THE ELECTROCHEMICAL ASPECTS OF D.C. ELECTROSLAG REMELTING

by

GORDON BEYNON

B.A.Sc., University of British Columbia, 1967

A THESIS SUBMITTED IN PARTIAL FULFILMENT OF THE

REQUIREMENTS FOR THE DEGREE

OF

DOCTOR OF PHILOSOPHY

in the Department

of

METALLURGY

We accept this thesis as conforming to the required standards

THE UNIVERSITY OF BRITISH COLUMBIA

October, 1971

In presenting this thesis in partial fulfilment of the requirements for an advanced degree at the University of British Columbia, I agree that the Library shall make it freely available for reference and study. I further agree that permission for extensive copying of this thesis for scholarly purposes may be granted by the Head of my Department or by his representatives. It is understood that copying or publication of this thesis for financial gain shall not be allowed without my written permission.

Department of Metallurgy

The University of British Columbia
Vancouver 8, Canada

Date Oct. 18, 1971

ABSTRACT

It is predicted from the known ionic properties of the slags used in electroslag melting, that the D.C. melting process should be accompanied by Faradaic reactions on the slag/ingot and slag/electrode interfaces. In the present work we have determined the magnitude of the overpotentials resulting from concentration polarization at these interfaces, for the case of pure iron in contact with $CaF_2 + Al_2O_3$ and $CaF_2 + CaO$ slags. This has been carried out using a galvanos tatic pulsing technique in an electrolytic cell.

The polarization overpotential existing on an electrode in an operating ESR unit has been measured essentially by the same technique. It was found that the potentials observed on melting ESR electrodes agree well with the results from the electrolytic cell. The primary anodic process is postulated to be the corrosion of iron, leading to an Fe^{2+} - saturated slag layer on the anode surface at sufficiently high current densities. The cathodic process is suggested to be the Faradaic reduction of Al^{3+} or Ca^{2+}, to produce a concentration of $[Al]_{Fe}$ or $(Ca)_{slag}$ in the cathode interface region.

The concentration polarization behaviour of other pure electrode materials (Cr, Ni, Co) was also investigated in $CaF_2 + Al_2O_3$ slags. For these materials, it has been postulated that the primary anodic process is the corrosion of the metal which again leads to interface saturation by the appropriate metal ions.

The concentration polarization behaviour of iron alloy electrodes (Fe-Cr, Fe-C) was also investigated. It was found that the more easily oxidizable alloying elements are preferentially removed from

these alloys when they are anodically polarized.

At very high current densities both the anodic and cathodic processes may convert to arcs, leading to process instability.

The chemical and thermal phenomena associated with D.C. ESR were studied by making ingots from pure electrode materials and iron-alloy electrode materials. Chemical effects which include metal oxidation and possible alloy loss were explained in terms of the Faradaic reaction mechanisms proposed in the electrolytic cell studies. Thermal effects were also explained on the same basis.

It was concluded that electrochemical reaction products were responsible for the formation of large numbers of small oxide inclusions in the pure metals. In the case of alloy materials, electrochemically produced oxidation resulted in significant losses of alloy components during melting.

TABLE OF CONTENTS

Page

TITLE PAGE. i

ABSTRACT. ii

TABLE OF CONTENTS iv

LIST OF TABLES. ix

LIST OF FIGURES x

ACKNOWLEDGEMENTS. xiii

CHAPTER 1. INTRODUCTION. 1

1.1 The Electroslag Remelting Process. 1

1.2 The problem. 2

1.2.1 Chemical effects. 3

1.2.2 Mechanical effects. 4

1.2.3 Thermal effects 5

1.3 Background to the problem. 5

1.3.1 Electronic conduction 6

1.3.2 Ionic conduction. 7

1.3.2.1 Interfaces at equilibrium. 10
1.3.2.2 Polarized electrode interfaces 11
1.3.2.3 Polarization mechanisms. 12
1.3.2.4 Mass transport 15
1.3.2.5 Transition time. 18
1.3.2.6 Ionic chemical and thermal effects 23

1.3.3 Arc discharge 24

1.4 Conclusions. 26

1.5 Experimental program outline 27

Page

CHAPTER 2. SMALL SCALE STUDIES. 29

2.1 Experimental considerations 29

2.2 Small scale polarization apparatus. 32

2.3 Electrode materials 41

2.3.1 Ferrovac-E pure iron 41
2.3.2 AISI 430 stainless steel 41
2.3.3 Fe - 1.0 wt. % Cr alloy. 41
2.3.4 Pure chromium 41
2.3.5 Pure nickel. 42
2.3.6 Pure cobalt. 42
2.3.7 Iron-carbon alloy. 42

2.4 Electroslag remelting polarization experiments. 43

2.5 Polarization results. 47

2.5.1 Ferrovac-E pure iron 47
2.5.2 AISI 430 stainless steel 56
2.5.3 Fe - 1.0 wt. % Cr alloy. 56
2.5.4 Pure chromium. 60
2.5.5 Pure nickel. 60
2.5.6 Pure cobalt. 65
2.5.7 Iron-carbon alloy. 65

2.6 Electroslag remelting polarization results. 65

CHAPTER 3. MELT PROGRAM 72

3.1 Melting procedure 72

3.2 Electrode materials 72

3.2.1 Low carbon mild steel: AISI 1018 73
3.2.2 Ferrovac-E pure iron. 73
3.2.3 Armco iron. 74
3.2.4 Ferritic stainless steel: AISI 430 74
3.2.5 Medium carbon mild steel: AISI 1095. 75

Page

3.2.6 Pure nickel. 75

3.3 Slag materials. 76

3.3.1 Calcium fluoride 76

3.3.2 Alumina. 77

3.3.3 Calcium oxide. 77

3.4 Atmospheric control 78

3.5 Melting conditions. 78

3.6 Melt records. 81

3.7 Melt record calculations. 82

3.7.1 Melt rate. 82

3.7.2 Specific coulombic density (Z) 83

3.7.3 Drop size and surface tension. 84

3.7.4 Melt program results 85

3.8 Ingot analysis. 85

3.8.1 Oxygen analysis of ingots. 85

3.8.2 Aluminum analysis of FVE ingots. 87

3.8.3 Analysis of AISI 1095 steel. 87

3.8.4 Analysis of AISI 430 stainless steel 87

3.9 Slag cap analysis 87

CHAPTER 4. DISCUSSION OF SMALL SCALE STUDIES. 99

4.1 Introduction. 99

4.2 Previous electrochemical work 99

4.3 Anodic polarization of pure iron in Al_2O_3 slags 101

4.3.1 Apparent transition time 115

4.4 Anodic polarization of pure iron in CaO slags 119

Page

4.5 Cathodic polarization of pure iron in ESR slags. 120

4.6 Polarization of Fe-Cr alloys and pure chromium 125

4.7 Polarization of pure nickel. 127

4.8 Anodic polarization of pure cobalt 129

4.9 Anodic polarization of an Fe-C alloy. 130

4.10 High current density polarization. 130

4.11 Electroslag process polarization 136

CHAPTER 5. DISCUSSION OF MELT PROGRAM RESULTS. 137

5.1 Introduction 137

5.2 Effect of electrode polarity on oxygen content 138

5.3 Inclusion types. 142

5.4 Effect of specific coulombic density (Z) on the final oxygen content 148

5.5 Effect of atmosphere control 148

5.6 Diffusion of oxygen into an anodic electrode 149

5.7 Drop size and surface tension. 153

5.8 Significance of iron in the slag caps. 154

5.9 Melt rate and heat generation. 156

5.10 Calcium oxide slags and ingot porosity 158

5.11 Effect of increasing ingot/electrode diameter ratio. 158

5.12 Effect of aluminum addition at the electrode during melting. 159

5.13 Alloy losses during remelting. 160

5.13.1 AISI 1095 steel. 160

5.13.2 AISI 430 stainless steel 162

Page

5.14 Remelting of nickel electrodes. 163

5.15 A.C. melting of pure iron 164

5.16 Electrochemical phenomena in commercial ESR 164

CHAPTER 6. CONCLUSIONS. 166

REFERENCES 168

LIST OF TABLES

Table		Page
I.	Melt Record Results of AISI 1018 Mild Steel.	.88
II.	Melt Record Results of FVE Ingots.	.89
III.	Melt Record Results of FVE Ingots	90
IV.	Melt Record Results of Armco Iron Ingots.	92
V.	Melt Record Results of Miscellaneous Ingots	93
VI.	Drop Size and Interfacial Tension Results for FVE	94
VII.	Total Aluminum Content of FVE Ingots.	95
VIII.	Composition of AISI 1095 Electrode and Ingots.	.96
IX.	Composition of AISI 430 Electrode and Ingots	.97
X.	Total Iron Content of FVE Slag Caps.	.98
XI.	Critical Current Density Estimation.	132

LIST OF FIGURES

Figure		Page
1.	Cell electrical circuitry	35
2.	General cell design	36
3.	Detail of cell assembly	37
4.	Method of obtaining overvoltage	39
5.	ESR furnace assembly	44
6.	Detail of reference electrode configuration	45
7.	Potential decay between the melting electrode and reference electrode observed at current interruption on an ESR anodic electrode	46
8.	Anodic polarization curves for pure iron in $CaF_2 + Al_2O_3$ slags	48
9.	Cathodic polarization curves for pure iron in $CaF_2 + Al_2O_3$ slags	49
10.	Anodic polarization curves for pure iron in $CaF_2 + CaO$ slags	50
11.	Cathodic polarization curves for pure iron in $CaF_2 + CaO$ slags	51
12.	Apparent transition time in the anodic polarization of pure iron in CaF_2 + 5 wt. % Al_2O_3	52
13.	High current density polarization curves for pure iron in CaF_2 + 5 wt. % Al_2O_3	53
14.	Sections through a pure iron electrode tip anodically polarized at high current density	55
15.	Anodic polarization curves for AISI 430 stainless steel in $CaF_2 + Al_2O_3$ slags	57
16.	Cathodic polarization curves for AISI 430 stainless steel in $CaF_2 + Al_2O_3$ slags	58
17.	Cr concentration gradient produced at anodic surface of AISI 430 stainless steel	59

Figure | Page

18. Anodic polarization curves for a Fe + 1 wt. % Cr electrode in a CaF_2 + 1 wt. % Al_2O_3 slag. 61

19. Anodic polarization curve for pure Cr in a CaF_2 + 1 wt. % Al_2O_3 slag. 62

20. Single polarization curve for an anodic pulse on pure nickel in a CaF_2 + 2.5 wt. % Al_2O_3 slag. 63

21. Section through a pure nickel electrode cathodically polarized in a CaF_2 + 8 wt. % Al_2O_3 slag 64

22. Single polarization curve for an anodic pulse on pure cobalt in a CaF_2 + 2.5 wt. % Al_2O_3 slag 66

23. Anodic polarization on Armco iron ESR electrodes in CaF_2 + Al_2O_3 slags. 67

24. Cathodic polarization on Armco iron ESR electrodes in CaF_2 + Al_2O_3 slags. 68

25. Anodic polarization on Armco iron ESR electrodes in CaF_2 + Al_2O_3 slags 69

26. Cathodic polarization on Armco iron ESR electrodes in CaF_2 + CaO slags. 70

27. Argon fume hood. 79

28. Argon gas cap. 80

29. Ingot sampling scheme. 86

30. Schematic representation of the anodic polarization curve for pure iron in CaF_2 + Al_2O_3 slags 102

31. Application of a limiting current density law to anodic polarization of pure iron in CaF_2 + Al_2O_3 slags 103

32. Partial phase diagrams of the system CaF_2 - CaO - FeO. 108

33. Estimated limiting current density for anodic polarization of pure iron in CaF_2 + Al_2O_3 slags 111

34. IR drop as a function of applied current, I, for anodic polarization of pure iron in a CaF_2 + 2.5 wt. % Al_2O_3 slag . . .112

Figure Page

35. Anodic pulse on pure iron in CaF_2 + 250 ppm CaO. 114

36. Application of transition time law to anodic polarization of pure iron in CaF_2 + 2.5 wt. % Al_2O_3 slag. 117

37. Successive anodic pulses applied to pure iron in a CaF_2 + 2.5 wt. % Al_2O_3 slag. 118

38. Cathodic polarization of pure iron in a CaF_2 + 1 wt. % Al_2O_3 slag plotted against the applied current 122

39. Section from interior of FVE electrode negative ingot. . . .143

40. Section from interior of AISI 430 stainless steel ingot. . .144

41. Alumina inclusions on the top of a FVE electrode negative ingot. 146

42. Al and O in liquid iron in equilibrium with unit activity Al_2O_3 at 1600°C. 147

43. Various electrode tips showing oxide present on an anodic iron electrode tip 155

A C K N O W L E D G E M E N T S

The author is indebted to Dr. A. Mitchell for his advice and assistance throughout the duration of this work.

Thanks are also due to my fellow graduate students and to various faculty members for innumerable helpful discussions.

The assistance of Mr. A. Thomas and other members of the technical staff is greatly appreciated.

The financial assistance of Stelco is gratefully acknowledged.

CHAPTER 1

INTRODUCTION

1.1 The Electroslag Remelting Process

Electroslag Remelting (ESR) is a process in which a metal electrode is consumably melted through a slag to solidify in a water-cooled mold forming an ingot. ESR is one of the few processes suitable for upgrading the quality of the more complex alloys in use in specialized structural applications. The most widely used process in North America is Vacuum Arc Remelting (VAR) which is the chief alternative to ESR. More expensive processes such as Electron Beam Melting are normally used to process only the rarer metals because of the high operating costs and the small melting capacity of those units.

Any refining action during VAR is a result of metal exposure to the vacuum and is therefore restricted to pressure sensitive reactions. In contrast, in ESR the melting metal spends a finite length of time in contact with the slag. For this reason composition changes requiring solid/liquid or liquid/liquid reactions are possible.

ESR appears to be a more satisfactory secondary refining process than VAR mainly because of the greater flexibility in melting conditions. With proper utilization of slag chemistry and melting parameters, it should be possible to achieve rigorous composition and structure control hence producing an ingot with better overall properties.

The rate of production of an ESR unit is controlled by the maximum tolerable freezing rate. In general a lower melt rate produces a

flatter pool profile while a higher melt rate produces a deeper pool profile and possibly unfavourable dendrite orientation. At present the maximum ESR ingot size is 150 tons with a diameter of 3 m., and this can be increased to 200 tons with a 3.5 m. diameter without requiring any major technological changes. Power consumption during ESR ranges from 120 to 2000 kwh per ton of metal, again depending on which parameters the operator chooses to control, in contrast to a typical 3 Ø-arc furnace consumption of 550-650 kwh/ton. Both VAR and ESR add approximately the same cost per ton of metal. In this cost structure electrical power consumption accounts for approximately 30-50% of the total direct and indirect costs. Optimization of this power consumption would evidently be a major advantage in furnace operation.

1.2 The problem

The majority of ESR units in operation today use single-phase, line frequency (60 Hz) A.C. power. It is desirable that the power supply cables have the shortest possible route from transformer to electrode connection and be sited on the same route as the baseplate return lines. Such an arrangement will reduce the inductive loop and maintain transmission efficiency. A power factor of between 0.85 and 0.92 is normally obtained on such equipment without correction measures. As larger electroslag furnaces are built, it is necessary to determine whether they will use A.C. or D.C. power. A.C. power factors tend to decrease with increasing ingot size, and although these furnaces could operate at low power factors, the supply authorities would not permit this because of wave-shape distortion on the incoming mains. Power factor correction can be

accomplished using variable capacitors but the cost is exceedingly high. D.C. melting, on the other hand, has no electroslag circuit power-factor problems and thus has advantages for very large ingot sizes.

Strictly from power considerations then, D.C. power is apparently preferable to A.C. power for very large electroslag furnaces, but such a decision must also be made with respect to possible electrochemical, and thermal phenomena which might be encountered during the passage of large amounts of D.C. current through the electroslag system. One must therefore attempt to answer the following questions about D.C. electroslag melting:

1. What electrochemical, chemical, and thermal changes will occur during remelting?
2. Why do they occur?
3. How important will they be in terms of affecting the final chemical and mechanical properties of the ingot metal?

1.2.1 Chemical effects

It is a generally accepted fact that D.C. melting of alloy materials produces a higher loss of easily oxidized alloying elements than occurs during A.C. melting, and also that the main concern is not with the loss of major alloying elements, but instead with changes in minor components such as Ti, Si, Al, O, S, etc. Etienne (1) reported titanium losses from AISI 321 stainless steel (0.5 wt. % Ti in the electrode) of 40% in the electrode negative mode and losses of 80% in the electrode

positive mode. Kennard (2) reported Ti losses of approximately 30% when remelting 18% Ni Maraging steel (0.80 wt. % Ti in electrode) in the electrode negative mode. Other workers (3, 4) have reported serious losses of Si (~10%) and Al (~15%) from iron alloys remelted with D.C. power. Whittaker (5) and Holzgruber (6) found varying levels of oxygen and sulphur in ingots made using electrode negative, electrode positive, and A.C. power. As mentioned previously, oxidation losses are higher during D.C. melting. These chemical effects must therefore be a result of electrochemically produced oxidation. The nature of this phenomenon is unclear due to the lack of definitive electrochemical studies of metal electrodes in calcium fluoride-based slags.

1.2.2 Mechanical effects

General concern for oxidative losses is not surprising, since some alloys, where a small concentration of an essential alloying element is present, are particularly sensitive to composition fluctuations. In Maraging steel type 300, for instance, which contains 0.8 wt. % Ti, a loss of 0.1 wt. % in Ti will cause the yield strength to drop by 10,000 psi (3%). It is apparent, then, that these observed alloy losses can be very serious indeed, and one must be aware of such potential losses during D.C. remelting in order to decide what mode of melting is most feasible in large remelting furnaces. Effective loss of alloying elements may also occur by formation of oxide inclusions in the ingot. In this case, the elements have not actually been lost, but they are no longer available to serve their intended purpose in the matrix. Consideration must also be given to the detrimental effect of inclusions on the mechanical properties of the metal.

1.2.3 Thermal effects

Thermal effects in D.C. Electroslag melting will arise directly if the mode of current passage at the metal/slag interfaces alters either the rate of heat generation or heat transfer. Depending on the type of current conduction in the slag, such changes might arise from a Peltier effect, from an electrochemical polarization resistance, or from the formation of an arc. These possibilities will be discussed subsequently. Heat effects apparently do exist during electroslag melting because it has been noted (7,8) that the three modes of melting (D.C. -ve, D.C. +ve, A.C.) produce differences in the specific melt-rate (kwh/ton), and, furthermore, these findings by different investigators are not in agreement as to which mode is the most efficient. These differences in specific melt-rate must arise, in part, from heat generation effects at the electrode, which in turn must result from electrochemical and chemical effects associated with the mode of current passage at the slag/metal interfaces.

Since it is apparent that chemical, mechanical and thermal effects are associated with using D.C. power for electroslag remelting, and that the results to date are contradictory regarding these effects, it is worthwhile investigating these phenomena on both small and large scales.

1.3 Background to the problem

Before one can study the occurrence of the effects discussed previously, it is necessary to understand fully all the possible methods of current passage in a liquid metal/fused salt system, and in each case to consider the possible mechanisms which could give rise to chemical and thermal effects. The three possible modes of current passage between a

liquid metal electrode and a fused salt are:

I. Electronic conduction.

II. Faradaic reactions.

III. Arc discharge.

Each of these have specific characteristics which may or may not be able to explain the effects being examined.

1.3.1 Electronic conduction

If current passage through such a system takes place by electronic conduction, i.e., the slag is an electronic conductor, there will be no Faradaic reactions occurring at the slag/metal interfaces. There will therefore be no electrochemically produced material to affect the chemistry of the metal and the slag. Any chemical changes would result only from chemical interaction between the slag and the melting metal. Heat generation in the bulk of the slag will occur by resistance heating, the amount of heat so generated being equal to the product of the process voltage and current. If any change in the CaF_2 stoichiometry is to be produced by high temperature reaction it would be most likely to lead to metal-excess compositions. Hence the slag would behave as an n-type semiconductor. It is possible during electronic conduction, to generate localized heating or cooling at an interface due to the Peltier effect, which is important when two materials have differing electron mobilities. The amount of heat so generated is given by:

$$q = \pi I$$

where π is the Peltier coefficient and I is the current. The Peltier coefficient is given by:

$$\pi = \alpha T$$

where α is the Seebeck coefficient and T is the absolute temperature. The Seebeck coefficient of one of the best commercial thermoelectric materials (PbTe), is approximately 400 $\mu V.°C^{-1}$, but that of a calcium-fluoride slag, would likely be much lower, say approximately 10 $\mu V.°C^{-1}$. At a temperature of 2000°K, and a current of 1000 A., the rate of Peltier heating at such a proposed interface would be 20 $cal.sec.^{-1}$, a negligible amount in comparison to the total process heat generation rate of 6.5 $Kcal.sec^{-1}$. Also, such heat generation at one electrode interface, would be complemented by an equivalent amount of heat loss at the other interface. One can therefore conclude that electronic conduction during ESR processing would produce no significant chemical changes and that localized heat generation arising from the Peltier effect would be insufficient to affect the melt rate of the electrode. In view of these deductions, one must account for any chemical and thermal effects observed during electroslag melting by means other than electronic conduction, even though the degree of electronic conduction in such a metal/fused salt system might be quite substantial (as will be discussed in Chapter 5).

1.3.2 Ionic conduction

If current passage between liquid metal electrodes in contact with calcium fluoride-based slags takes place by ionic conduction, Faradaic processes must take place at the electrode/slag interfaces. This requirement has two important consequences. The first is that Faradaic reaction products are available in the system to react chemically with the metal and the slag. The second is that polarization can occur at the metal/

slag interfaces which could result in localized excess heat generation and modify iso-potential surfaces in the bulk of the slag. This would affect the local dynamic heat balance at the metal/slag interfaces, and would be reflected either in melting efficiency or in process temperature distributions.

Although it has been stated that calcium fluoride-based slags are completely ionic in nature (9), this in fact means that the degree of electronic conduction is extremely small. In pure liquid CaF_2, the transport number of electrons is approximately 10^{-4}(10), and arises from a small degree of nonstoichiometry which is inherent in all compounds at high temperature (11). Calcium fluoride will have significant electronic conductivity when calcium is dissolved in it, calcium being completely miscible with calcium fluoride (12). Although the effect of dissolved calcium on the electrical conductivity of calcium fluoride has not been studied, data are available on the effect of sodium addition to sodium fluoride and similar halide systems (12). From these data it appears that a 30→40 increase in conductivity for 2→5 mole % addition of calcium to calcium fluoride is not unreasonable. This would represent a large degree of nonstoichiometry and therefore a substantial degree of n-type electronic semiconduction.

For the moment, calcium fluoride slags will be presumed to conduct ionically, and therefore during electroslag remelting with D.C. power, cathodic and anodic Faradaic reactions take place continuously at the appropriate sites. It is difficult to justify the presence of substantial net Faradaic reactions in an electroslag furnace in view of the fact that the slag chemistry is essentially unchanged during melting. The

overall system reaction efficiency must therefore be very low, approximately 1%, a condition that can arise in two ways. The first possibility is that the individual total anodic and cathodic processes themselves operate at very low current efficiencies. This would be the case if there was a substantial amount of electronic conduction. The second possibility is that, if the reaction current efficiencies are high, the individual reaction products continuously recombine during remelting such that during melting a small steady state amount of anodic and cathodic products are present in the slag. Observation of the system as a whole would therefore indicate that the reactions behave efficiently but that the net electrochemical composition changes in the slag are small.

The lack of substantial chemical changes in the slag implies that the chemical changes which occur in the metal are also small, although even small losses in some alloying elements can have very serious effects on the mechanical properties of the metal. The purpose of this study is then to formulate Faradaic reaction mechanisms occurring at liquid metal/fused salt anodic and cathodic interfaces which can account for the following phenomena:

I. Chemical changes in the slag are small.

II. Easily oxidized alloying elements are preferentially removed from the melting metal.

III. Chemical changes in the metal are small.

IV. Thermal effects have been observed and are apparently related to the mode of power used during melting.

1.3.2.1 Interfaces at equilibrium

It is useful at this point to consider the type of metal/slag interface that would exist between pure iron and a calcium fluoride-based slag at equilibrium, (no net current flow across the interface). If a solid iron electrode is immersed in a liquid calcium fluoride-calcium oxide slag, equilibrium between the metal and slag will be attained by dissolution of iron ions in the slag at the interface. Although the iron surface is in equilibrium with the slag, the interface is not a static one. An exchange current flows, in which the forward current equals the reverse current. Aqueous systems generally have low exchange current densities ($10^{-12} \rightarrow 10^{-3}$ A.cm^{-2}) but some liquid metal/fused salt systems have comparatively high exchange current densities (i_o = 210 A.cm.$^{-2}$ for the Cd(II)-Cd reaction) (13). The exchange current density can be considered to be a measure of the reversibility of an electrochemical reaction, which in turns indicates the ease with which an electrode may be polarized.

A high exchange current density implies that an electrode is difficult to polarize. The behaviour of polarized electrode interfaces will now be discussed since polarization phenomena can be used to answer some of the questions previously presented with respect to chemical and thermal effects. At a simple liquid metal/fused salt electrode interface, polarization phenomena have the following consequences.

1. The presence of polarization at such an interface implies that excess heat will be generated by current passage through the thin polarized slag layer

representing part of the irreversibility of the reaction. Significant polarization could therefore account for any observed thermal effects during remelting.

2. Polarization will take place by Faradaic reactions, the products of which may lead to small but important composition changes of the metal during melting.

1.3.2.2 Polarized electrode interfaces

At equilibrium, the potential, with respect to a reference electrode, of an Fe electrode in contact with a calcium fluoride-calcium oxide slag is determined by the concentration of Fe^{2+} ions at the slag/metal interface. This concentration is governed by the half-cell reaction:

$$Fe \rightarrow Fe^{2+} + 2e^{-} \qquad (1\text{-}1)$$

For the case of a simple metal/ion electrode having the electrode reaction valence $\eta = z$:

$$Me \rightarrow Me^{z+} + ze^{-} \qquad (1\text{-}2)$$

the equilibrium electrode potential, E, is written in the form of a Nernst equation:

$$E = E^{\circ} + \frac{RT}{\eta F} \ln \frac{a_{me^{z+}}}{a_{Me}} \qquad (1\text{-}3)$$

where E° is the standard electrode potential when all reactants and products are at unit activity. It must be stressed that all half-cell potentials are measured with respect to a reference electrode whose potential is constant for a given electrolyte. Ideally, a reference electrode consists of an electrode surface in contact with electrolyte of a known and invarient

composition such that a standard reference electrode of known potential can be used. An example of a standard reference electrode is the saturated calomel electrode. A difficulty that arises with such electrodes is that it is frequently necessary to have two different solutions in contact, which gives rise to a liquid junction potential. The value of the liquid junction potential can be minimized by using a salt bridge. In aqueous systems where the solution resistances are generally high it is necessary to utilize this type of reference electrode in order that the IR drop between a working electrode and the reference electrode can be minimized by having the reference electrode very close to the working electrode. In fused salt systems, the resistances are much lower and it is possible to use a remote reference electrode in contact with the bulk liquid if the range of liquid compositions studied do not grossly alter the reference electrode potential. This will be discussed in detail in Chapter 2. The important point at issue is that a reversible reference electrode must be used to measure the potential of the working electrode being studied. If current is passed through an electrode at equilibrium and the current is such that the concentration of the electrochemical reactants or products is altered, the electrode is said to be polarized, and the potential of the electrode interface is altered from the equilibrium potential by the polarization overvoltage.

1.3.2.3 Polarization mechanisms

Vetter (14) defines four types of overvoltage, each one of which is operative at an interface if that particular step of the overall

electrochemical reaction is the slowest or rate-determining process. The types of overvoltage are given below.

1. η_t - charge-transfer overvoltage.

   The transfer of charge carriers across the electrical double layer is rate-controlling.

2. η_r - reaction overvoltage.

   A slow chemical step in the overall electrode reaction is rate controlling, and the rate constant is, by definition, independent of potential.

3. η_d - diffusion overvoltage.

   Supply of reactants to or removal of reaction products from the electrode is rate controlling.

4. η_c - crystallization overvoltage.

   Hindrance of the process by which atoms are incorporated into or removed from the crystal lattice leads to crystallization overvoltage.

In a liquid metal/fused salt system at high temperature (~1400°C) it is unlikely that activation processes other than diffusion would be rate controlling. Further discussion will therefore be concerned with diffusional processes and associated phenomena.

Diffusion overvoltage. Diffusion overvoltage, η_d, appears when the supply of reactants to the electrode or the removal of reaction products from the electrode is rate determining. If all chemical processes, including the crystallization processes and also the charge-transfer reaction, are in equilibrium, only diffusion overvoltage is present.

The potential of an electrode experiencing pure diffusion polarization can be calculated in terms of the Nernst equation in which the concentration of the components directly at the surface must be used and not those in the interior of the electrolyte. Therefore, the diffusion overvoltage η_d is equal to the difference:

$$\eta_d = E' - E \tag{1-4}$$

between the equilibrium potential E and the impressed potential E' required for current flow.

To correlate the diffusion overvoltage η_d with concentration changes, a general overall electrode reaction will be given.

$$(-v_1)S_1 + (-v_2)S_2 + \ldots \overset{\rightarrow}{\leftarrow} v_1 S_1 + \ldots + v_q S_q + ne^- \tag{1-5}$$

The stoichiometric factors v_j are positive for oxidized components and negative for reduced components. At equilibrium the overall electrode reaction leads to the equilibrium electrode potential E whose concentration dependence is expressed by the Nernst equation:

$$E = E^\circ + \frac{RT}{nF} \Sigma\, v_j \cdot \ln \bar{a}_j \tag{1-6}$$

In equation (1-5) $\bar{a}_j$ are the activities $\bar{a}_j = f_j \bar{c}_j$ of the components S_j of the overall electrode reaction. On current flow the concentrations c_j directly before the surface, are functions of the current density i and of the time t. Hence $a_j = a_j(i, t) \neq \bar{a}_j$. Therefore, the potential E'(i, t) is given in accordance with the Nernst equation by:

$$E'(i,t) = E^\circ + \frac{RT}{nF} \cdot \Sigma v_j \cdot \ln a_j(i,t) \tag{1-7}$$

and by substraction of equation (1-6) from (1-7), the diffusion overvoltage is:

$$\eta_d = E'-E = \frac{RT}{nF} \cdot \Sigma v_j \cdot \ln \frac{a_j(i,t)}{\bar{a}_j} \qquad (1\text{-}8)$$

Diffusion polarization therefore results when mass transport of reactants or products to or away from the electrode interface is rate-controlling. This produces concentration changes in components S_j at the interface and the resulting diffusion overvoltage is expressed as a Nernst equation in terms of concentration or activity changes.

1.3.2.4 Mass transport

The concept of a diffusion boundary layer must be used when discussing diffusional transport of species to or away from an electrode interface. For the simplest case, one assumes a planar electrode surface with a diffusion layer of thickness δ, which is assumed to be stationary. Transport of the component S_j having the activity a_j can take place only if an activity gradient da_j/dx exists for this component. x is the perpendicular distance from the electrode surface. The number of moles N_j of substance S_j diffusing through a cross-section of 1 $cm.^2$ per second is given by Fick's first law. For simplicity, the concentration c_j will be used in place of the activity a_j, and the flux is written as:

$$N_j = D_j \cdot \frac{dc_j}{dx} \qquad (1\text{-}9)$$

All components S_j of the overall electrode reaction (1-5) must diffuse through this diffusion layer. A transfer of one mole of S_j corresponds to a charge amounting to $n \cdot F/v_j$ coulombs. Therefore the current density divided by $n \cdot F/v_j$ represents mass transfer in mole. $cm.^{-2}$ $sec.^{-1}$, which passes from the electrode through the layer to the

electrolyte. With due consideration to sign

$$\frac{i \cdot v_j}{nF} = -D_j \cdot \frac{dc_j}{dx} \qquad (1\text{-}10)$$

is obtained. In the stationary state and in the absence of homogeneous chemical equilibria through the entire layer, the flow of the components $|S_j|$ must be constant and a linear concentration gradient $dc_j/dx = -(c_j-\bar{c}_j)/\delta$ = constant is established throughout the entire layer. Equation (1-10) may now be written as:

$$\frac{i \cdot v_j}{n \cdot F} = + D_j \cdot \frac{c_j - \bar{c}_j}{\delta} \qquad (1\text{-}11)$$

In principle, with the movement of ions through the diffusion layer, the influence of an electric field must also be taken into account. This field causes an additional migration current which is superimposed on the diffusion current. A high excess of an indifferent electrolyte minimizes this electric field effect within the diffusion layer to a large extent, since the excess electrolyte causes the transport number t_j of the reacting components S_j to become very small. By assuming that the concentration of ions involved in the electrochemical reaction is small, the effect of the electric field can be neglected.

The value of the concentration gradient $(c_j-\bar{c}_j)/\delta$ is proportional to the current density i , [equation (1-11)], and in the case of ions diffusing to the electrode surface, the concentration gradient will have a maximum value which is reached when the current density is such that the ionic concentration c_j of species S_j becomes zero at the electrode surface (c_j=0). This maximum concentration gradient is then $\bar{c}_j/\delta$

and the corresponding current density is called the limiting diffusion current density $i_{d,j}$ with respect to substance S_j. For each substance S_j in the overall electrode reaction equation (1-5) there is such a limiting diffusion current density which is characterized by the index j.

$$i_{d,j} = -\frac{n}{v_j} \cdot F \cdot \frac{D_j}{\delta} \cdot \bar{c}_j \qquad (1\text{-}12)$$

The electrode reaction can take place no faster than the value determined by this limiting current density. However, if a potential is impressed on the cell sufficient to produce a current density i higher than the limiting current density $i_{d,j}$, the potential at the electrode will change to such an extent that a second electrode process may take place at the current density $(i-i_d)$.

The ratio of the concentration $c_j/\bar{c}_j$ is important for the calculation of the diffusion overvoltage according to equation (1-8). This ratio is easily derived from equations (1-11) and (1-12), i.e.,

$$\frac{i}{i_{d,j}} = \frac{\bar{c}_j - c_j}{\bar{c}_j} = 1 - \frac{c_j}{\bar{c}_j}$$

or

$$\frac{c}{\bar{c}_j} = 1 - \frac{i}{i_{d,j}} \qquad (1\text{-}13)$$

Equation (1-13) is valid for every component S_j in the overall electrode reaction, so that one obtains the general expression for the total diffusion overvoltage after substitution into equation (1-8), i.e.,

$$\eta_d = \frac{RT}{nF} \cdot \Sigma v_j \cdot \ln\left(1 - \frac{i}{i_{d,j}}\right) \qquad (1\text{-}14)$$

The diffusion overvoltage resulting from transport of species S_j is written in terms of the current density, i, and the limiting current density, $i_{d,j}$. Examination of equations (1-14)and (1-12) shows that i_d contains the mass transport variables inherent in η_d.

1.3.2.5 Transition time

The term chronopotentiometry is applied to the techniques of electrolysis at constant current under conditions of linear diffusion control. It must be stressed that chronopotentiometry is a selected form of unsteady state. An important experimental quantity in chronopotentiometry is the "transition time" τ. This time is the time interval subsequent to the onset of constant current electrolysis during which the surface concentration of diffusing material undergoing electrode reaction reaches zero and a rapid increase of electrode potential occurs. The value of the transition time can be calculated from linear diffusion theory, derived from the following conditions:

1. Uniform initial concentration $\bar{c}_j$ of diffusing species S_j.

2. Constant concentration gradient at the electrode surface equal to $i \cdot v_j/nFD_j$.

The concentration of species S_j at the interface can then be found by solving the partial differential equation for diffusion (Fick's Second Law) under the appropriate initial and boundary conditions. The interface concentration c_j varies with the distance x and the time t such that $c_j = c_j(x, t)$ and is written:

$$c_j(x,t) = \bar{c}_j - \frac{2 N_j t^{1/2}}{D^{1/2} \pi^{1/2}} \cdot e^{-\frac{x^2}{4 D_j t}} + \frac{N_j x}{D_j} \cdot \operatorname{erfc} \frac{x}{\sqrt{4 D_j t}} \qquad (1\text{-}15)$$

where N_j is the constant flux imposed by the current density i. As stated in equation (1-10) the flux N_j is equivalent to $i \cdot v_j/nF$ at the electrode interface, and this can be substituted into equation (1-15) for the boundary condition x = 0 to obtain

$$c_j(x = 0,t) = \bar{c}_j - \frac{2 i v_j}{nF} \cdot \sqrt{\frac{t}{\pi D}} \qquad (1\text{-}16)$$

By writing

$$P = + \frac{2 i v_j}{nF} \cdot \sqrt{\frac{1}{\pi D}} \qquad (1\text{-}17)$$

equation (1-16) becomes

$$c_j(x = 0,t) = \bar{c}_j - P t^{1/2} \qquad (1\text{-}18)$$

The expression gives the variation of concentration of species S_j at the interface with time, after application of a constant current density, but one seeks also to know the time variation of the potential difference across the interface at which the reaction is occurring. To obtain this relationship, the Nernst equation can be used to relate the potential difference to the interface concentration. That is, by substituting (1-18) into the Nernst equation, the electrode potential measured with respect to a reference electrode is given by:

$$E'(x = 0,t) = E^\circ + \frac{RT}{nF} \ln (\bar{c}_j - P t^{1/2}) \qquad (1\text{-}19)$$

Before one can develop this equation further, consideration must be given to the material produced by the electrochemical reaction. A simple

example is the electro-reduction of ferric ions to form ferrous ions ($Fe^{3+} + e^{-} \rightarrow Fe^{2+}$) where the reactant and product are in solution, and one must take into account the diffusion of the electron donor away from the electrode and the variation of its interfacial concentration with time. If the reacting species is S_a and the product species S_b, equation (1-19) can be written as:

$$E'(x = 0,t) = E^\circ + \frac{RT}{nF} \ln \frac{c_a(x = 0,t)}{c_b(x = 0,t)} \tag{1-20}$$

where $c_a(x=0,t) = \bar{c}_a - Pt^{1/2}$. (1-21)

If 1 mole of S_b is formed from 1 mole of S_a and their diffusion coefficients are the same, one obtains

$$c_b(x = 0,t) = \bar{c}_b + Pt^{1/2} \tag{1-22}$$

and equation (1-20) becomes:

$$E'(x = 0,t) = E^\circ + \frac{RT}{nF} \ln \frac{\bar{c}_a - Pt^{1/2}}{\bar{c}_b + Pt^{1/2}} \tag{1-23}$$

If at zero time, the concentration of S_b is negligible, then $\bar{c}_b = 0$ and equation (1-23) becomes:

$$E'(x = 0,t) = E^\circ + \frac{RT}{nF} \ln \frac{\bar{c}_a - Pt^{1/2}}{Pt^{1/2}} \tag{1-24}$$

Consider the expression (1-24) for the time variant potential of the working electrode at which a diffusion controlled electro-reduction reaction is stimulated by a constant current switched on at $t = 0$. The product $Pt^{1/2} = 0$ at $t = 0$. Hence, $\bar{c}_a/Pt^{1/2}$ tends to infinity as does its logarithm. At values of time greater than $t = 0$ the term $Pt^{1/2}$ is

finite and at some value of time is equal to $\bar{c}_a$. This time has been previously defined as τ, the transition time, and $\ln(\bar{c}_a - Pt^{1/2})$ tends to minus infinity, and the potential changes rapidly. In fact, it sinks till it has become sufficiently negative so that the electro-reduction of some other ionic species can occur. By definition, therefore, when $t = \tau$ and $(\bar{c}_a - Pt^{1/2}) = 0$, $\bar{c}_a = P\tau^{1/2}$ and equation (1-24) can be written as:

$$E'(x = 0,t) = E^\circ + \frac{RT}{nF} \ln \frac{P\tau^{1/2} - Pt^{1/2}}{Pt^{1/2}} \tag{1-25}$$

where P was defined by equation (1-17) to be

$$P = + 2 \frac{i}{nF} \sqrt{\frac{1}{\pi D}}, (\nu_j = 1)$$

and equation (1-25) becomes

$$E'(x = 0,t) = E^\circ + \frac{RT}{nF} \ln \frac{\tau^{1/2} - t^{1/2}}{t^{1/2}} \tag{1-26}$$

Prior to current passage, the equilibrium electrode potential determined by the concentration of species S_a is written as:

$$E = E^\circ + \frac{RT}{nF} \ln \bar{c}_a \tag{1-27}$$

As defined by equation (1-4), the diffusion overvoltage η_d can then be written as:

$$\eta_d = E' - E = A + \frac{RT}{nF} \ln \frac{\tau^{1/2} - t^{1/2}}{t^{1/2}} \tag{1-28}$$

where the constant A is given by:

$$A = - \frac{RT}{nF} \ln \bar{c}_a \tag{1-29}$$

By manipulation of the equation

$$\bar{c}_a = P\tau^{1/2} \tag{1-30}$$

and substitution of equation (1-17), it can be shown that

$$i\tau^{1/2} = \frac{nF\bar{c}_a \pi^{1/2} D^{1/2}}{2} \tag{1-31}$$

The product $i\tau^{1/2}$ is seen to be constant for diffusion controlled electrolysis regardless of the current density. Equation (1-31) therefore constitutes a simple experimental criterion of diffusion control.

The preceeding discussion on ionic conduction has presented the basic information regarding diffusion polarization processes.

General expressions were presented to show that the polarization overvoltage can be described in terms of concentration changes of reactant or product species at the electrode surface, and these changes can be considered in terms of a Nernst equation:

$$\eta_d = \frac{RT}{nF} \cdot \Sigma v_j \ln \frac{c_j(i, t)}{\bar{c}_j} \tag{1-32}$$

Using the concept of mass transport at constant current density in unstirred solutions, the definition of a limiting diffusional current was discussed and it was shown that the diffusion overvoltage can also be expressed in terms of the current density(i) and the limiting current density ($i_{d,j}$):

$$\eta_d = \frac{RT}{nF} \cdot \Sigma v_j \cdot \ln \left(1 - \frac{i}{i_{d,j}}\right) \tag{1-33}$$

The transition time, τ, was defined as the time after the onset of constant current that the concentration of reacting ionic species becomes zero at the electrode interface. The diffusion overvoltage can also be expressed in terms of τ and t:

$$\eta_d = A + \frac{RT}{nF} \ln \frac{\tau^{1/2} - t^{1/2}}{t^{1/2}} \qquad (1\text{-}34)$$

1.3.2.6 Ionic chemical and thermal effects

Chemical effects. The Faradaic reaction products produced at the electrode surfaces are available in the system to interact chemically with the metal and the slag. Therefore ionic conduction can account for chemical effects observed during D.C. electroslag melting.

Thermal effects. A polarized electrode interface through which high current densities pass will behave in a quite different thermal manner from an unpolarized interface. Current passage through ionic slags produces heat by Joule heating according to the relationship:

$$P = Vi \qquad (1\text{-}35)$$

where P is the power generation in watts, and v is voltage drop in the slag. At an unpolarized electrode, the voltage gradient in the slag at the electrode interface is the same as that in the bulk of the slag. At a polarized electrode, the voltage gradient is higher than normal in the polarized layer and heat generation in this layer will be accordingly higher. The increased voltage gradient is produced by the polarization overvoltage and the excess heat generation is given by:

$$P = \eta i \qquad (1\text{-}36)$$

In this way polarization at liquid metal/liquid slag interfaces can account for thermal effects observed during D.C. electroslag melting.

It is interesting to consider the possibilities of chemical and thermal effects when melting with A.C. power. If slow diffusional processes are responsible for D.C. melting effects, and if the diffusion times are long in comparison to the half-wave time of 60 Hz. A.C. power, net chemical effects should be zero. This is to say that reaction products produced on the anodic half-cycle should be entirely removed by the cathodic half-cycle. However, any polarization resistance heating would not behave reversibly.

1.3.3 Arc discharge

Consideration will now be given to the case in which current transfer between a melting electrode and liquid CaF_2 based slag takes place by arc discharge. This possibility will be discussed in terms of thermal effects and chemical effects, and it is assumed that the slag conducts ionically. Very little is known about the mechanisms of current movement through a high current arc, especially for arcs between high-temperature slag and metal surfaces.

In metal electrodes, charge is conducted by a "degenerate gas" of free electrons, but they remain loosely associated with atoms. Within the plasma region of an arc, electrons and ions exist and move as separate entities but very little is known about the transition from one type of conduction to the other at the arc terminals. In the case

of arcing during electroslag melting the conduction sequence in going from the metal to the slag is electronic → electronic + ionic → ionic.

At a metallic arc cathode, thermionic emission is most often proposed as the primary mechanism of electron liberation, but there is doubt as to the source of energy needed to sustain emission. Also, the effect of ion current in reducing requirements for electronic emission must be recognized.

The anodes of high-current metallic arcs appear to function primarily as collectors of electrons and secondarily as contributors of vapours and ions to the plasma. The principal means of anode heating is electron bombardment. Hence, it is generally concluded that the current at the anode is almost entirely electronic.

With respect to a metal/slag arc, one can propose that current transfer through the arc plasma takes place by electron plus ionic conduction. There will be Faradaic reaction products deposited at both the metal/plasma interface and the plasma/slag interface. Electrochemical reactions are therefore possible, but the most important aspect of arc phenomena are those of heat generation in the arc. During electroslag melting, an arc could be initiated at the electrode in two ways.

1. By evolution of a Faradaic reaction product which is gaseous or has a very high vapour pressure (e.g., Ca_{1}, O_{2g}). This product would facilitate electron emission at the ionic liquid surface. An arc so formed would be self-sustaining by virtue of continued production of the materials.

2. By passage of sufficient current at the electrode to heat the slag at this point to its boiling point and vapourize it.

Both possibilities will be considered in the discussion, but, at this point, it is sufficient to say that the most important aspect of arc discharge will be the high rate of heat production at the electrode. This should produce anomalously high electrode consumption rates. Chemical effects would be possible but would be secondary in importance to the thermal effects.

1.4 Conclusions

The conclusions of this chapter are as follows:

1. Chemical and thermal effects do exist using D.C. electroslag melting. Chemical effects result in oxidation loss of important alloying elements from the metal, the magnitude of which can be sufficient to alter ingot mechanical properties. Thermal effects are apparently manifested as differences in the specific melt rate.

2. Electronic conduction in the slag cannot account for the observed chemical or thermal effects.

3. Ionic conduction in the slag can account for the reported observations, through Faradaic reactions and their consequent associated polarization effects.

4. Arc discharge at a melting electrode is possible and is important in regard to thermal effects.

5. Definitive small scale and large scale studies are justified in order to establish the chemical and thermal effects, and to propose suitable electrochemical mechanisms.

1.5 Experimental programme outline

It is now necessary to decide what experimental results are needed to satisfactorily explain the chemical and thermal phenomena observed during D.C. electroslag remelting. In view of the contradictory nature of these phenomena as reported by other workers in the field, the following questions must be asked.

A. Are the reported effects real in experiments in which the following parameters are controlled?

- atmosphere
- process voltage and amperage
- alloy composition
- slag composition

B. What is the magnitude of these effects?

C. What is the nature of the electrochemical reactions at liquid metal/calcium-fluoride based slag interfaces?

The experimental programme designed to answer these questions consisted of two areas of work, and these are:

A. The investigation of metal/slag interfaces polarized at realistic current densities.

B. The production of ESR ingot from pure metals and alloys using various modes of power under controlled atmosphere and slag chemistry conditions.

CHAPTER 2

SMALL SCALE STUDIES

2.1 Experimental considerations

As was outlined in the preceeding section, one experimental objective was the study of electrochemical phenomena occurring on metal electrodes in CaF_2 slags. As will be shown later, for experimental reasons, cylindrical electrodes were used in these studies and it was therefore necessary to consider the effect of cylindrical geometry on diffusional process occurring in the slag. The diffusion problem can be treated in terms of two variables, the distance r from the cylinder axis and time elapsed from the beginning of electrolysis. The flux through a cylinder of radius (r + dr):

$$q(r,t) + [\partial q(r,t)/\partial r] \cdot dr \qquad (2\text{-}1)$$

The change in concentration of the substance being reduced at the electrode is, in a shell of thickness dr per unit time:

$$\frac{\partial C_o(r,t)}{\partial t} = \frac{2\pi (r + dr)q(r + dr,t) - 2\pi r\, q(r,t)}{2\pi r dr} \qquad (2\text{-}2)$$

The cylinder surface area is $2\pi r$ and the cylinder height is one unit of length.

The flux of the diffusing substance through the surface of a cylinder of radius r is proportional to the concentration gradient. Thus

$$q(r,t) = D_o \frac{\partial C_o(r,t)}{\partial r} \qquad (2\text{-}3)$$

By combining (2-2) and (2-3) one obtains:

$$\frac{\partial C_o(r,t)}{\partial t} = D_o \cdot \left[\frac{\partial^2 C_o(r,t)}{\partial r^2} + \frac{1}{r} \frac{\partial C_o(r,t)}{\partial r} \right] \qquad (2\text{-}4)$$

Equation (2-4) will be solved for the case in which the substance is reduced at the electrode surface as soon as it reaches it. The boundary and initial conditions are as follows:

$$C_o(r_o,t) = 0$$

where r_o is the cylinder radius.

$$C_o(r_o,o) = C^o$$

$$C_o(r,t) = C^o \text{ for } r \to \infty$$

Integration of equation (2-4) is rather complicated and only the expansion for the current density will be presented in terms of expanded Bessel functions:

$$i = nFAD_o C^o \frac{1}{r_o} \left[\frac{1}{\pi^{\frac{1}{2}} \phi^{\frac{1}{2}}} + \frac{1}{2} - \frac{1}{4} \left(\frac{\phi}{\pi}\right)^{\frac{1}{2}} + \frac{1}{8} \phi \ . \ . \ . \right] \qquad (2\text{-}5)$$

where ϕ represents the dimensionless group $D_o t/r_o^2$. When ϕ is sufficiently small, all but the first term in the bracket in equation (2-5) vanish, and the current is the same as for linear diffusion. This will be so when the quantity $1/(\pi^{\frac{1}{2}}\phi^{\frac{1}{2}})$ is smaller than 0.01. The electrodes used in the small scale studies had $r_o = 0.363$ cm. and for an average diffusion coefficient $D_o = 10^{-4}$ cm.^{2} sec.$^{-1}$ in CaF_2 slags, a maximum value of t can be calculated below which the current will be the same as for linear diffusion ($\phi = 0.01$).

$$\phi = \frac{D_o t}{r_o^2}$$

$$\text{so} \quad t = \frac{\phi r_o^2}{D_o}$$

$$= \frac{10^{-2} \times 1.32 \times 10^{-1}}{10^{-4}}$$

so t = 13.2 seconds.

Therefore, if electrolysis times less than ~10 seconds are used with the electrodes considered, conditions of linear diffusion can be applied to subsequent analysis.

Galvanostatic pulsing. The technique of galvanostatic pulsing was used in the small scale electrochemical studies rather than a potentiostatic technique because of the design aspects of the electrochemical cell. The reference electrode was well removed from the working electrode and the potential difference produced by the cell resistance when current flowed was significant, and occasionally as large as the measured overvoltage. It was therefore necessary that, for a given slag composition at a given current density, the iR product remain constant which is the case with a galvanostatic technique. When using a potentiostatic technique, the iR product would decrease continuously as the working electrode polarized and reliable overvoltage values would be difficult to obtain.

2.2 Small scale polarization apparatus

The apparatus used in these experiments evolved through a series of designs in which many problems were encountered. The aim of the experiments was to study metal/slag interfaces at high temperatures and high current densities. The slags of interest are very corrosive to most high temperature structural materials. The crucibles were machined from graphite, and lined with molybdenum foil to avoid carbon contamination of the slag. A disc of molybdenum, 0.25 in. thick, was placed in the bottom of the crucible to prevent molten metal which had fallen from the electrode corroding the graphite crucible and therefore exposing the slag to graphite. Since there is no material known that will hold liquid iron and calcium fluoride slags isothermally, it was necessary to hang the working electrode from above so that it was in contact only with the slag. The entire assembly was enclosed in a silica tube thermally insulated with carbon felt and purged with argon. Induction heating was used in spite of its drawbacks in giving rise to electrical noise. It was attempted at all times to keep the temperature of the slag below the melting point of the electrode material to ensure that the electrode tip did not change shape and therefore surface area. It was also necessary to use only slags forming a primary phase with a lower melting point than the electrode material. This restriction arose through the formation of slag skins on the electrode tip which could not be removed without completely melting the electrode tip. We have therefore had to confine all our studies to slags with CaF_2 as the primary phase. The

graphite crucible acted as the counter electrode and was supported on a graphite pedastal mounted on the water cooled bottom plate of the furnace assembly. The top plate on the silica tube was water cooled and it served to suspend the working electrode, the slag thermocouple and the reference electrode. The reference electrode was a short graphite rod encased in a closed end boron-nitride sleeve and supported by a single bore alumina tube. A small hole was drilled in the side of the boron-nitride tube to expose an area of the graphite to the slag to act as the reference electrode. A molybdenum wire was used as the electrical contact to the graphite. Before initiating the galvanostatic pulse, the reference electrode was anodically polarized and the reference potential was established by the reaction:

$$C_{gr} + O^{2-} \rightleftarrows CO_g + 2e^- \qquad (2\text{-}6)$$

Reference electrodes of similar design have been used in cryolite systems, and were found to behave reversibly (15, 15a). Ideally a reference electrode should be isolated from the system by an ionic membrane such as a boron-nitride filament carrying slag to act as a salt bridge, but due to the dimensional limitations of our system this was not feasible and the absolute reference electrode potential therefore contains an inherent variation due to the oxide-ion activity variations in the slags used.

However, these variations would be small (~30 mv between CaF_2 + 0.5 wt. % Al_2O_3 and 8 wt. % Al_2O_3) compared with the experimental error in individual measurements. In no case did we find that the potential between the reference electrode and the unpolarized iron

electrode was outside the range 80 - 110 mv.

Finally, the nature of the high current density experiments dictates that a transient method must be used to avoid gross chemical and thermal changes in the system. The method used was that of galvanostatic pulsing, essentially as used by Gosh and King (16), and as outlined theoretically by Delahay (17). Since we wanted to investigate high current densities we could not use the more usual methods of fast-rise time constant-current pulsing, and instead used constant-current generators (Hewlett-Packard Models 6269A and 6203B). These have rise times well within the polarization times we investigated, except at very high currents (~20 A), and in these regions we used the voltage decay rather than rise, measurements. At the higher current densities (> 5 A. $cm.^{-2}$), we would expect to find a significant effect of the electrical field superimposed on the chemical diffusion gradient. Hence in these regions also we have used the voltage decay measurements. The voltage-time transients were recorded on a Tektronics storage oscilloscope model 564 B calibrated against a Kiethly Model 153 electrometric potentiometer. The apparatus is shown in Figures 1, 2, and 3.

All the slags used in these small scale studies were prepared by mixing weighed quantities of prefused calcium fluoride (British Drug House "extra pure") with the required oxide additions of alumina (Norton fused alumina) or recrystallized calcium oxide. The calcium fluoride was prefused under argon in the experimental apparatus. The mixed dry slag was then fused in the apparatus at a high temperature to ensure complete solution of the oxide. The slag temperature was then lowered to the working temperature which was always 20 to 30°C lower than the

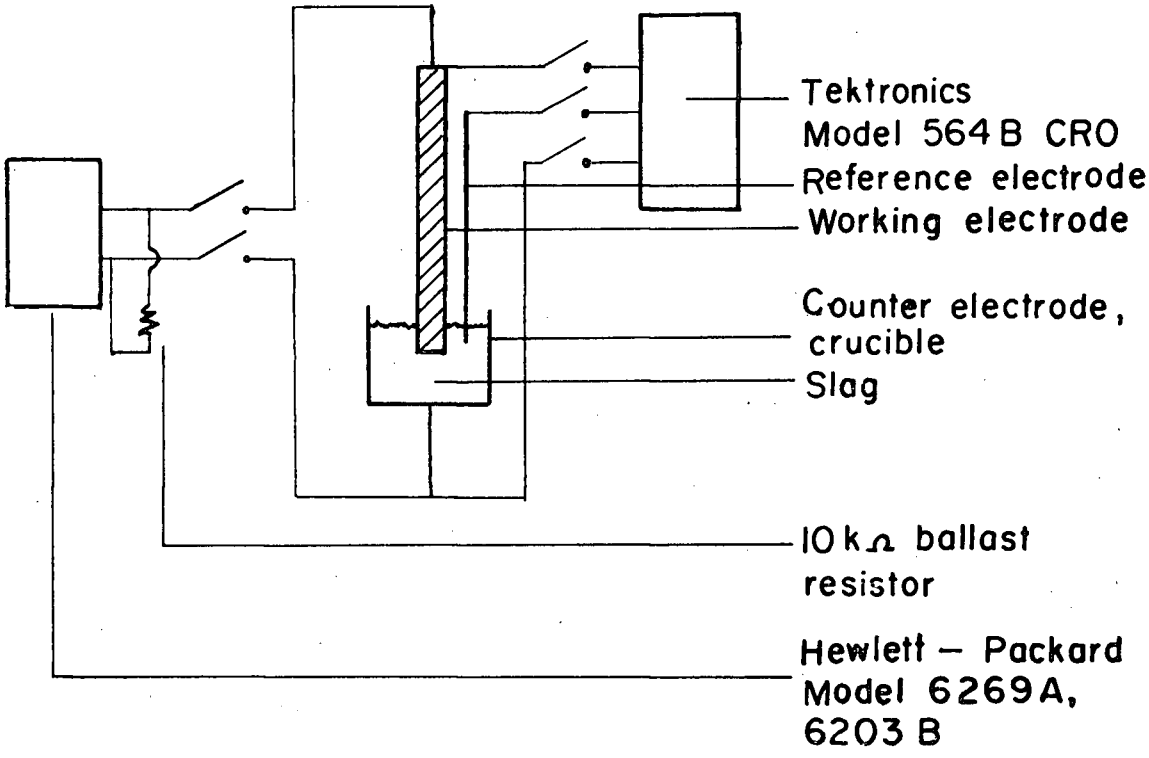

Figure 1. Cell electrical circuitry.

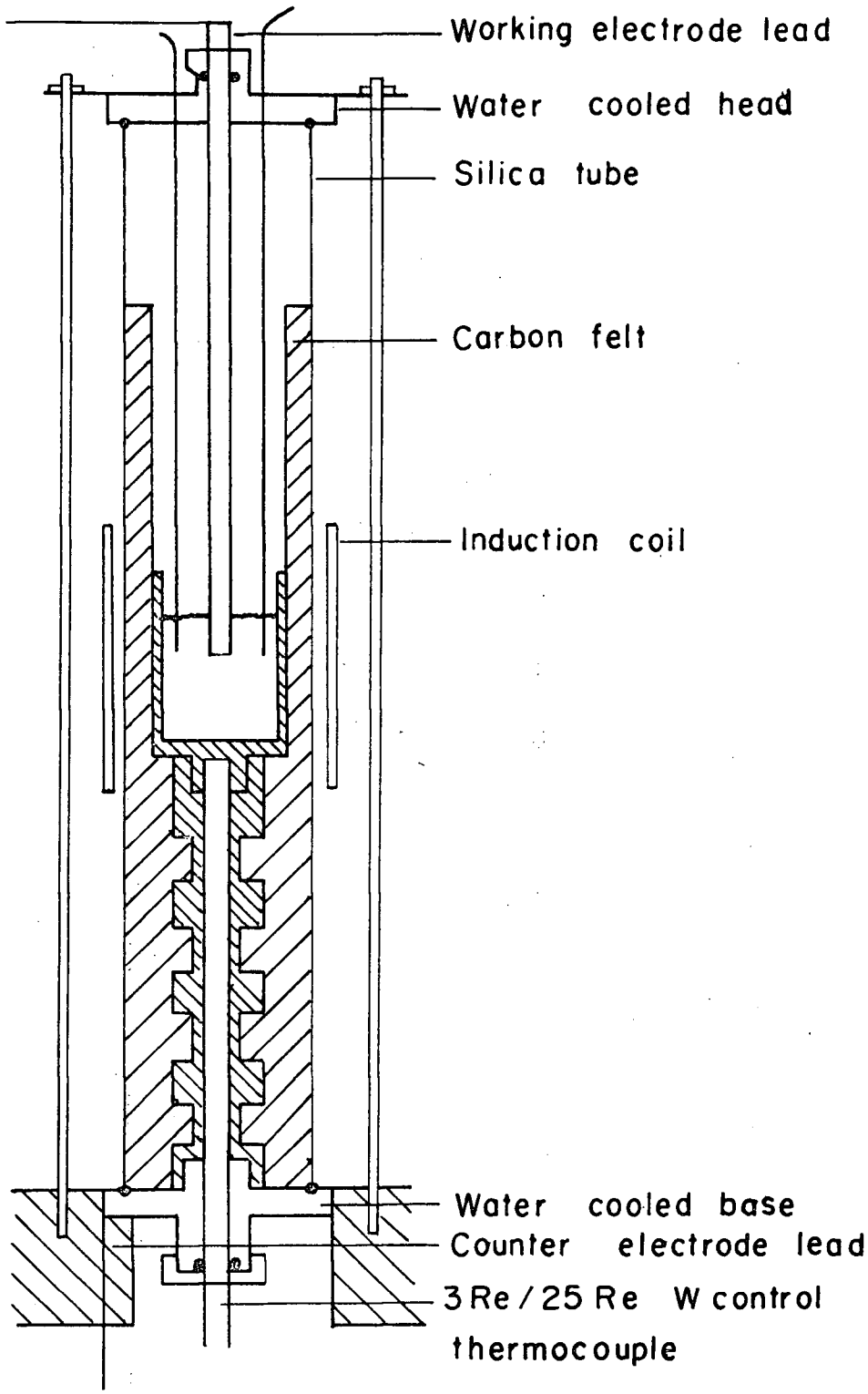

Figure 2. General cell design.

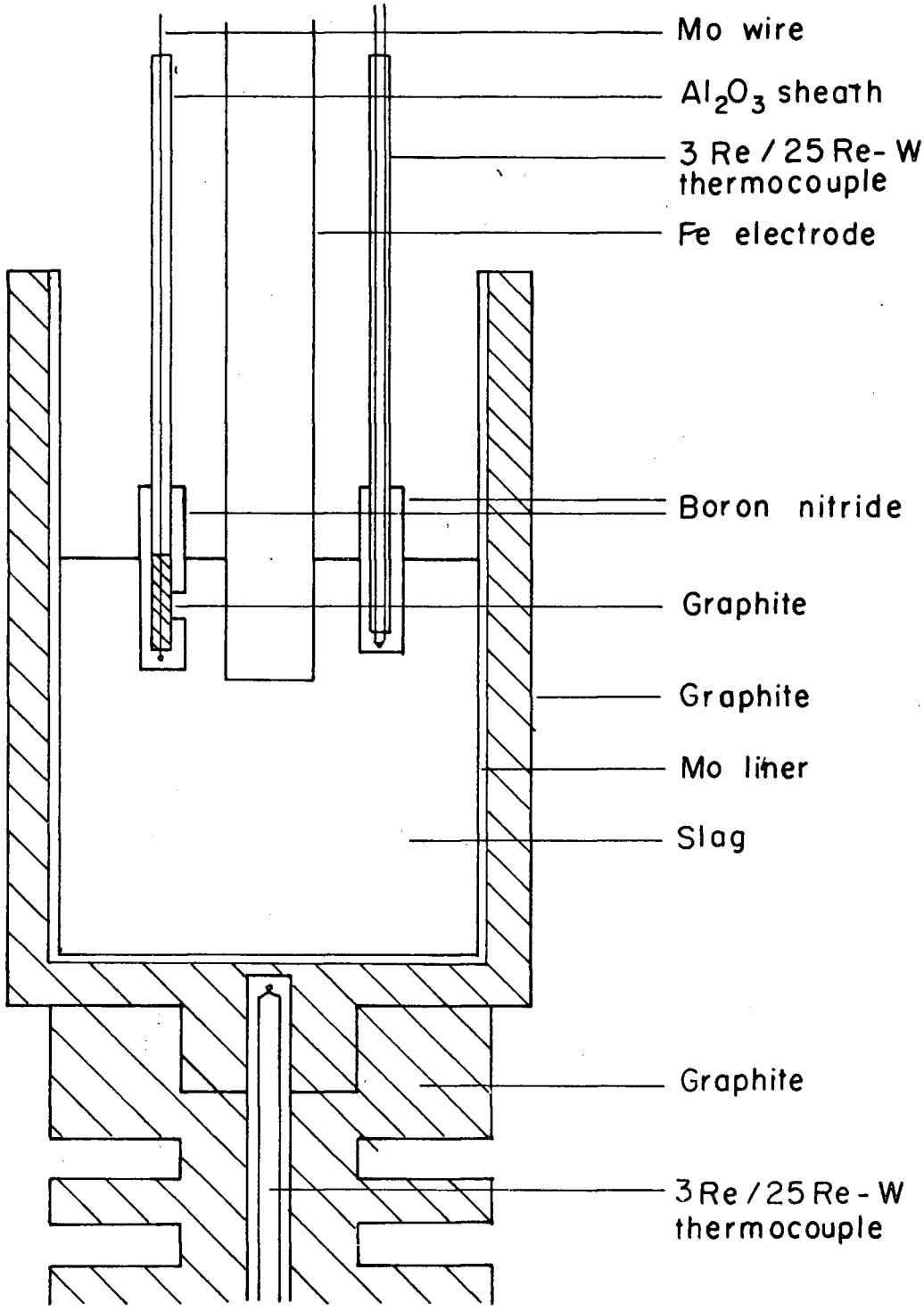

Figure 3. Detail of cell assembly.

melting temperature of the electrode material being studied. When the temperature was stable, the working electrode was lowered slowly towards the slag until initial electrical contact was made in the current supply circuit. This position was taken as a zero point and the electrode was then lowered a predetermined distance (normally 1.0 cm.) into the slag to present a known surface contact area between the electrode and the slag. The temperature of the system was measured and controlled by two separate W3Re/W25Re thermocouples.

At this point, the reference electrode potential was measured with respect to the working electrode, and established to be stable and within the range 80 - 110 mv. It was found that a stable reference electrode potential could be achieved much more quickly by passing a low current (100 ma. for 10 sec.) between the two electrodes with the reference electrode being anodic. Once the system was stable, the induction generator was switched off, and the current was completed between the counter electrode (crucible) and the working electrode at a pre-determined constant current setting. The voltage rise between the reference and working electrodes was traced on the oscilloscope and followed to its constant value, usually established in less than 10 sec., and also followed as it decayed when the current supply was stopped. A typical low current test oscilloscope trace is shown in Fig. 4. This shows the gradual buildup of potential difference between the two electrodes. The schematic below the oscilloscope picture shows the method of obtaining the overpotential from the trace. The iR potential drop between the two electrodes is established very quickly and is not traced

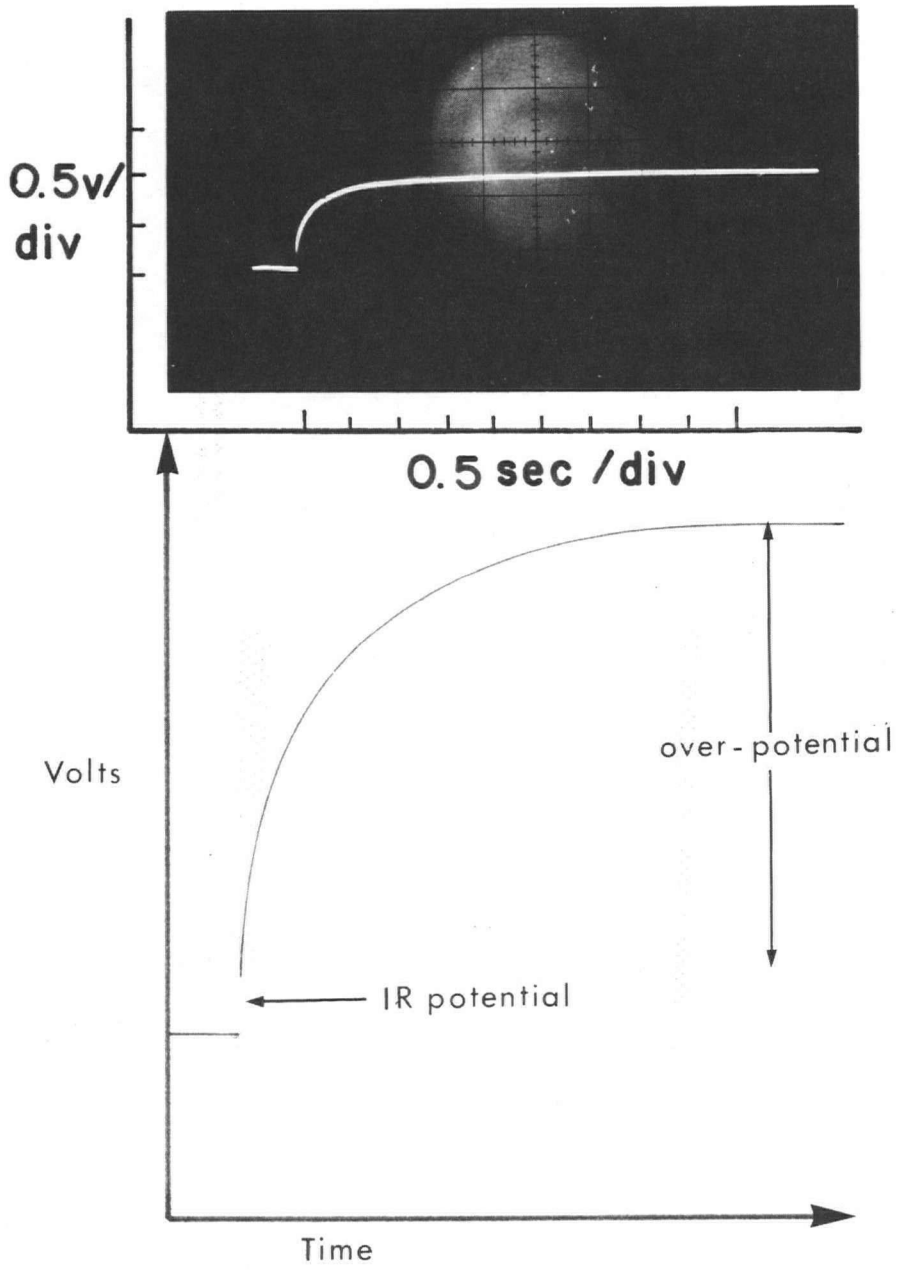

Figure 4. Method of obtaining overvoltage.

on the screen. The total charge passed through the system during one such test is small as are the bulk chemical changes so produced. Approximately 5 minutes was allowed between tests to allow the working electrode to re-equilibrate with the liquid slag as the slag was slowly brought back up to temperature. By testing at increased applied currents each time, the polarization of a given electrode material in a given slag can be plotted against the current density to give a galvanostatic polarization curve.

It was found that the largest part of the experimental error arose from the difficulty of defining a precise and constant electroactive surface area on the working electrode. The immersion of the electrode was known but chemical reactions at the interface gave rise to changes in interfacial tension which when combined with overheating and partial melting of the electrode tip resulted in a change in the electrode shape. The second major source of experimental error lies in the nature of the polarization. As will be shown later, this is a concentration effect, and is therefore modified by both electrical and liquid-shear fields. Any error arising from electrical effects was eliminated by using decay measurements, but the thermal effects producing convection are unknown and cannot be stabilized in this type of apparatus. The degree of temperature control in the system was considered to be $\pm$ 5°C and it was decided that errors arising from intrinsic thermal effects were small in comparison to the others.

2.3 Electrode materials

2.3.1 Ferrovac-E pure iron

The Ferrovac-E pure iron electrodes were made by machining the 1.25 in. diameter bar down to 0.50 in. diameter stock and then swaging this down to 0.285 in. in diameter. This rod was then cut to 4 in. lengths and a female thread machined on one end for attachment to the electrode holder.

2.3.2 AlSl 430 stainless steel

This material was found to be unsuitable for swaging in the as received condition, therefore these electrodes were machined directly from the 1.0 in. diameter bar.

2.3.3 Fe-1.0 wt. % Cr alloy

This alloy was produced by melting a piece of Ferrovac-E together with a piece of AlSl 410 stainless steel to produce a final alloy of 1 wt. % Cr in iron. The melt was deoxidized with aluminum wire prior to solidification. The solid slug was then welded to a piece of mild steel rod, 0.75 in. in diameter, machined down to the diameter of the rod, and then swaged down to the desired diameter of 0.285 in.

2.3.4 Pure chromium

This material was made by hot extrusion of steel clad chromium metal. The purpose of the cladding was to prevent excessive oxidation

of the chromium during the hot working stage. After extrusion, the cladding was dissolved in acid. The material had an irregular surface but because of its brittleness, machining was not attempted, and it was used in the as received condition by silver soldering it to a threaded mild steel stub.

2.3.5 Pure nickel

These electrodes were made by swaging the as received 0.375" dia. nickel rod down to the desired size, and then cutting to the appropriate length.

2.3.6 Pure Cobalt

Because of the difficulty in obtaining pure cobalt in the appropriate size range, this electrode was made from a deformed single crystal of cobalt which had a slightly irregular surface. The single crystal was silver-soldered into a threaded mild steel stub.

2.3.7 Iron-carbon alloy

These electrode materials were supplied by the Babcock and Wilcox Company. They were machined to the correct size when received and had only to be threaded before use. Only one experiment was carried out with this material, the purpose of which was to see if an anodic iron-carbon alloy would experience carbon loss. Carbon analyses was carried out on the tip after electrolysis had been completed.

2.4 Electroslag remelting polarization experiments

It was thought that it would be meaningful to measure the degree of polarization of an electrode during electroslag remelting in order to correlate the small scale experiments with the conditions existing during actual remelting. These experiments were carried out with Armco iron electrodes, and reference electrodes of the same design as used in the small scale studies. As shown in Figures 5 and 6, the reference electrode was attached to the electrode by means of iron wire and mullite spacers, such that it entered the slag after steady-state melting had taken place for approximately 30 minutes. When the reference electrode entered the slag (Fig. 6), the process current was switched off and the voltage decay between the reference electrode and the melting electrode was traced on the oscilloscope. An example of this trace is given in Fig. 7. The voltage decay times observed were short compared to the time taken for the slag to solidify in the electrode region, which is approximately one minute. It was essential that the power be interrupted immediately after the reference electrode entered the slag. If this was not the case the physical distance between the reference and melting electrodes was too great and the ohmic potential drop following current interruption exceeded the full scale defection of the oscilloscope. This prevented any measurement of the polarization potential.

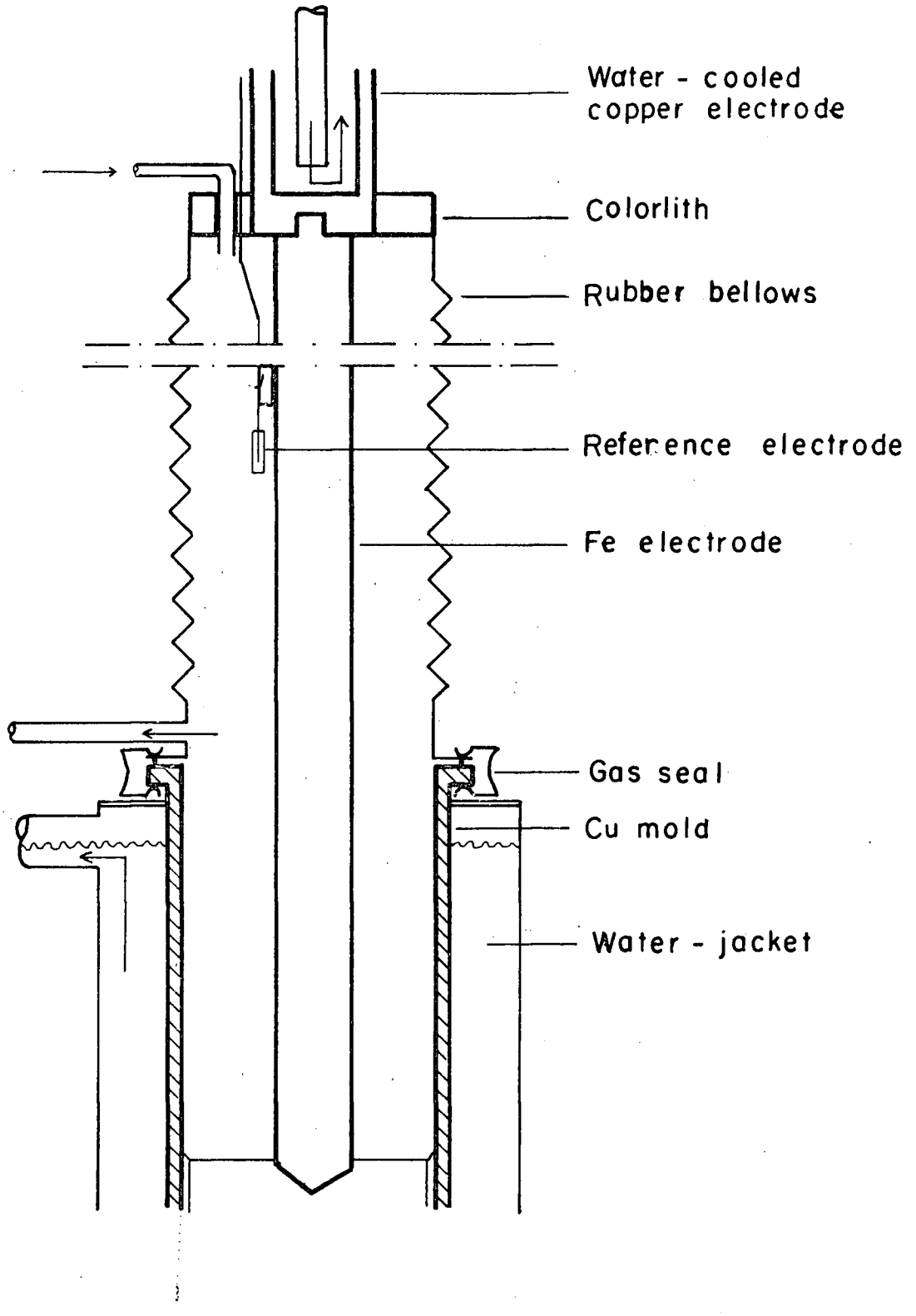

Figure 5. ESR furnace assembly.

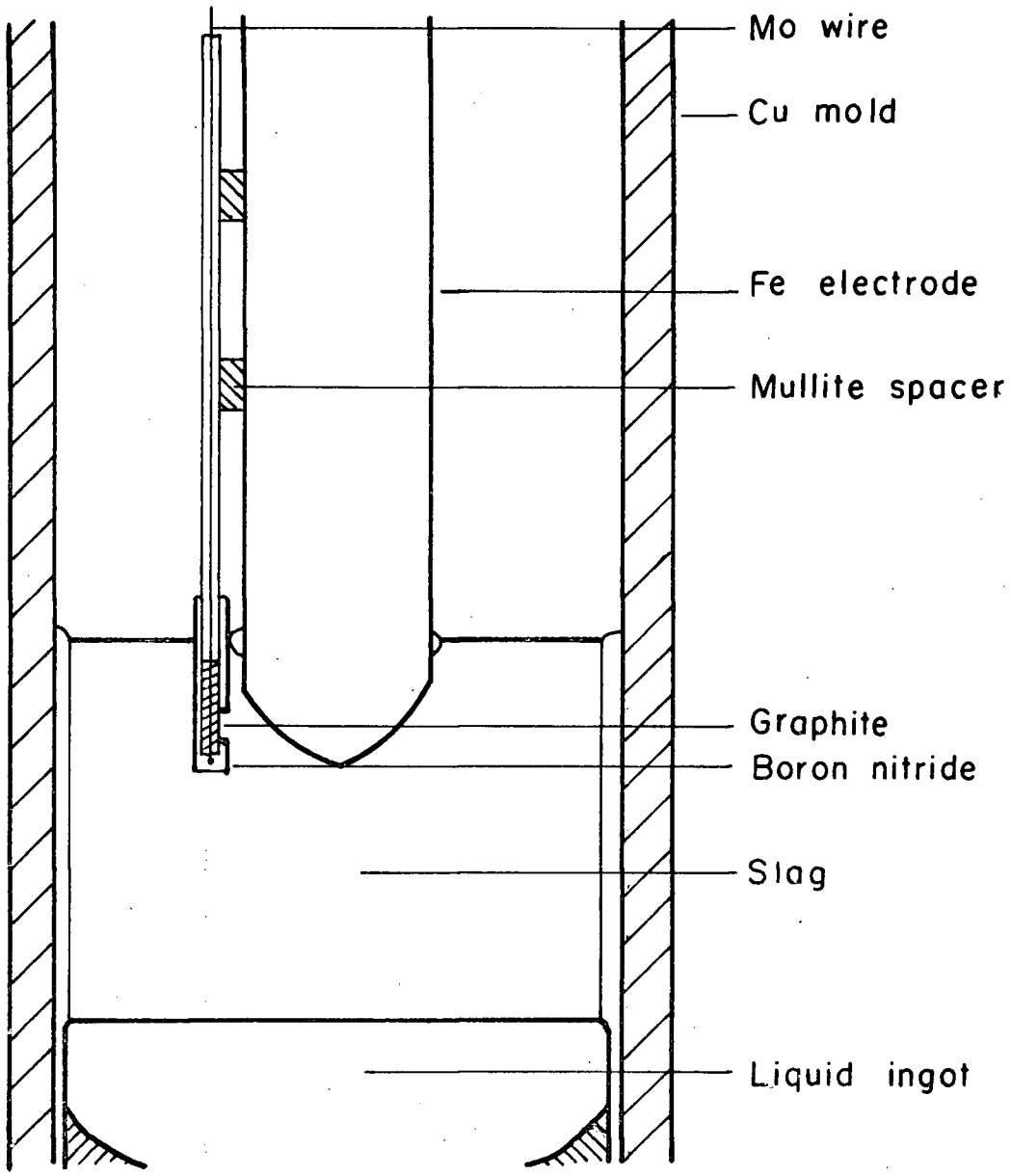

Figure 6. Detail of reference electrode configuration.

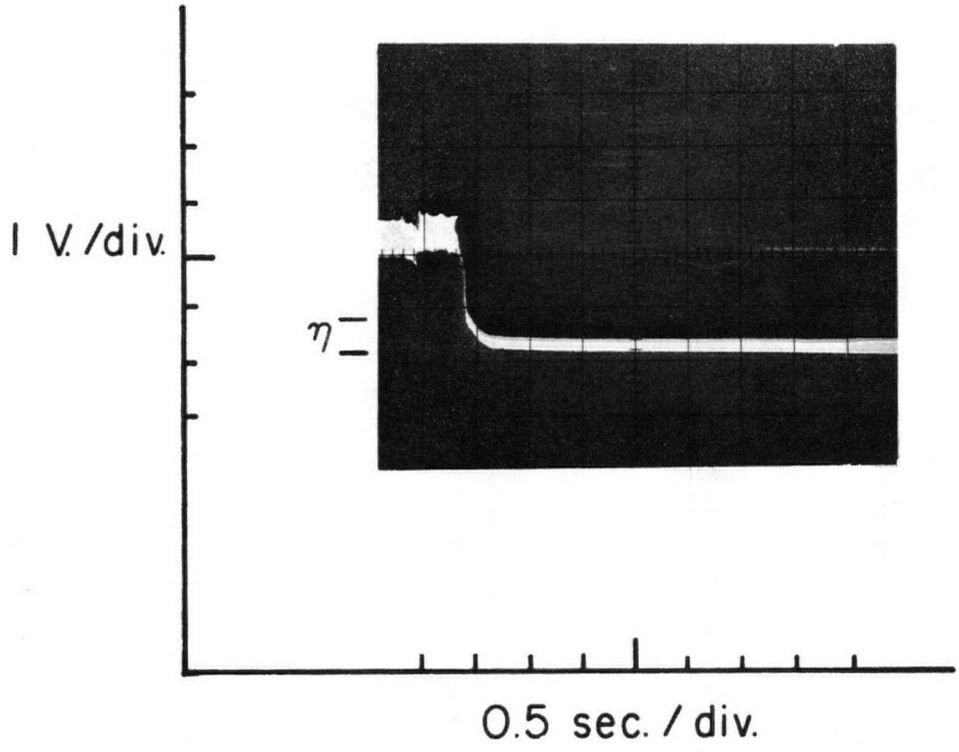

Figure 7. Potential decay between the melting electrode and the reference electrode observed at current interruption on an ESR anodic electrode.

2.5 Polarization results

2.5.1 Ferrovac-E pure iron

The anodic and cathodic polarization curves for Ferrovac-E pure iron electrodes in calcium fluoride-alumina slags and calcium fluoride-calcium oxide slags are given in Figures 8, 9, 10 and 11. In certain slags (5 wt. % Al_2O_3) at certain current densities (1 A. $cm.^{-2}$) anodically polarized Ferrovac-E electrodes exhibited apparent transition times as shown in Fig. 12. This behaviour was not observed during cathodic polarization of the same electrode material.

The usual electrode current density during melting in the electroslag unit is much higher than the current densities normally applied during the small scale tests. It was therefore thought to be useful to carry out small scale tests at normal remelting current densities. This was done for both anodic and cathodic Ferrovac-E electrodes in a CaF_2 + 5 wt. % Al_2O_3 slag using a bank of 12 volt lead-acid storage batteries to produce current densities up to several hundred A. $cm.^{-2}$. The results of this work are given in Fig. 13. At these high current densities the electrode melted to some extent during each test due to localized heat production at the interface as well as resistance heating of the slag. These results, although quite inaccurate, appear to agree well with the lower current density results in the same slag. It was noted that, at current densities above points X in Fig. 13, an arc was established at the electrode. This was seen as a sudden increase in radiation when the test current was passed through the cell, and was

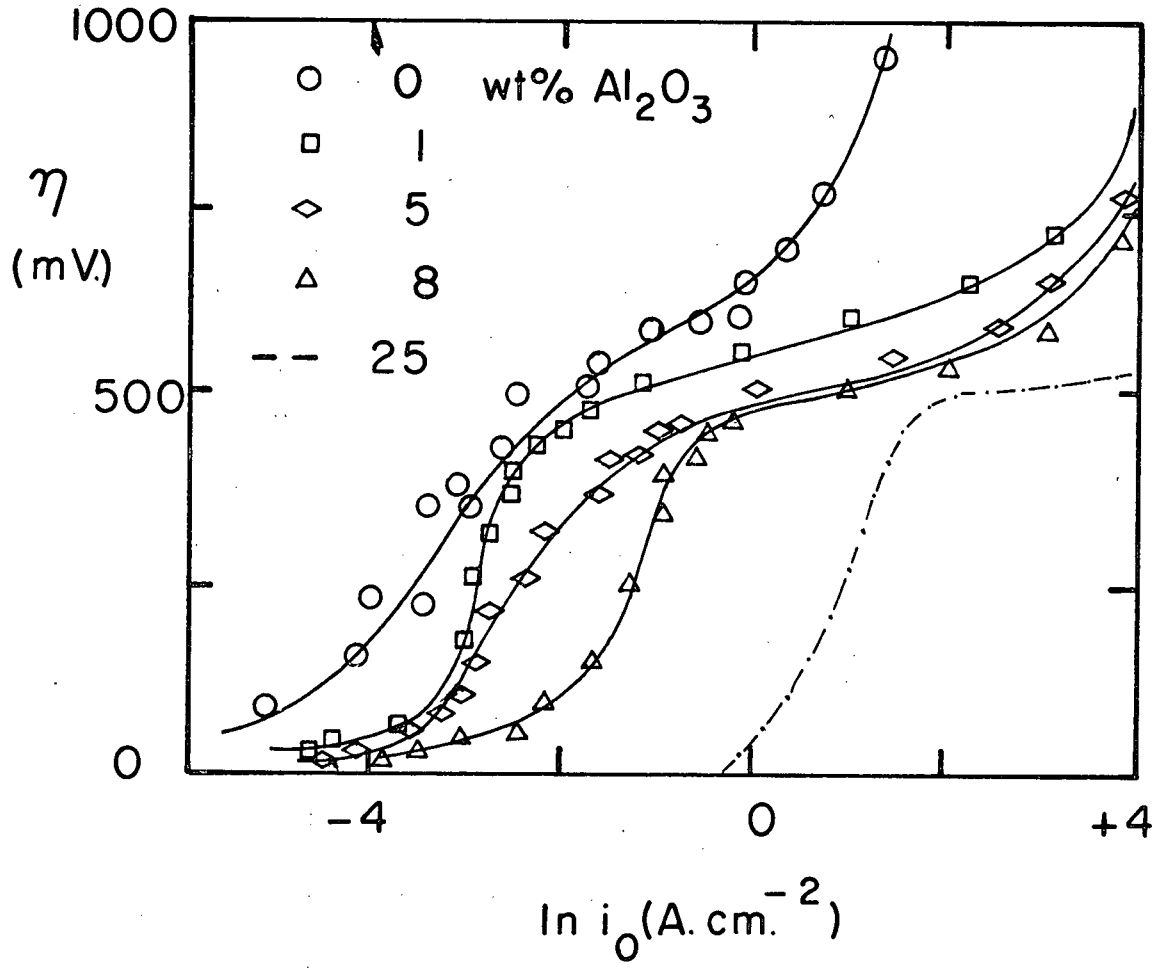

Figure 8. Anodic polarization curves for pure iron in CaF_2 + Al_2O_3 slags.

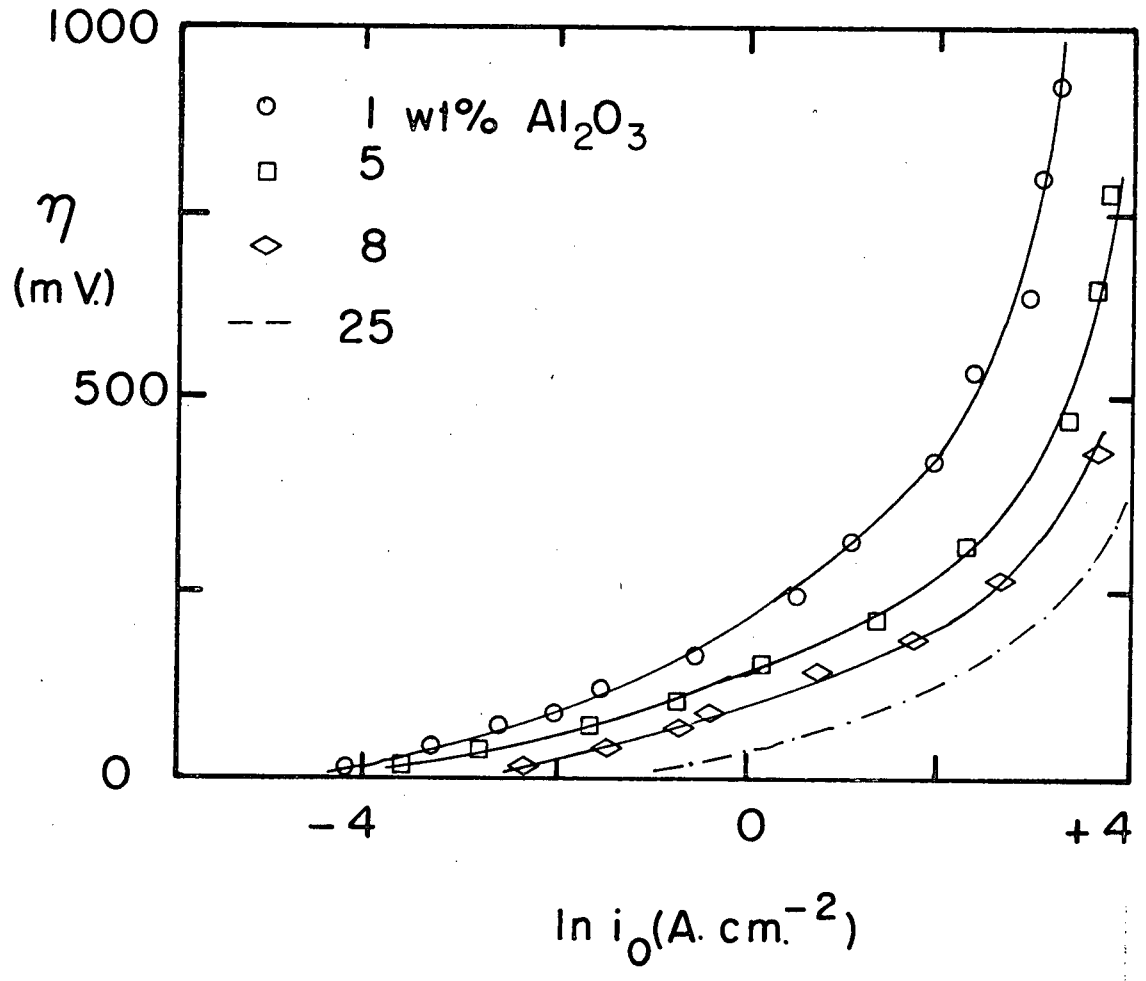

Figure 9. Cathodic polarization curves for pure iron in $CaF_2 + Al_2O_3$ slags.

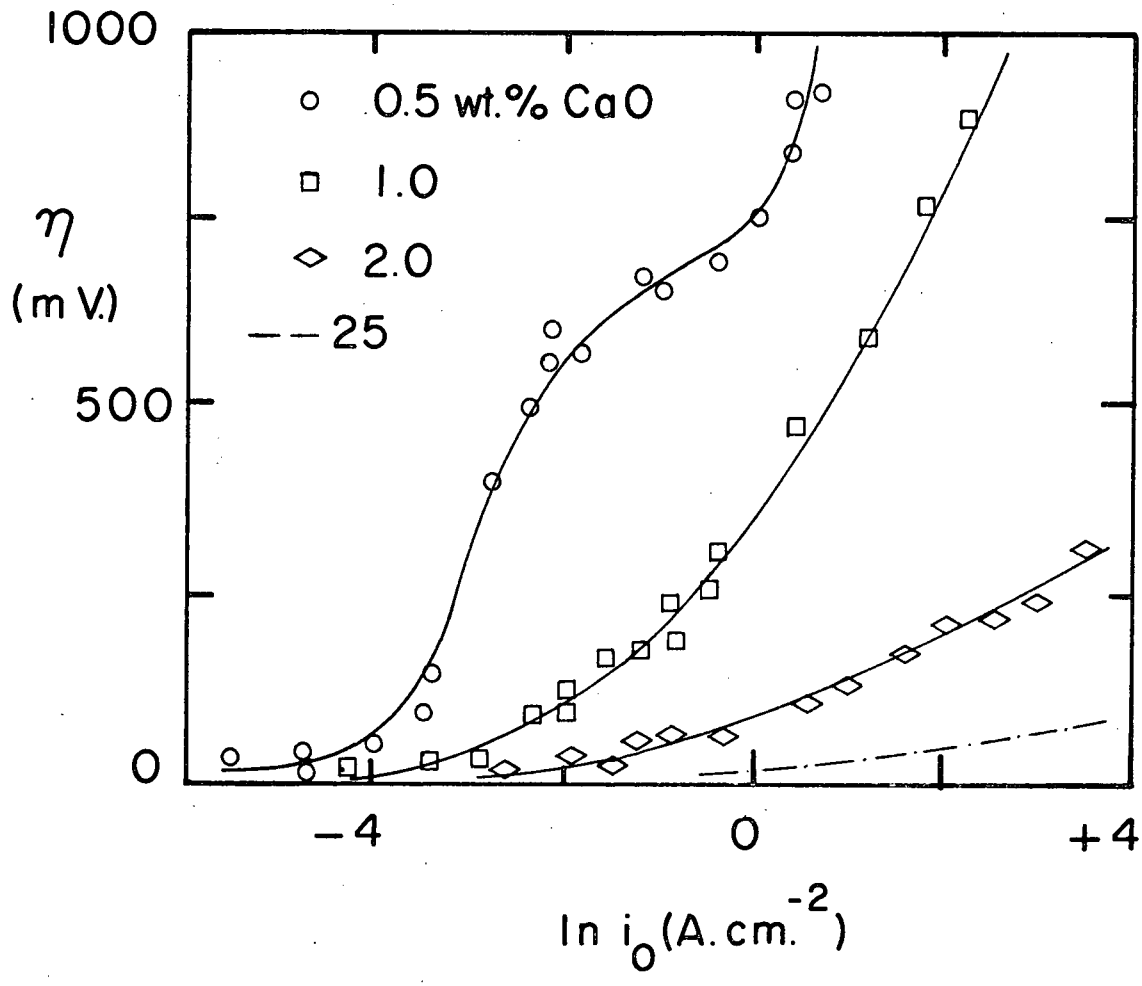

Figure 10. Anodic polarization curves for pure iron in CaF_2 + CaO slags.

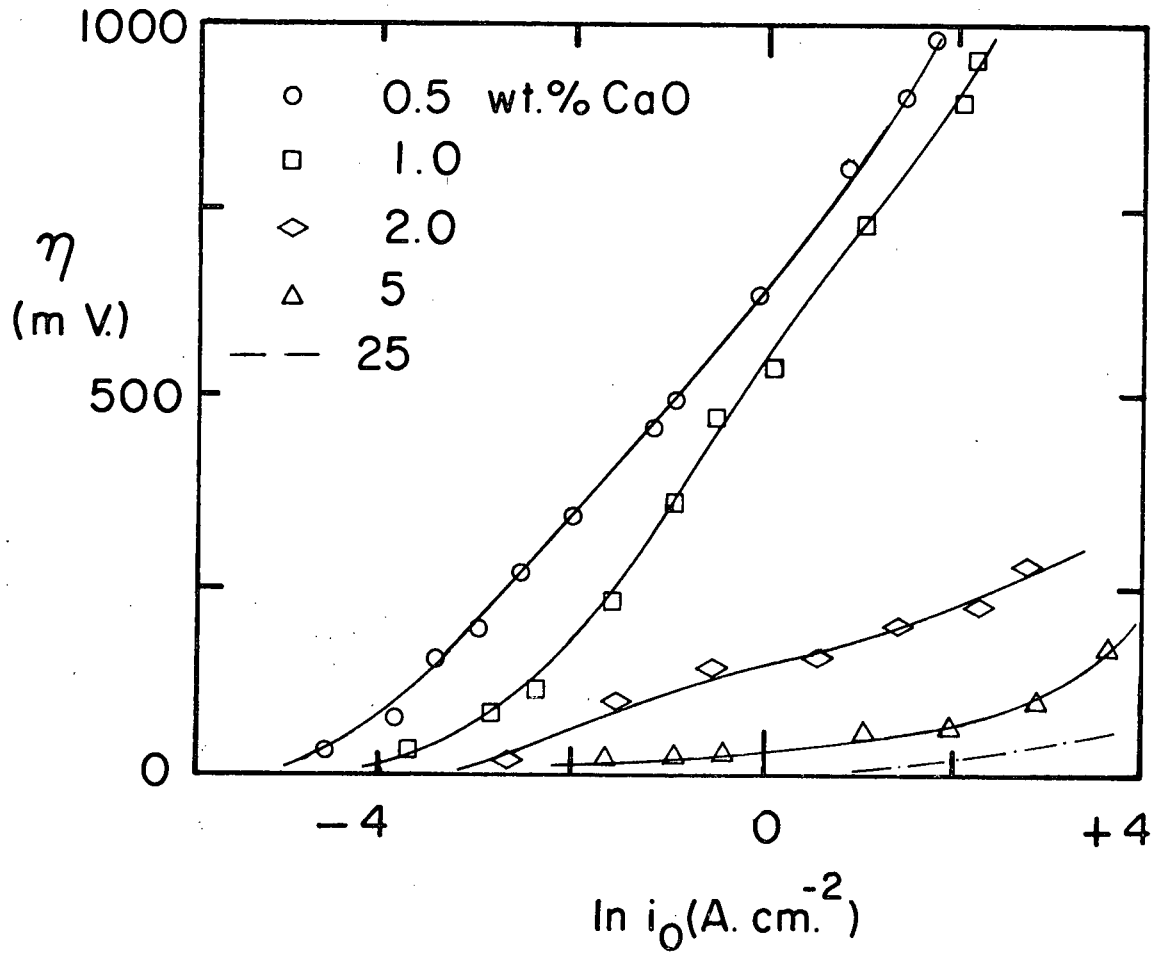

Figure 11. Cathodic polarization curves for pure iron in CaF_2 + CaO slags.

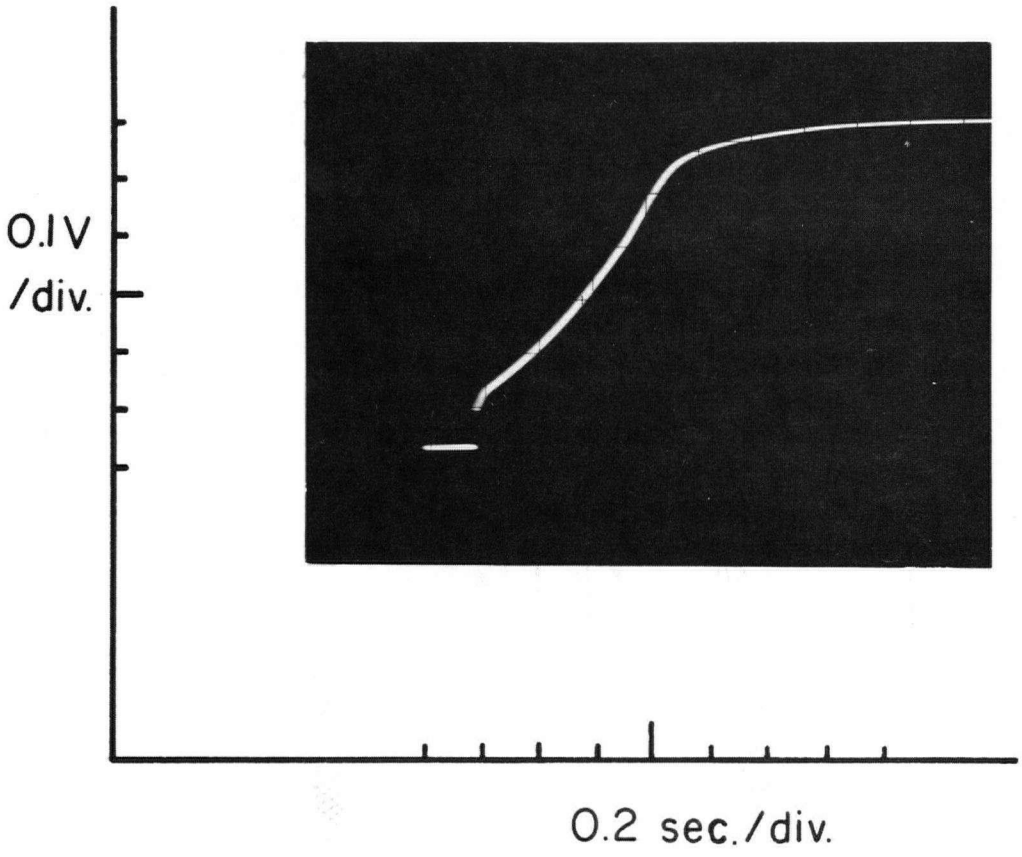

Figure 12. Apparent transition time in the anodic polarization of pure iron in CaF_2 + 5 wt.% Al_2O_3, at i_o = 1 $A.cm^{-2}$.

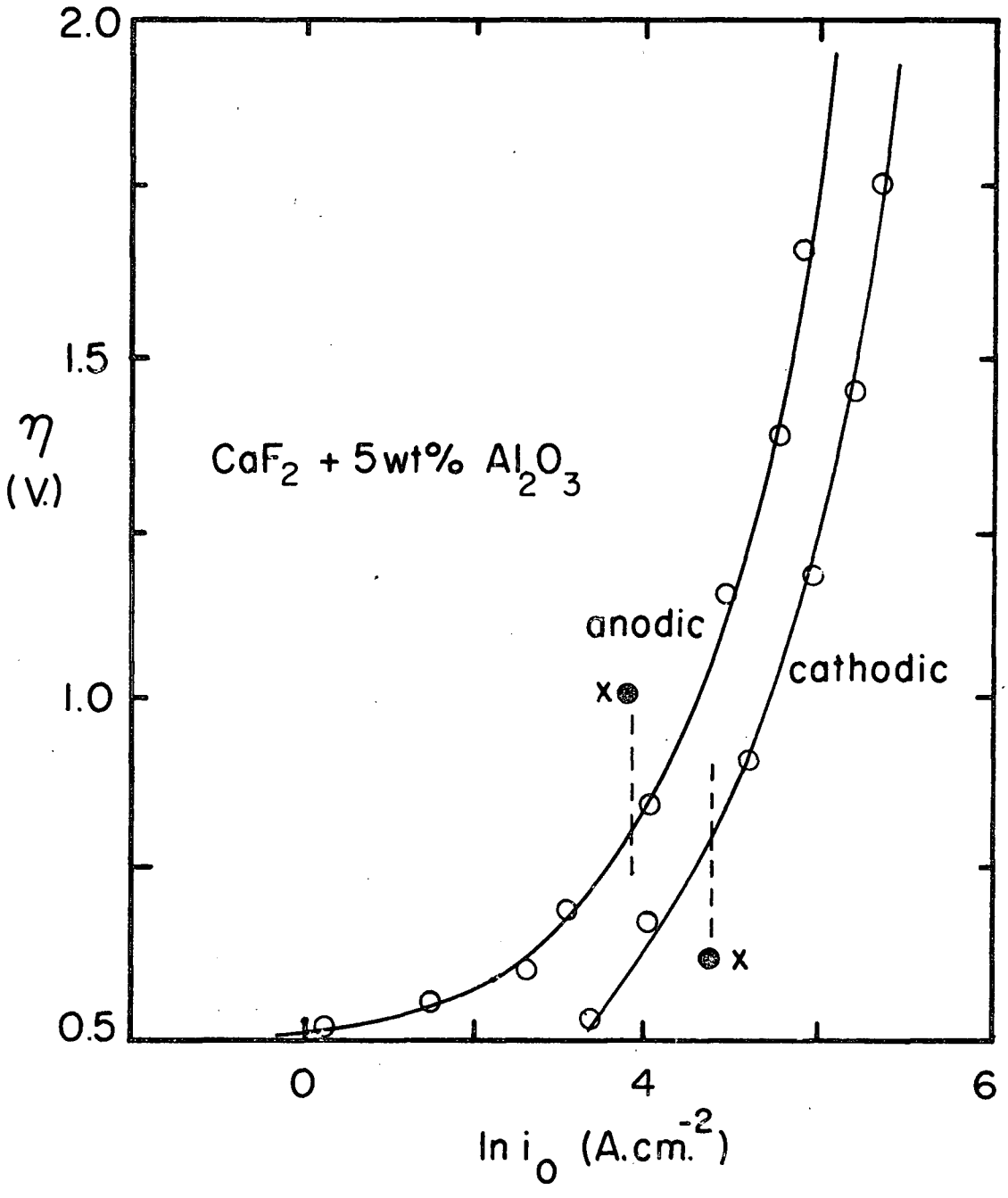

Figure 13, High current density polarization curves for pure iron in CaF_2 + 5 wt.% Al_2O_3. Points X indicate the onset of visible arcing.

often accompanied by excessive electrode melting.

In this small scale work on CaF_2 + Al_2O_3 slags, no work was carried out successfully at Al_2O_3 concentrations greater than 10 wt. %, which is the eutectic composition (18). This arises in the fact that pure Al_2O_3 is the primary precipitate upon cooling a hypereutectic composition, and once a layer of Al_2O_3 had been formed on the electrode tip, it could not be removed without completely melting the electrode tip. The large experimental scatter observed in the "pure" CaF_2 measurements in Fig. 8 is probably due to the variable (100 - 500 ppm) CaO content of this material. The data points shown are the average of three separate experiments.

Polarization of Ferrovac-E electrodes in Al_2O_3 slags results in significant concentration changes in the electrode. Fig. 14 shows optical and electronmicroprobe scans of a section through an anodic electrode tip. This initially low oxygen (20 ppm) electrode was polarized at high current density in a CaF_2 + 5 wt. % Al_2O_3 slag for several 10 sec. periods, and then removed from the slag. The optical picture shows the resulting "dirty" microstructure, and the probe pictures show areas of oxygen-containing material, probably iron-oxide. The other half of this tip was analyzed for total oxygen and found to contain 400 ppm.

An equivalent Ferrovac-E electrode was cathodically polarized in a CaF_2 + 8 wt. % Al_2O_3 slag for 1 hour at a current of 1 A. A significant portion of the tip had melted off, but the remaining portion was analyzed for Al on the electron microprobe. The concentration of Al in the matrix was calculated from the probe X-ray intensities using the "MAGIC" computer program, and was found to be 3.0 wt. %. In no case did we detect fluorine or calcium in either electrode tip.

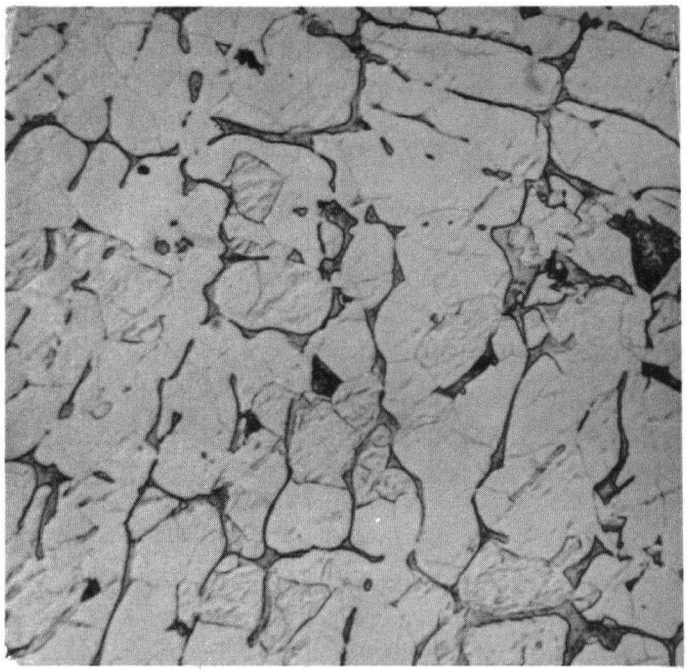

Optical X260

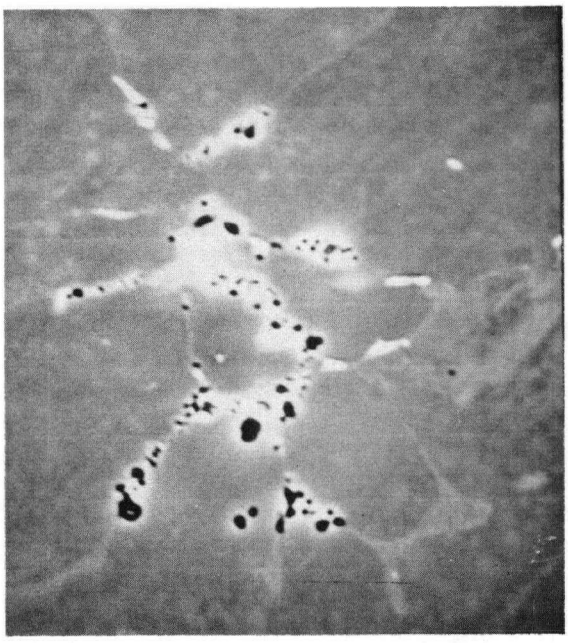

A.E.I. X650

O X-ray X650

Figure 14. Sections through a pure iron electrode tip anodically polarized at high current density for several 10 sec. periods in a CaF_2 + 5 wt.% Al_2O_3 slag.

2.5.2 AISI 430 stainless steel

The polarization curves obtained for AISI 430 stainless steel in CaF_2 + Al_2O_3 slags are given in Figures 15 and 16. In addition to these experiments, one test was carried out for the purpose of studying chromium depletion of the alloy. An electrode was anodically polarized in a CaF_2 + 8 wt. % Al_2O_3 slag at a current of 1 A. for 915 sec. The electrode tip was then cut veritcally for examination on the electron microprobe. A horizontal traverse was made from the outside edge towards the center and Cr counts were taken at 20 μ steps. These X-ray counts were corrected to give wt. % Cr using the "MAGIC" program, and the results are given in Figure 17. This figure shows a diffusion profile in which the Cr concentration falls from the bulk concentration of approximately 17 wt. % Cr, to a value of approximately 9 wt. % at the electrode-slag interface. The purpose of this experiment was to show that easily oxidizable alloying elements can be selectively oxidized at an anodic interface during anodic polarization. The Cr loss so observed indicates a build-up of Cr^{n+} ions in the slag. The current efficiency of Cr removal, assuming Cr goes to Cr^{3+} in the slag, was calculated by assuming the concentration profile in Fig. 17 is linear between 9 wt. % Cr and 17 wt. % Cr at 300μ depth. The total Cr lost during electrolysis is therefore approximately 20 mg. which gives a current efficiency for chromium removal of approximately 10%.

2.5.3 Fe - 1 wt. % Cr alloy

The anodic polarization curves for an Fe + 1 wt. % Cr alloy in

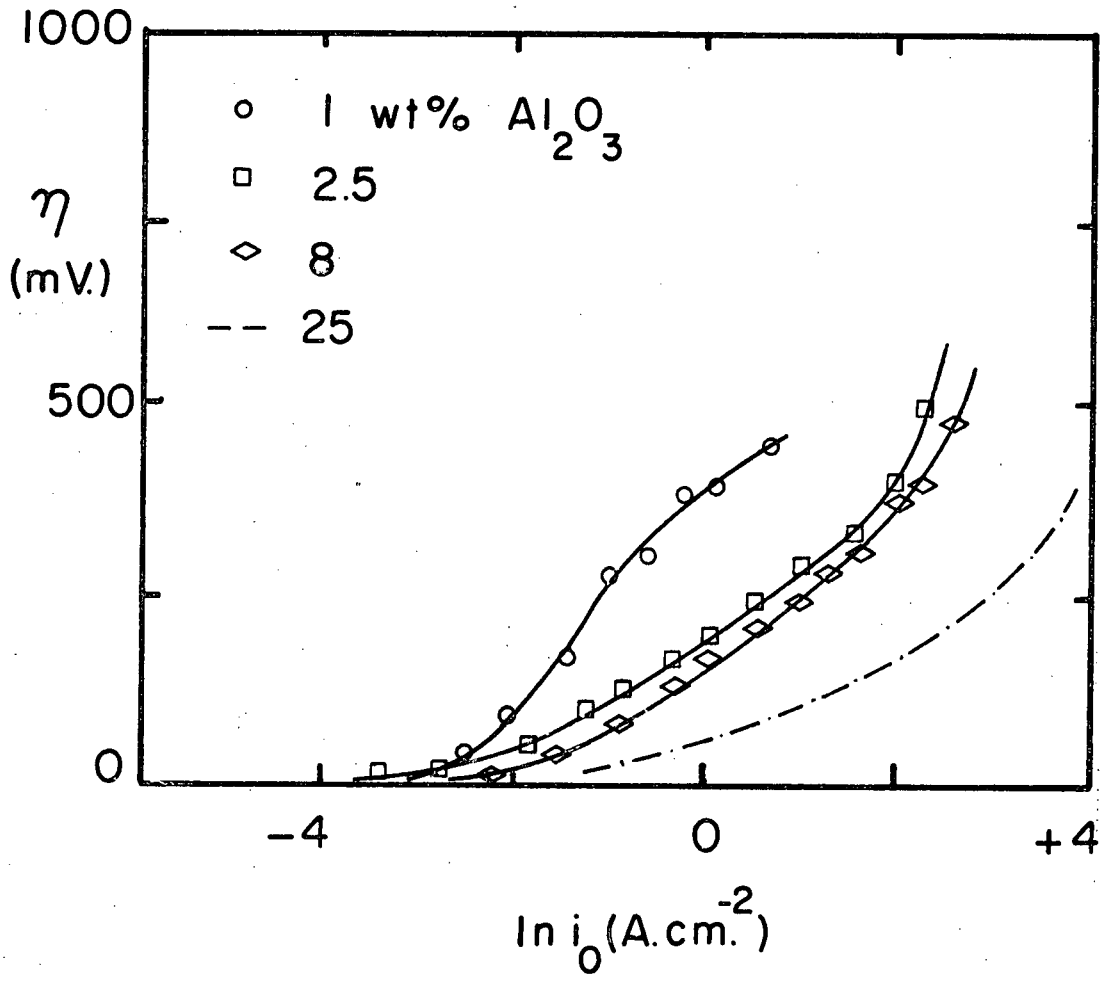

Figure 15. Anodic polarization curves for AISI 430 stainless steel in CaF_2 + Al_2O_3 slags.

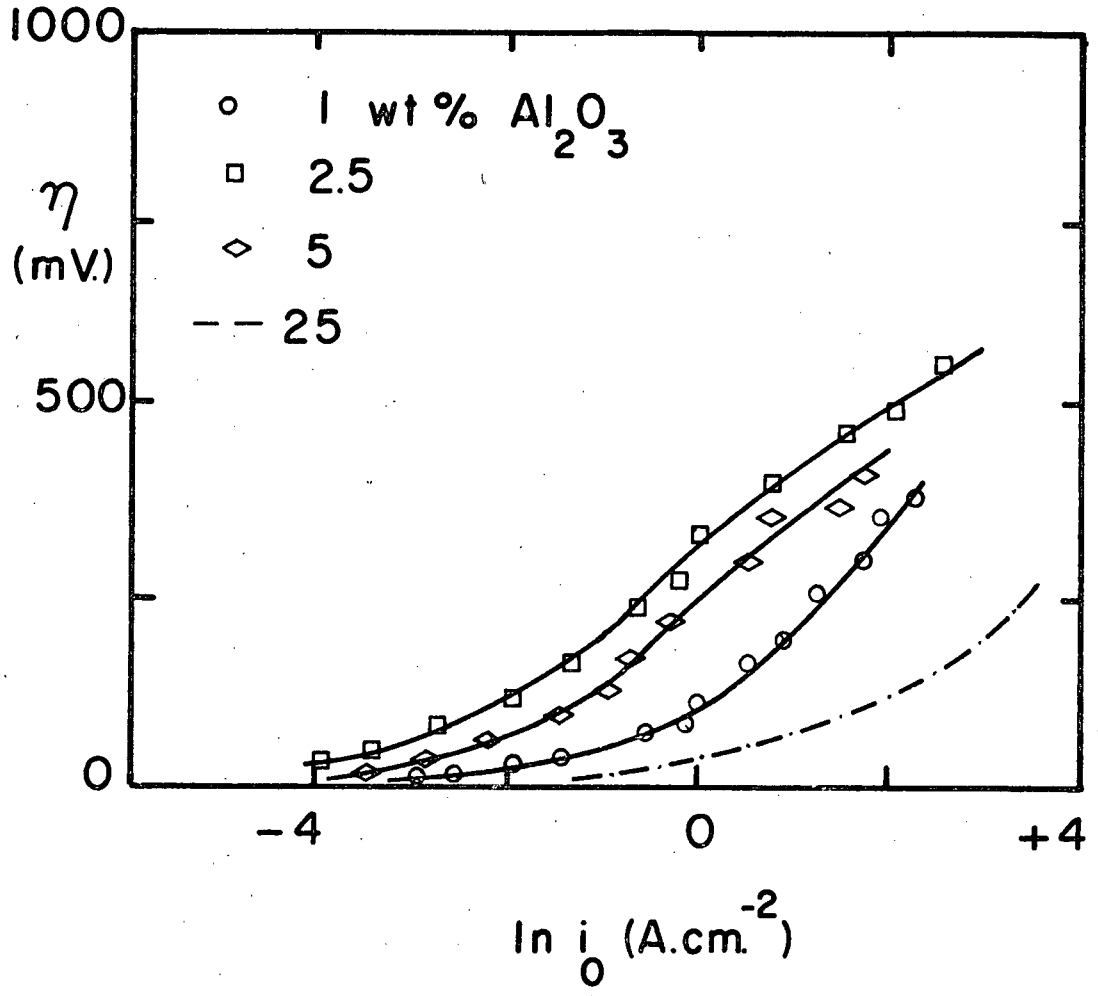

Figure 16. Cathodic polarization curves for AISI 430 stainless steel in CaF_2 + Al_2O_3 slags.

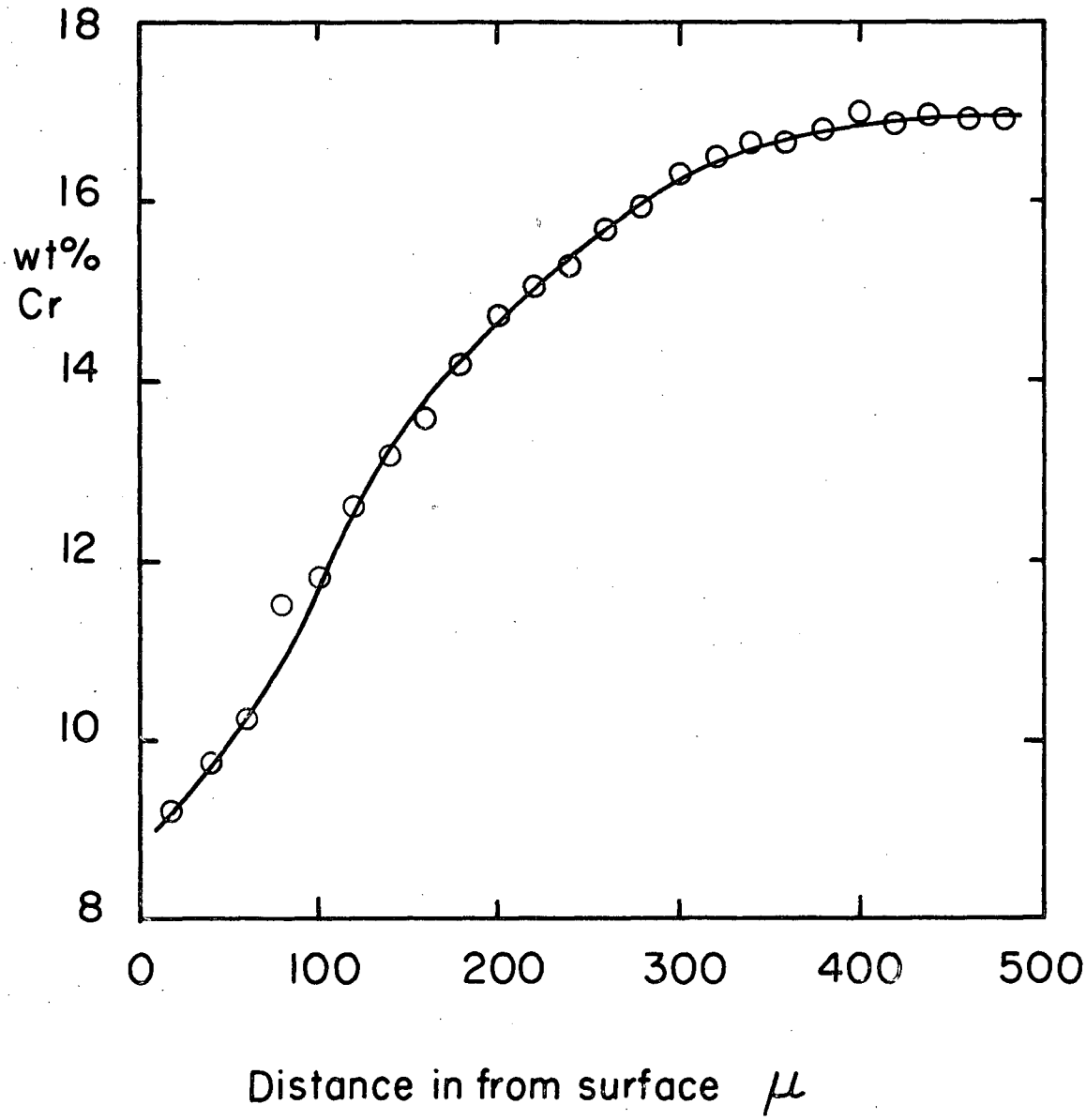

Figure 17. Cr concentration gradient produced at the surface of an AISI 430 stainless steel electrode anodically polarized for 915 sec. at i_o = 360 ma.cm.$^{-2}$ in a CaF_2 + 8 wt.% Al_2O_3 slag.

a CaF_2 + 1 wt. % Al_2O_3 slag are given in Fig. 18. The two curves drawn correspond to the rise overpotential measured when the cell circuit is closed, and the decay overpotential measured on current interruption.

2.5.4 Pure chromium

The anodic polarization curve for a pure Cr electrode in a CaF_2 + 1 wt. % Al_2O_3 slag is shown in Fig. 19.

2.5.5 Pure nickel

A pure nickel electrode was anodically polarized in a CaF_2 + 2.5 wt. % Al_2O_3 in order to establish that its anodic behaviour was similar to that of a pure iron electrode in Al_2O_3 slags. The behaviour of the nickel electrode is shown in Fig. 20. This figure is a picture of the oscilloscope trace at a current of 3 A. A steady state plateau is observed, which is established quickly, and is followed on current interruption by a relatively slower potential decay.

A nickel electrode was cathodically polarized at a current of 1.25 A. for 900 sec. in a CaF_2 + 8 wt. % Al_2O_3 slag, and then sectioned and examined in the electron microprobe for Ca and Al. The appropriate electron microprobe scans are given in Fig. 21. These show a strong con centration of matrix Al and a significant number of Ca containing areas corresponding to the lighter areas on the AEI.

The electrode tip gave a strong response for aluminum X-ray counts, and these results were corrected using the "MAGIC" program to give a matrix concentration of aluminum of 8.9 wt. %. However there was

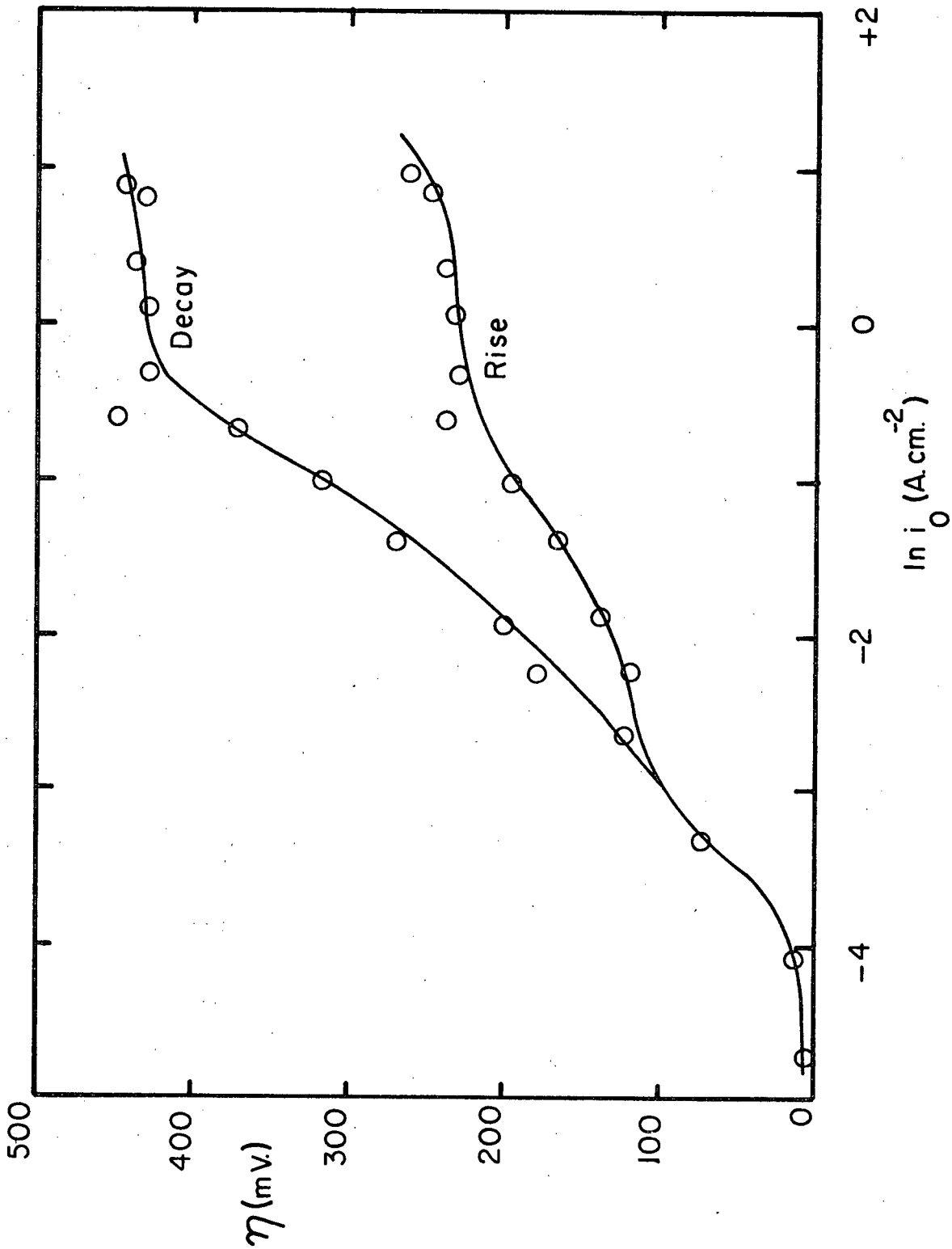

Figure 18. Anodic polarization curves for a Fe + 1 wt.% Cr electrode in a CaF_2 + 1 wt.% Al_2O_3 slag.

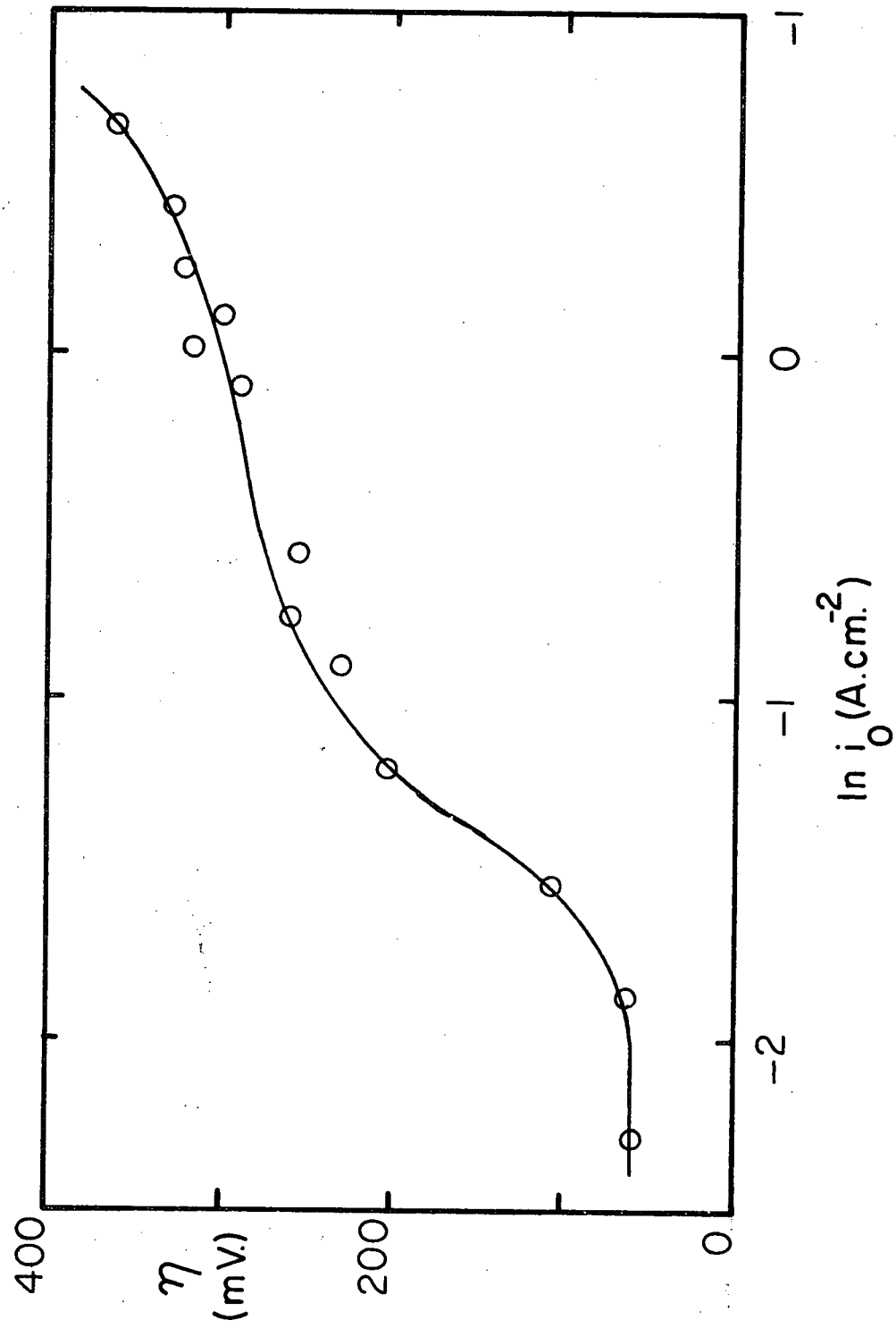

Figure 19. Anodic polarization curve for pure Cr in a CaF_2 + 1 wt.% Al_2O_3 slag.

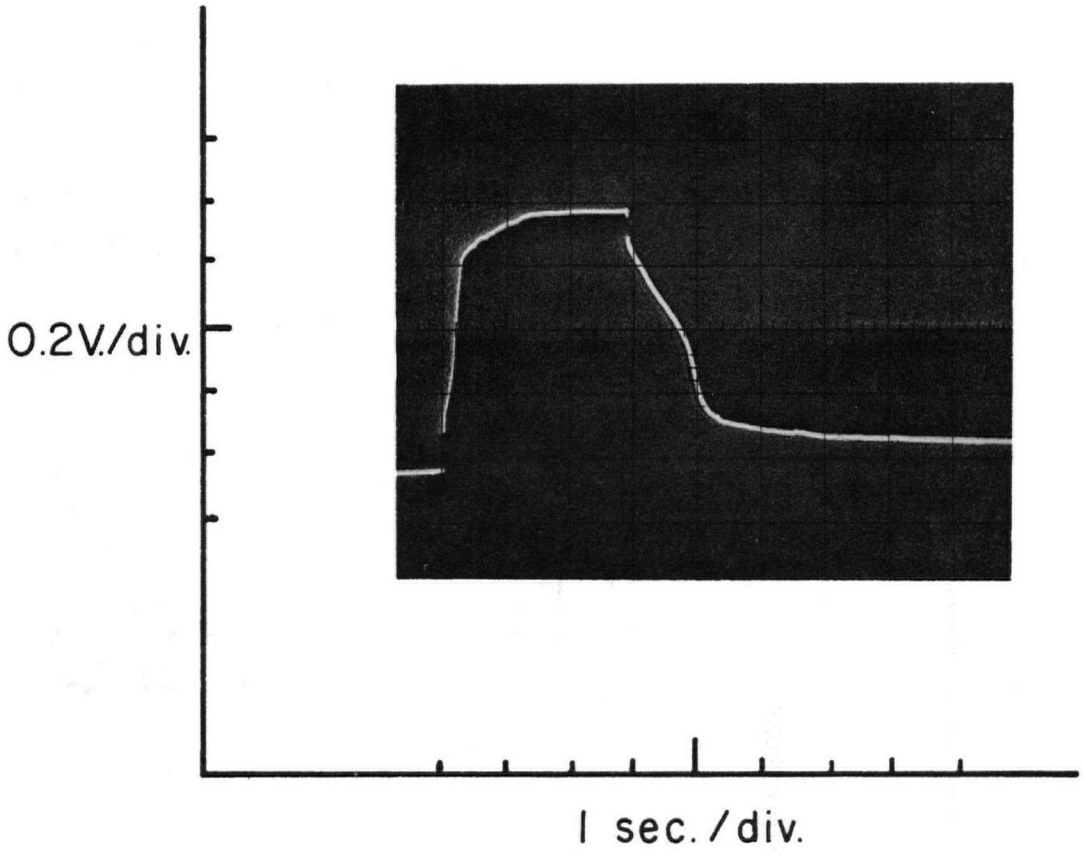

Figure 20. Single polarization curve for an anodic galvanostatic pulse on pure nickel in a CaF_2 + 2.5 wt.% Al_2O_3 slag. i_o = 1.10 $A.cm^{-2}$.

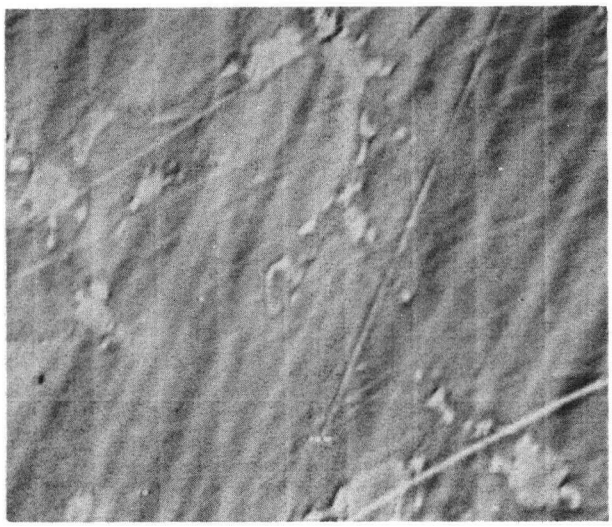

A.E.I. X 1020

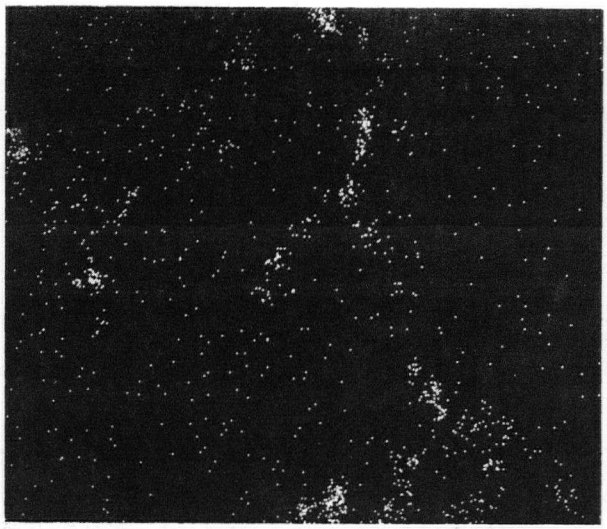

Ca X-ray X 1020

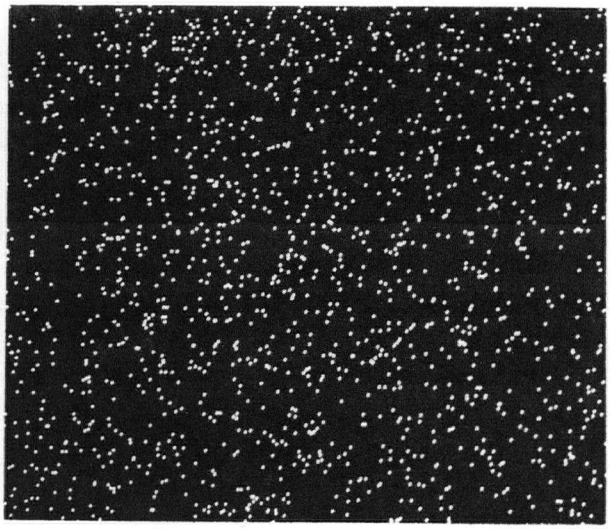

Al X-ray X 1020

Figure 21. Section through a pure nickel electrode cathodically polarized for 900 sec. at i_o = 450 ma.cm^{-2} in a CaF_2 + 8 wt.% Al_2O_3 slag.

no response when Ca X-rays were counted in the matrix, despite the fact that there were Ca rich areas as shown in Fig. 21.

2.5.6 Pure cobalt

A pure cobalt electrode was polarized anodically in a CaF_2 + 2.5 wt. % Al_2O_3 slag. Fig. 22 shows its polarization rise and decay at a current of 3 A. The similarity is to be noted for the case of an anodic nickel electrode (Fig. 20).

2.5.7 Fe - C alloy

An Fe + 0.83 wt. % C alloy was anodically polarized at a current of 1 A. for 200 sec. in a CaF_2 + 2.5 wt. % Al_2O_3 slag in order to study the carbon loss. Approximately one-half of the electrode tip melted off during this time.

The remaining part of the tip was cut from its base and analyzed for total carbon. The carbon content had dropped to 0.31 wt. % C.

2.6 Electroslag remelting polarization results

The electroslag polarization results are given in Figures 23→26 for Armco iron electrodes being remelted in Al_2O_3-containing and CaO-containing slags. Figures 23 and 25 are anodic polarization results while Figures 24 and 26 are cathodic results. These results are superimposed on the small scale results given in Figures 8→11, and although some extrapolation was necessary to extend the small scale results into the current density range experienced during remelting, good agreement is found. The

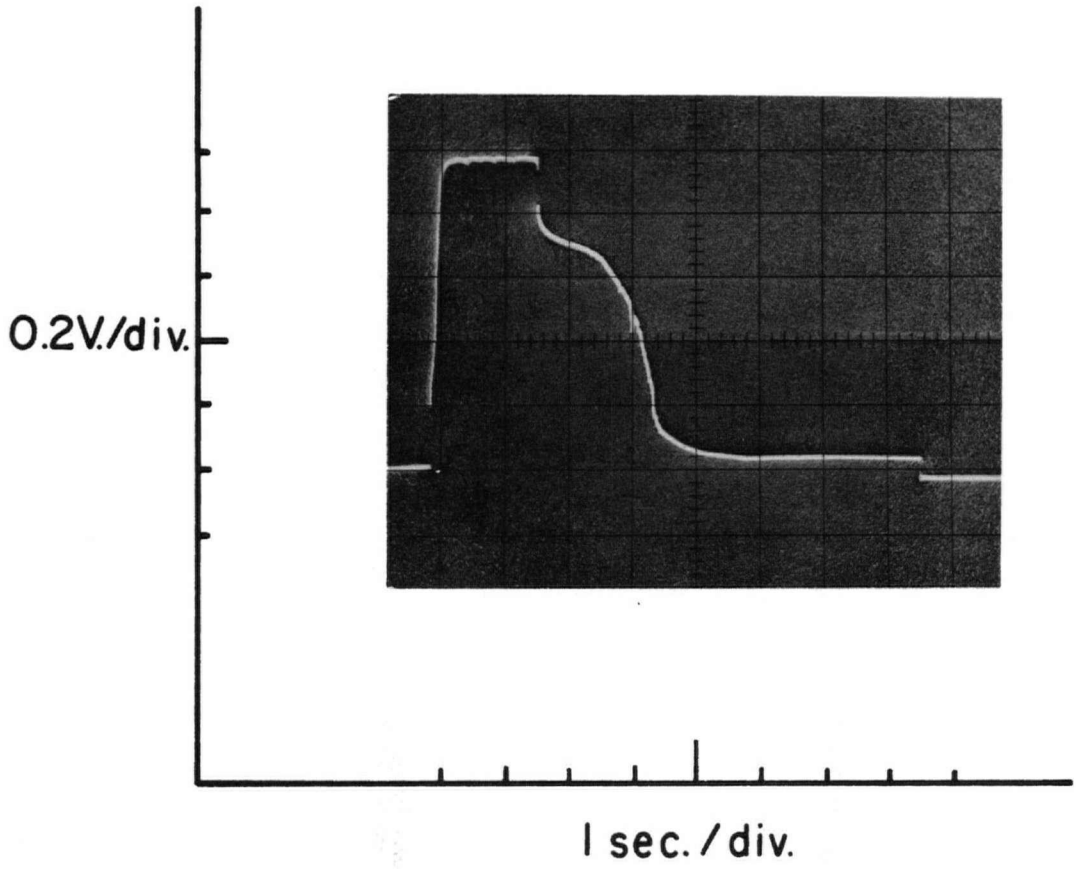

Figure 22. Single polarization curve for an anodic galvanostatic pulse on pure cobalt in a CaF_2 + 2.5 wt.% Al_2O_3 slag. i_o = 1.8 $A.cm^{-2}$.

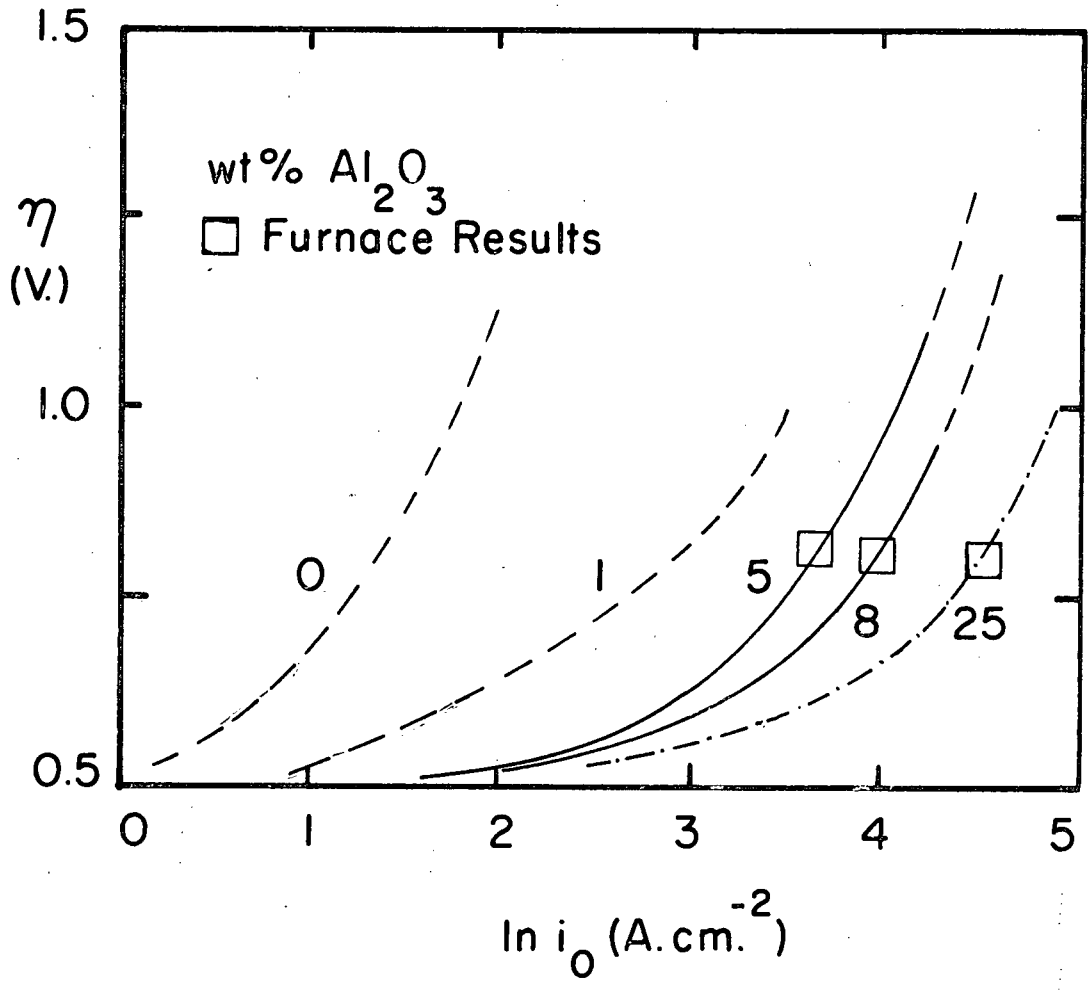

Figure 23. Anodic polarization on Armco iron E.S.R. electrodes in CaF_2 + Al_2O_3 slags.

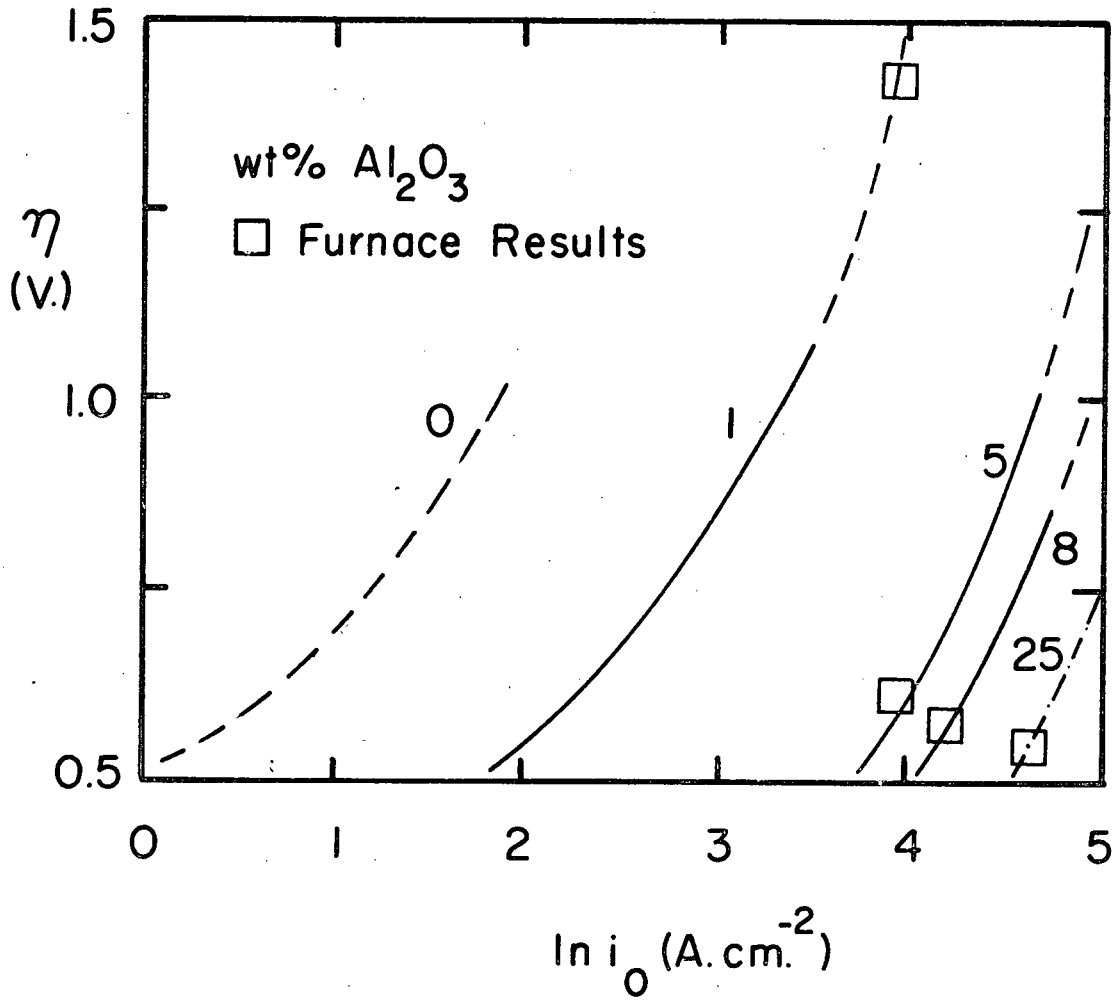

Figure 24. Cathodic polarization on Armco iron ESR electrodes in CaF_2 + Al_2O_3 slags.

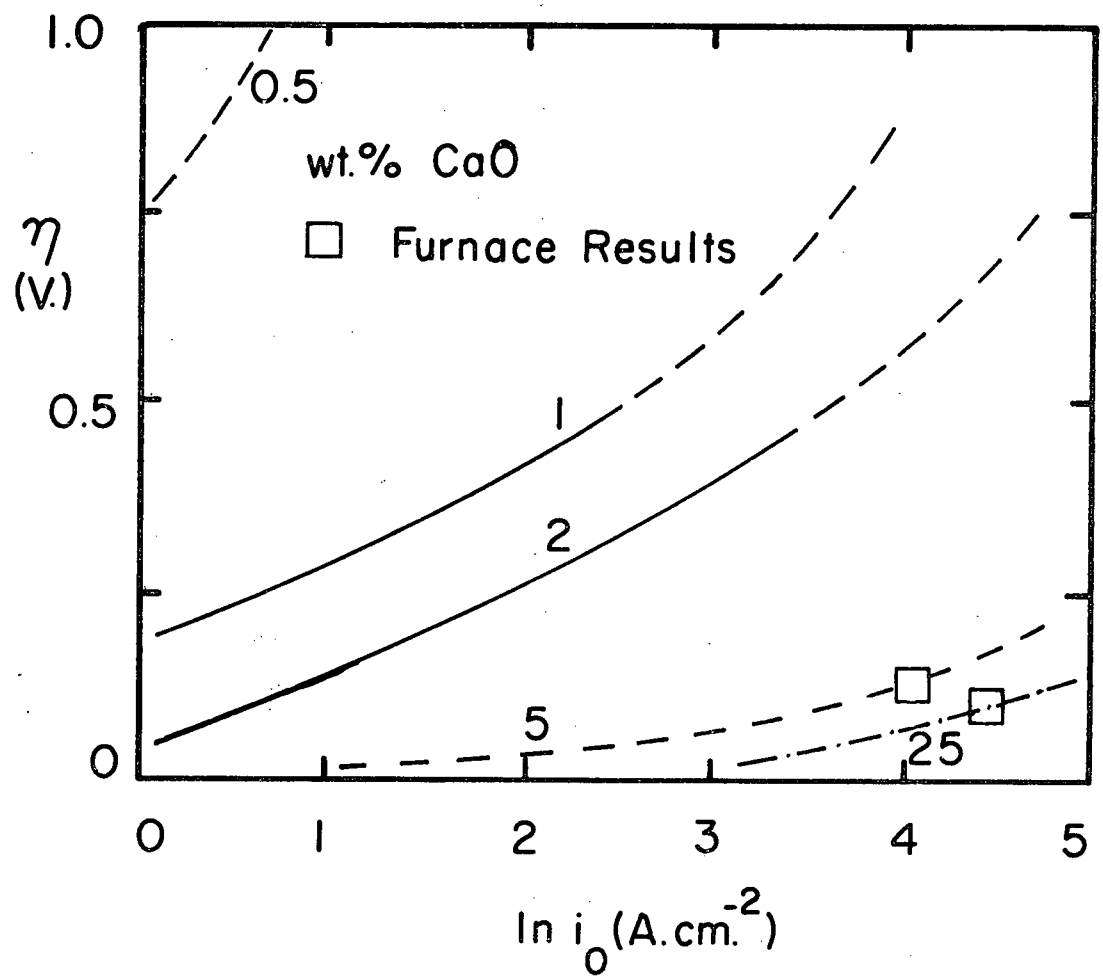

Figure 25. Anodic polarization on Armco iron ESR electrodes in CaF_2 + CaO slags.

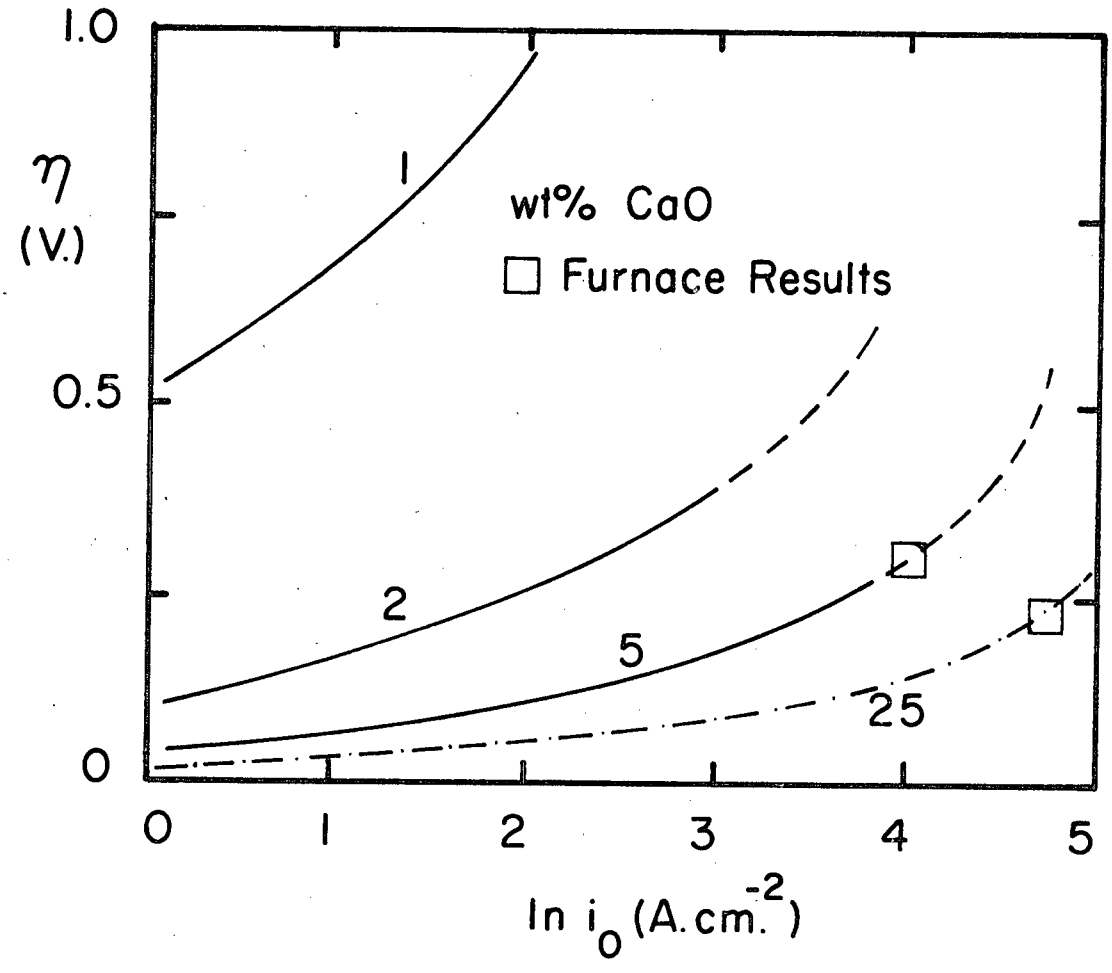

Figure 26. Cathodic polarization on Armco iron ESR electrodes in CaF_2 + CaO slags.

extent of polarization was also measured on AISI 430 stainless steel electrodes and AISI 1095 steel electrodes. The results are too inconclusive to present in graphical form, but will be discussed in Chapter 5.

CHAPTER 3

MELT PROGRAM

3.1 Melting procedure

All the ingots used in this investigation were made on the U.B.C. Electroslag Unit, the design and operation of which have been described by Etienne (4). Each run was started using a compact consisting of metal turnings and calcium-fluoride power, the metal turnings being machined from the electrode material. When the slag was completely molten and the melting conditions were stable, the operators proceeded to record the pertinent process parameters at regular time intervals. In this manner, a complete record of each ingot was taken and used for subsequent analysis.

3.2 Electrode materials

The electrode materials used in this program of experiments can be classified into two types, the first type consisting of essentially pure metals and the second being iron-base alloys containing other potentially oxidizable elements. The reasons for using each material are given together with the analysis of the electrode materials in the as received condition. All compositions are given in weight per cent.

3.2.1 Low carbon mild steel: AISI 1018 grade

(Supplied by Stelco)

C	Mn	P_{max}	S_{max}	O	Fe
.15-.20	.60-.90	.040	.050	.0155	Bal.

This electrode material, because of its low cost, was used in the initial experiments where the melting conditions were uncertain.

3.2.2 Ferrovac-E: vacuum melted (Supplied by the Crucible Steel Company, Sorel, Quebec)

C	Mn	P	S	Si	Ni
.010	.001	.002	.004	.006	.01
Cr	Mo	N	O	H	
<.01	.001	.0002	.00092	.000018	
Co	Cu	V	W	Fe	
.006	.006	<.002	.02	Bal	

Ferrovac-E pure iron was the ideal electrode material on which to study electrochemical phenomena during ESR. Because of its very low oxygen content, any oxygen found in the ingots must have arisen directly as a result of remelting the metal whether by chemical or electrochemical means.

A later series of ingots were made using a second batch of Ferrovac-E which was excessively high in oxygen (316 ppm). Apart from this, it was essentially pure iron as was the previous batch of Ferrovac-E. Since it had been found that this high initial oxygen content would

be lost during remelting, and would have very little effect on the final ingot oxygen content, this material was used in the same way as was the initial batch of Ferrovac-E. Two ingots were made using this second batch of Ferrovac-E with lengths of aluminum wire held in shallow grooves machined on the electrode surface. The purpose of this was to investigate whether or not excess aluminum would control the ingot oxygen content in spite of electrochemical oxidation. The amount of wire added would produce 2000 ppm of Al in the final ingot if none were to be lost during melting.

3.2.3 Armco iron: (Supplied by Armco Steel Corporation)

C	Mn	P	S	Si	O	Fe
.012	.017	.005	.025	trace	.070	Bal.

Armco iron was used in place of Ferrovac-E pure iron for several runs as it was found that despite the high oxygen content of the Armco iron, ingots made from it had oxygen contents very close to the O contents of Ferrovac-E ingots made under the same conditions. This resulted in substantial savings in electrode materials.

3.2.4 Ferritic stainless steel: AISI 430 grade

(Supplied by Allegheny Ludlum Industries, Inc.)

C	Mn	P	S	Si	Cr	O
.06	.44	.024	.015	.26	17.35	.0115

It was desired to make ingots from an iron alloy containing a second major element which could be oxidized during remelting. AISI 430

stainless steel was chosen because it is essentially an iron-chromium alloy containing little else which could interfere with Cr oxidative losses. Another advantage of this alloy was that its melting point is very close to that of pure iron.

3.2.5 Medium carbon mild steel: AISI 1095 grade

(Supplied by Stelco, Hamilton, Ontario)

C	Mn	Si	P_{max}	S_{max}	O	Fe
.975	.39	.34	.040	.050	.0020	Bal.

Ingots were made from this electrode material to study the effect of a substantial amount of carbon on the final oxygen content of these ingots.

3.2.6 Pure Ni: Supplied by Falconbridge Nickel Mines

C	Si	Mg	Fe	O
.01	.17	.18	1.9	.0011

Ingots were made from Falconbridge Nickel to investigate the behaviour of pure nickel during ESR and to compare this behaviour to the melting behaviour of pure iron.

3.3 Slag materials

The slags used during this melting program were all based on calcium-fluoride with additions of aluminum-oxide (Al_2O_3) or calcium-oxide (CaO) to alter the melting point, the conductivity, and the activities of the various components.

3.3.1 Calcium fluoride

The calcium-fluoride used in these slags was a fine power produced by a hydro-fluorination process. Approximately two-thirds of the calcium-fluoride used in each run was pre-fused in graphite crucibles by induction heating under an argon cover. The slag was held as a liquid for only a very short time in the graphite crucible to minimize carbon pick-up from the crucible. After fusion, the cold slag was crushed into small particles (approx. 1/8" in diameter) before being mixed with the other slag components.

It was found from experience that if these calcium-fluoride granules were too large they could bind between the electrode and the mould wall thus stopping electrode travel and causing the current path to be broken during the start-up period of a melt. If the slag was too fine, sintering of the solid particles would occur, again preventing electrode travel during the start-up. Another reason for fusing part of the calcium-fluoride was to drive off the surface moisture on the fine powder. Moisture in the slag can alter the slag composition according to the reaction:

$$CaF_2 + H_2O \rightarrow CaO + 2\ HF_g \qquad (3\text{-}1)$$

to form calcium-oxide in the slag. Calcium-oxide is the main slag impurity and is usually found to be at a level of 500 ppm although it would vary from melt to melt. This impurity was only important when the slag used during remelting was kept low in oxide content. For higher oxide content slags (5 wt. % Al_2O_3 or more) the calcium-oxide impurity content is unimportant in comparison to the total oxide content of the slag.

When it was desired to make ingots in low oxide content slags, BDH extra pure calcium-fluoride was prefused in graphite crucibles and used for the entire calcium-fluoride content of the slag. The as received analysis of this calcium-fluoride is given below as maximum impurity limits in wt. %.

Chloride (Cl)	.005 %
Sulphate (SO_4)	.01 %
Iron (Fe)	.005 %
Lead (Pb)	.005 %
Silica (SiO_2)	.05 %

3.3.2 Alumina

Norton granular alundum (Al_2O_3) of 99.3% purity was used in the as received condition for making alumina containing slags. This material is electrically fused from Bayer process alumina.

3.3.3 Calcium oxide

Recrystallized calcium oxide (CaO) of 99.5% purity was used to make calcium-oxide containing slags. This material was supplied by Dynamit Nobel, Germany.

3.4 Atmospheric control

Ingots were made under two types of atmospheric control equipment. The initial 24 ingots, as well as some later ones were made using a crude type of argon fume hood as shown in Fig. 27. This fume hood directed an argon flow down towards the slag/atmosphere surface and collected most of the fumes given off during remelting.

A more sophisticated design was used to make the balance of the ingots. As shown in Fig. 28, it consisted of a number of rubber bellows, clamped at the lower end to a flanged section of pipe and fixed above to a water-cooled copper electrode carrier, such that the downward travel of the electrode caused the bellows to collapse. The flanged pipe, which was held to the top of the ingot mould by C-clamps, had two aluminum foil blow-out windows. This design provides an atmosphere the quality of which depends almost exclusively upon the purity of the argon used. By contrast, chromatographic analysis of the argon fume hood atmosphere indicates that it may contain up to 1% O_2 with an argon flow rate of 100 l/hr.

3.5 Melting Conditions

Most of the ingots produced in this melt program were made under stable melting conditions which in turn were determined by such factors as slag composition, electrode polarity, and electrode materials.

In general, it was found that melting using either A.C. or electrode negative was quite stable but melting with electrode positive at the same voltage and current as used in electrode negative was very un-

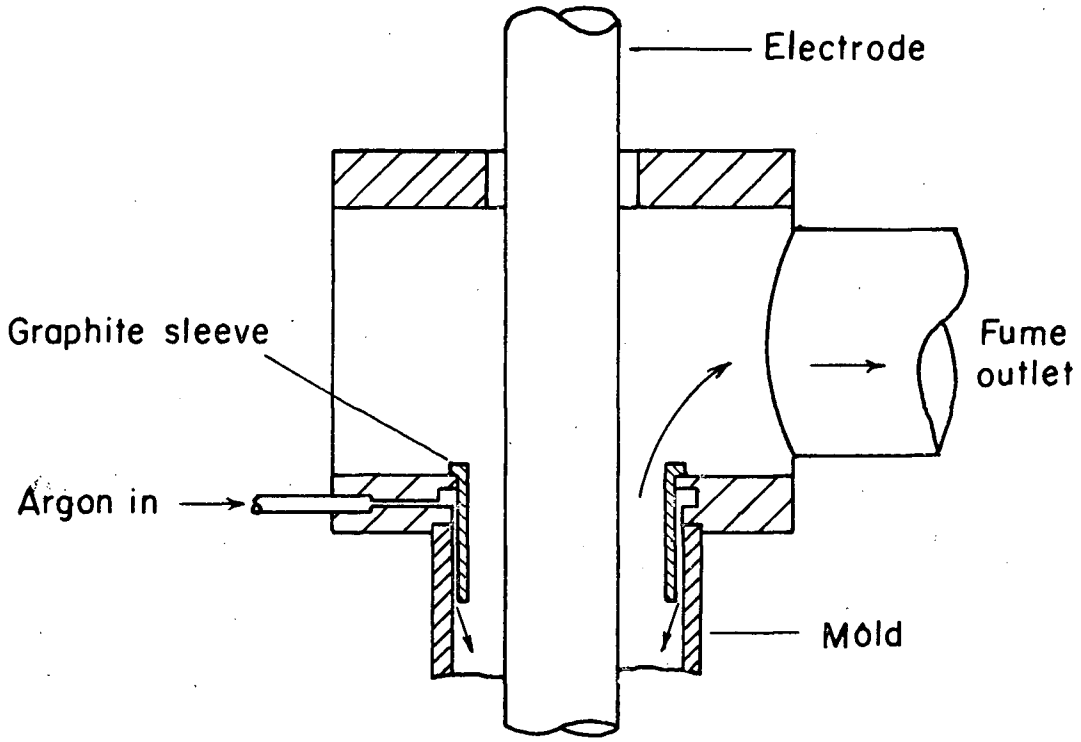

Figure 27. Argon fume hood.

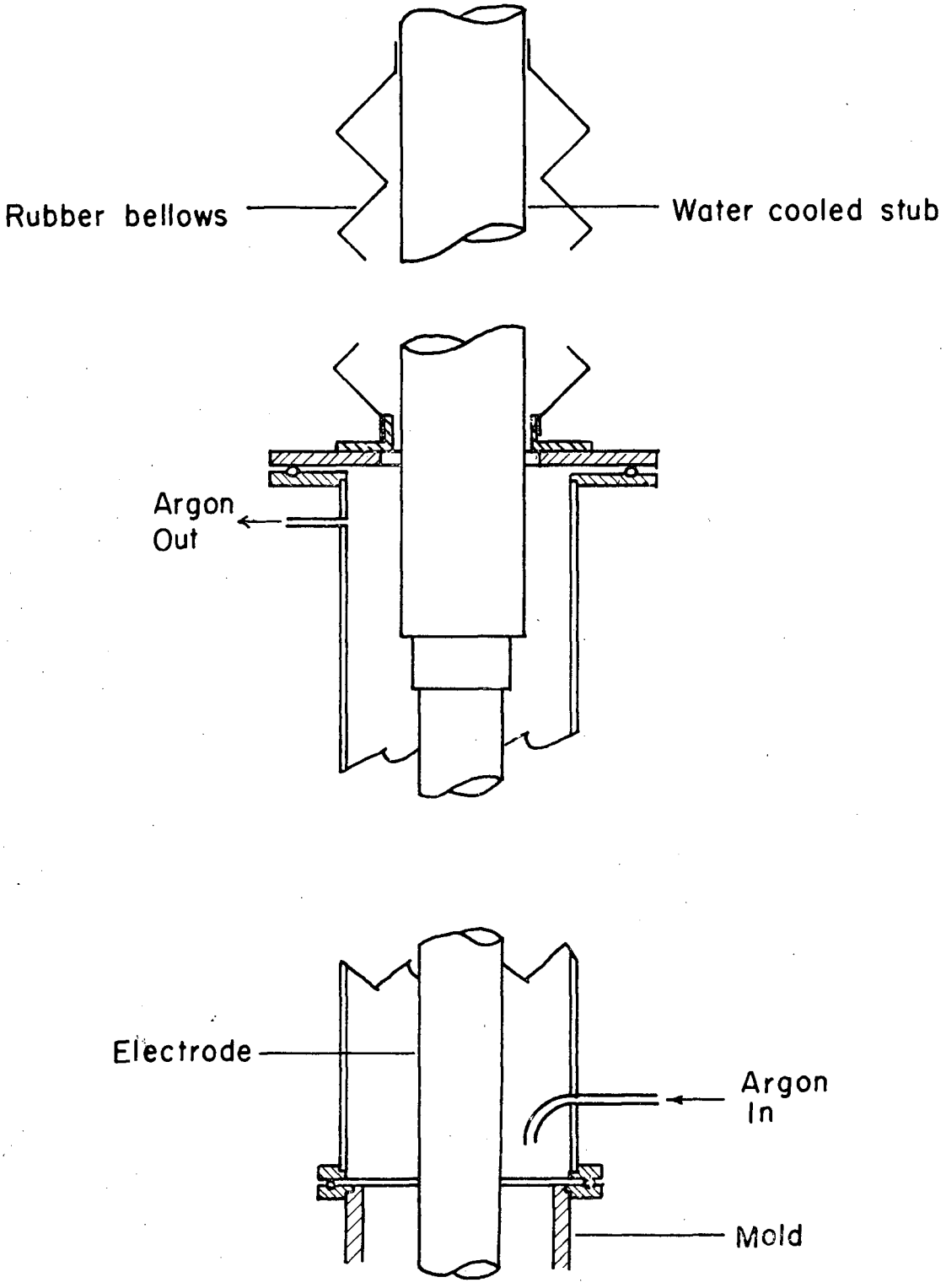

Figure 28. Argon gas cap.

stable, if not impossible. This instability was the result of arcing between the radial slag segment around the electrode and the mould wall and occurred even though the mould was insulated from the base plate (19).

The problem of arcing was overcome by painting the inside of the Cu mould with Boron-Nitride paint (type S) which is an electrical insulator but has a high thermal conductivity. Using this technique, it was possible to make ingots using the electrode positive mode at higher operating voltages while still maintaining the desired electrode-slag-ingot current path.

In a number of cases, ingots were made using a live mould. This was done by connecting separate leads directly to the bottom of the mould putting it in parallel with the base plate thereby allowing the process current to flow through either the mould or the ingot/base plate on the return path.

3.6 Melt records

During the melting of an ingot, detailed accounts were kept of all the important operating parameters. A Sargent Model SR Millivolt Recorder was used to keep a continuous record of the operating current. When the electrode was melting in a stable fashion (the slag was completely molten) the following data were recorded in the log book at 100 sec. intervals:

V - process voltage → D.C. or A.C.

A - process current → D.C. or A.C.

t - time in seconds with t = 0 the beginning of recording the data

C - total coulombs passed x 2×10^{-2}

P - total electrode travel in mm. from the beginning of the run

M.S. - speed of electrode travel drive motor

ΔT - temperature difference in °C between the inlet and outlet temperature of the mould cooling water.

Also recorded for each ingot were any operating peculiarities evident during melting.

3.7 Melt record calculations

3.7.1 Melt rate

The average melt rate of each ingot was calculated using the following mathematical approach. The starting point for the calculation is the actual distance traveled by the electrode, this distance being recorded at regular time intervals during a run. The diameter of the electrode is known (D_e) and the average diameter of the ingots (D_i) is measured. To convert the electrode travel into ingot rise as a function of ingot diameter, it is assumed that the electrode ingot separation remains constant during a run and that the ingot is fully dense. The amount of ingot rise resulting from 1 mm. of electrode travel is given by:

$$X = [1 + (\frac{R_e}{R_i})^2] \cdot [(\frac{R_e}{R_i})^2] \quad (3\text{-}2)$$

where R_e, R_i are radii of electrode ingot.

The weight of ingot formed per mm. of electrode travel is given by:

$$Y = X \cdot \pi R_i^2 \rho_m \quad (3\text{-}3)$$

where ρ_m is the density of the metal. The melt rate is then calculated according to:

$$M.R. = \frac{Y \cdot P}{t} \quad (\frac{gm}{sec}) \tag{3-4}$$

where P is the electrode travel in mm. and t the time in seconds over which the travel occurred.

3.7.2 Specific coulombic density (Z)

A parameter was required reflecting the rate at which the electrochemical reaction products entered the ingot metal during melting. This parameter could then be compared to the measured final oxygen content of the ingot. Such a parameter must take into account three terms; the current at the surface in question, the area of this surface, and the melt rate (which is a crude measure of the rate at which this surface is receiving fresh metal). An appropriate area was assumed to be the area of the ingot top, which was also considered to be flat. The rate of formation of electrochemical products would be proportional to the process current (assuming 100% current efficiency of any Faradaic processes) and inversely proportional to the surface area as well as the melt rate. This parameter Z could then be calculated as follows:

$$Z = \frac{\text{Process current (A.)}}{\text{Ingot top area } (cm.^2) \times \text{melt rate } (gm.sec^{-1})}$$

$$= \frac{\text{coul. sec.}^{-1}}{cm.^2 \times gm. \ sec^{-1}}$$

$$Z = \frac{\text{coul.}}{cm.^2 \times gm.}$$

3.7.3 Drop size and surface tension

It is known that oxygen is surface active in liquid iron as are many other elements (B, Se, S) and that the effect of oxygen in iron is to reduce its surface tension quite markedly. It was therefore thought to be desirable to measure the size of drops produced at the melting electrode during electroslag melting and to correlate the drop size to the surface tension of the drop, hence ultimately to the presence or absence of oxygen in the drops.

Campbell (20) studied droplet formation in electroslag remelting and derived the relation given below using a dimensional argument.

$$r^2 = \frac{k\,\gamma}{g\Delta\rho} \qquad (3\text{-}5)$$

r - drop radius

γ - interfacial tension between two liquids

g - acceleration due to gravity

$\Delta\rho$ - density diff. between liquids at T

k - a constant

He assumed that the drop radius, r, is independent of the electrode radius for a sufficiently large electrode and he states the relationship is valid for conical electrode tips, such as is the case during the melt program. In order to use this relationship it is first necessary to calculate r from the melt records. This is done by counting the drop rate on the process current recorder chart, each drop coinciding with a peak on the chart. Combining the drop weight with the melt rate, one can find the drop size, then r, and calculate γ using the appropriate physical constants. This was done for Ferrovac-E electrodes melted under various conditions.

3.7.4 Melt program results

The melt record data, the calculated parameters (melt rate and the specific coulombic density [Z]), and the average oxygen content of the ingots are summarized in Tables I→V. The drop size and interfacial tension results are given in Table VI.

3.8 Ingot analysis

3.8.1 Oxygen analysis of ingots

All of the ingots produced in this melt program were analyzed for their average total oxygen content using a Leco Rapid Oxygen Analyser (No. 734-300). It must be noted that the oxygen in these ingots is in the form of non-metallic inclusions formed by the reaction of dissolved oxygen with either metals dissolved in the base metal or the base metal itself.

Ingots to be analysed for total oxygen are sectioned as shown in Fig. 29 giving individual 1 g. specimens. An ingot is cut horizontally one-third of the way up from the bottom, and then a vertical slice one-quarter of an inch thick is cut from the top portion. This slice is then cut horizontally into 10 1/4" square slices and the desired slice can then be cut into 1/4" cubes for analysis. Normally, five cubes would be cut from the outside into the center from the second, fifth, and tenth slices to give 15 specimens for analysis from each ingot. Portions of these slices were also used for metallographic and electron microprobe examination of the inclusions in the ingots.

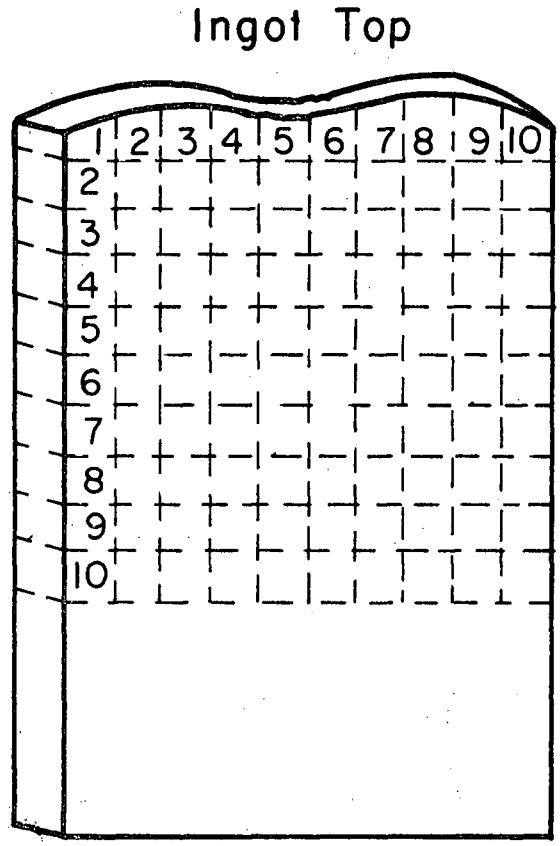

Figure 29. Ingot sampling scheme.

3.8.2 Aluminum analysis of FVE ingots

Five Ferrovac-E ingots were analyzed for total aluminum using the neutron activation method (21). The results of these analyses are given in Table VII.

3.8.3 Analysis of AISI 1095 steel

Electrode material and ingots made from 1095 steel were analysed spectrographically to determine what alloy losses took place during remelting. The results are given in Table VIII.

3.8.4 Analysis of AISI 430 stainless steel

Electrode material and ingots made from 430 stainless steel were also analysed spectrographically. The results are given in Table IX.

3.9 Slag cap analysis

Several of the slag caps were observed to contain dark green or brown phases, usually near the ingot region. These regions were thought to contain a high concentration of iron-oxide. Segments of four slag caps from FVE runs (-, +, +(im), A.C.) were crushed and analysed for total iron by caustic fusion and acid dissolution to make solutions suitable for analysis by the atomic absorption technique. The results are given in Table X.

TABLE I

MELT RECORD RESULTS OF AISI 1018 MILD STEEL

Atmosphere - Argon fume hood
Electrode Dia. = 3.82 cm.
Ingot Dia.(av.) = 7.5 cm.
Electrode 0 content = 150 ppm.
CA → calcium aluminate

INGOT NO.	SLAG ADD'N. (wt. %)	ELECTRODE POLARITY	VOLTS	AMPS	MELT RATE ($gm.sec.^{-1}$)	OXYGEN (ppm)	Z ($coul.cm.^{-2}\ gm.^{-1}$)
4	30 CA	—	24.6	1160	2.94	481	8.9
5	30 CA	—	23.8	1200	2.40	500	11.3
11	30 CA	—	23.5	1177	2.97	500	8.9
17	30 CA	—	23.2	1025	2.21	475	10.5
18	30 CA	—	23.2	1350	3.08	375	9.9
15	30 CA	— (mo insert)	n.a.		0	2000	n.a.
14	nil	—	22.2	1181	2.50	205	10.7
6	10 MgF_2	—	20.5	1150		510	
7	10 MgF_2	—	21.0	1100		505	
1	30 CA	+	22.1	1020	2.45	55	9.4
2	30 CA	+	22.5	1015	2.86	50	8.0
3	30 CA	+	23.0	1058	3.13	50	7.6
21	30 CA	A.C.	trial runs			180	
22	30 CA	A.C.				200	

TABLE II

MELT RECORD RESULTS OF FVE INGOTS

Atmosphere - Argon fume hood

Electrode Dia. = 3.18 cm.

Ingot Dia.(av.) = 5.5 cm.

Electrode O content = 9 ppm.

* → new FVE O content = 316 ppm.

CA → calcium aluminate

INGOT NO.	SLAG ADD'N. (wt. %)	ELECTRODE POLARITY	VOLTS	AMPS	MELT RATE ($gm.sec^{-1}$)	OXYGEN (ppm)	Z ($coul.cm.^{-2}\ gm.^{-1}$)
8	24 CA	-	23.5	689	1.28	1075	21.8
9	24 CA	-	23.2	862	1.63	788	21.4
10	24 CA	-	23.5	1047	2.06	730	21.4
16	24 CA	+	20.5	782	1.32	250	23.2
23	24 Al_2O_3	-	23.3	966	2.33	425	16.7
72*	25 Al_2O_3	-	22.7	892	1.49	569	22.7
24	24 Al_2O_3	+	20.2	749	1.59	150	19.0
74*	25 Al_2O_3	+(im)	22.5	878	1.68	174	17.9
73*	25 Al_2O_3	A.C.	23.3	558	2.99	165	8.7
19	25 CaO	-	22.4	1000	2.20	800	17.8
20	30 CaO	-	22.5	1040	1.58	550,	26.6

TABLE III

MELT RECORD RESULTS OF FVE INGOTS

Atmosphere - Argon gas cap.

Electrode Dia. = 3.18 cm.

Ingot Dia.(av.) = 5.5 cm.

Electrode O content = 9 ppm.

* → new FVE O content = 316 ppm.

INGOT NO.	SLAG ADD'N. (wt. %)	ELECTRODE POLARITY	VOLTS	AMPS	MELT RATE ($gm.sec^{-1}$)	OXYGEN	Z^{-2} ($coul.cm.^{-2}\ gm.^{-1}$)
25	25 Al_2O_3	-	22.6	833	1.38	450	27.3
26	25 Al_2O_3	-	22.5	949	1.75	450	22.8
27	25 Al_2O_3	-	23.3	924	1.77	470	22.8
28	25 Al_2O_3	-	22.2	750	1.28	450	26.6
29	25 Al_2O_3	-	24.5	859	1.64	500	23.3
30	25 Al_2O_3	-	24.0	748	1.43	680	22.0
39	25 Al_2O_3	-	23.5	991	1.83	460	23.6
77*	25 Al_2O_3	-	26.0	1160	3.55	378	13.7
31	25 Al_2O_3	+	19.0	652	1.30	67	21.2
32	25 Al_2O_3	+	19.1	655	1.11	317	23.9
33	25 Al_2O_3	+	18.9	748	1.28	171	22.9
37	25 Al_2O_3	+(im)	22.0	791	1.77	175	18.1
38	25 Al_2O_3	+(im)	22.4	917	1.58	70	24.4
41	25 Al_2O_3	+(im)	22.2	957	2.50	170	16.7
35	25 Al_2O_3	+ (lm)	21.5	857	1.15	690	32.7
83*	25 Al_2O_3	+ (lm)	22.5	933	1.76	834	22.3
34	25 Al_2O_3	A.C.	24.2	655	2.22	225	12.9

TABLE III (Continued)

INGOT NO.	SLAG ADD'N. (wt. %)	ELECTRODE POLARITY	VOLTS	AMPS	MELT RATE ($gm.sec^{-1}$)	OXYGEN (ppm)	Z ($coul.cm.^{-2} gm.^{-1}$)	
40	25 Al_2O_3	A.C. (im)	22.9	819	2.62	200	13.1	
36	25 Al_2O_3	A.C. (lm)	23.8	810	2.15	225	15.9	
79*	25 CaO	-	22.6	1065	2.06	342	20.8	
78*	25 CaO	+ (im)	21.4	828	2.22	119	15.0	
82*	25 CaO	+ (lm)	21.5	908	2.11	230	18.1	
75*	25 Al_2O_3	-	23.8	1150	3.07	548	8.7	large mold (7.6 cm) Al wire
76*	25 Al_2O_3	+(im)	24.5	1045	2.31	153	10.2	
80*	25 Al_2O_3	-	23.8	779	2.59	548	12.7	
81*	25 Al_2O_3	+(im)	22.0	792	1.75	526	22.1	

TABLE IV

MELT RESULTS OF ARMCO IRON INGOTS

Atmosphere - Argon gas cap
Electrode Dia. = 3.18 cm.
Ingot Dia. (av.) = 5.5 cm.
Electrode O content = 700 ppm.

INGOT NO.	SLAG ADD'N. (wt. %)	ELECTRODE POLARITY	VOLTS	AMPS	MELT RATE ($gm.sec.^{-1}$)	OXYGEN (ppm)	Z ($coul.cm.^{-2}\ gm.^{-1}$)
42	25 Al_2O_3	-	22.4	908	1.49	550	26.5
49	25 Al_2O_3	-	22.6	954	2.14	470	18.7
47	10 Al_2O_3	-	23.0	886	1.70	820	21.1
65	5 Al_2O_3	-	22.3	896	2.37	820	15.3
48	1 Al_2O_3	-	22.5	910	1.77	810	22.6
50	nil	-	20.0	536	1.79	660	16.3
54	25 Al_2O_3	+	20.0	732	1.72	300	17.9
57	25 Al_2O_3	+	18.5	757	1.80	195	17.0
58	25 Al_2O_3	+	19.0	768	1.80	290	17.3
55	10 Al_2O_3	+	18.5	808	1.53	250	22.1
56	10 Al_2O_3	+	18.8	786	1.53	260	21.5
59	5 Al_2O_3	+	19.0	827	1.58	285	21.3
44	25 Al_2O_3	+(im)	22.2	899	1.82	255	20.8
43	25 Al_2O_3	A.C.	23.0	710	2.94	260	10.9
60	25 Al_2O_3	A.C.	26.4	588	3.06	245	8.1
66	30 CaO	-	23.0	973	2.10	505	19.1
52	25 CaO	-	23.0	1062	1.91	580	23.4
51	5 CaO	-	20.0	1104	0.98	1200	45.7

TABLE V

MELT RECORD RESULTS OF MISCELLANEOUS INGOTS

Atmosphere - Argon gas cap.

Ingot Dia.(av.) = 5.5 cm.

MATERIAL	ELECTRODE DIA.(cm.)	O CONTENT (ppm)
AISI 430	2.54	115
AISI 1095	2.54	20
Pure Nickel	3.50	11

	INGOT NO.	SLAG ADD'N. (wt. %)	ELECTRODE POLARITY	VOLTS	AMPS	MELT RATE ($gm.sec.^{-1}$)	OXYGEN (ppm)	Z ($coul.cm.^{-2}\ gm.^{-1}$)
430	61	25 Al_2O_3	-	22.7	834	1.75	125	20.0
	62	25 Al_2O_3	-	22.7	877	1.85	115	19.8
	63	25 Al_2O_3	-	23.1	858	1.79	225	20.1
	64	12 Al_2O_3	-	23.0	843	1.95	170	18.2
	70	25 Al_2O_3	+ (im)	very unstable			91	
1095	68	25 Al_2O_3	-	24.0	910	2.15	145	17.8
	67	25 Al_2O_3	+ (im)	22.0	790	2.45	50	13.6
Ni	69	10 Al_2O_3	-	23.0	780	1.96	7	15.6
	71	10 Al_2O_3	+ (im)	22.0	628	2.23	362	11.4

TABLE VI

DROP SIZE AND INTERFACIAL TENSION RESULTS FOR FVE

ELECTRODE POLARITY AND CONDITIONS	DROP WT. (gm)	γ (DYNES cm.$^{-2}$)
-	2.57	421
+ (includes +im and +1m)	1.11	240
A.C.	3.51	517
- (Ingot 80- Al wire)	3.46	513
+ (Ingot 81- Al wire)	1.17	250

TABLE VII

TOTAL ALUMINUM CONTENT OF FVE INGOTS

INGOT NO.	MELT CONDITIONS	ppm. Al
25	-	522
41	+(im)	55
83	+(1m)	169
80	-[Al wire]	1962
81	+(im)[Al wire]	2621

TABLE VIII

COMPOSITION OF AISI 1095 ELECTRODE AND INGOTS

ELEMENT	ELECTRODE	INGOT 68 [el. - ve]	INGOT 67 [el + ve(im)]
C	.975	.903	.914
Mn	.39	.37	.38
Si	.34	.27	.37
O	.0020	.0145	.0050

TABLE IX

COMPOSITION OF AISI 430 ELECTRODE AND INGOTS

ELEMENT	ELECTRODE	INGOT 63 [el - ve]	INGOT 70 [el. + ve(im)]
Cr	17.35	17.16	16.90
Mn	0.44	0.47	0.40
Si	0.26	0.15	0.19
C	0.060	0.051	0.060
P	0.024	0.024	0.022
S	0.015	0.006	0.009
O	0.0115	0.0225	0.0091

TABLE X

TOTAL IRON CONTENT OF FVE SLAG CAPS

INGOT NO.	POLARITY	(CaF_2 + 25 wt. % Al_2O_3) (wt. % Fe)
39	-	0.52
31	+	1.74
37	+ (im)	1.34
34	A.C.	1.01

CHAPTER 4

DISCUSSION OF SMALL SCALE STUDIES

4.1 Introduction

The small scale studies were carried out with the purpose of formulating electrochemical reaction mechanisms responsible for current transfer across liquid metal/liquid slag interfaces, under ESR conditions. The reaction mechanisms so proposed must be able to account for chemical and thermal phenomena which exist during D.C. electroslag melting. It has been stated that CaF_2 slags conduct ionically and this was found to be essentially true, except when there were significant amounts of Ca and Al metals dissolved in the slag.

The mechanism responsible for polarization in such systems is the slow diffusion of reaction products away from the reaction interface into the slag and the metal.

In the following section we shall show that the anodic Faradaic reaction for pure iron in CaF_2 - Al_2O_3 slags is at low current densities, the anodic corrosion of iron leading to FeO saturation in the slag at the interface at sufficiently high current densities. In addition we shall demonstrate that the cathodic Faradaic reaction involves deposition of Al and/or Ca such that some Al dissolves in the iron and Ca and Al dissolve in the slag.

4.2 Previous electrochemical work

There have been very few studies in which the electrochemical phenomena of liquid metal electrodes in slags at relatively high tempera-

tures have been investigated. In the case of chloride melts (22), it has been shown that there exists clear evidence for electrochemical reactions in which the slow step is the adsorption of a complex species. This is an activation process and has a very short transition time (< 1 μ sec.). At higher temperatures there are only a few studies involving the steady state polarization of a carbon-saturated iron/oxide slag interface. Shantarin (23) studied the anodic polarization of carbon saturated iron surfaces in oxide melts and, although he did not find the nature of the electrochemical reactions, he mentioned that the anodic dissolution of Fe to give Fe^{2+} ions in the slag was accompanied by considerable current efficiencies, and was assumed to lead to concentration polarization at the interface. Other workers (24) studied the cathodic processes of carbon saturated steels in various fluoride-oxide slags but they were mainly concerned with alloy content increases resulting from electrolysis. Gosh and King (16) studied the discharge kinetics of oxide ions from lithium silicate melts on platinum anodes. They employed a galvanostatic pulse technique, and observed electrode polarization phenomena produced by evolution of oxygen gas at the electrode. In another case, the concentration polarization of iron and nickel surfaces in oxide-free and nickel oxide saturated fluoride melts was studied in the temperature range 500 - 600°C (25). It was found that an important aspect of the reaction characteristics in the oxide containing melts was the semi-conducting nature of the passive oxide layer formed on the metal electrode surface. For the case of most low temperature studies, the aim has been to define the electrochemical reaction steps, while eliminating concentration polarization from the cell.

This means that all these experiments had to be carried out at low (<1 A. $cm.^{-2}$) current densities. However, in the case where polarography has been studied in fused salts (26), the system has been found to follow closely the ruling equations derived for analogous aqueous situations under similar hydrodynamic control.

4.3 Anodic polarization of pure iron in Al_2O_3 slags

The anodic behaviour of pure iron in CaF_2 - Al_2O_3 slags is shown in Fig. 8. These polarization curves can be represented schematically in Fig. 30. The curve has three sections denoted A, B and C. Part A of the anodic polarization curves fits an exponential form which, together with the observed long times (.5 → 5 sec.) required to establish steady state polarization, implies that the mechanism is a diffusion controlled process, leading to a limiting current density, i_D. Values of i_D were obtained from the curves for 1, 5, and 10 wt. % Al_2O_3 slags by extrapolating the sections A of the curve. The curves were then plotted according to the equation (1-14):

$$\eta_d = \frac{RT}{nF} \cdot \ln\left(\frac{i_D - i}{i_D}\right) \qquad (4\text{-}1)$$

as shown in Fig. 31. Values of n between 1 and 0.1 are obtained which seems to indicate that the electrochemical mechanism responsible for section A is indeed a diffusion limited reaction. Such processes generally involve the depletion of a dilute ionic species in the solvent electrolyte near the electrode to such an extent that the rate of diffusion of this

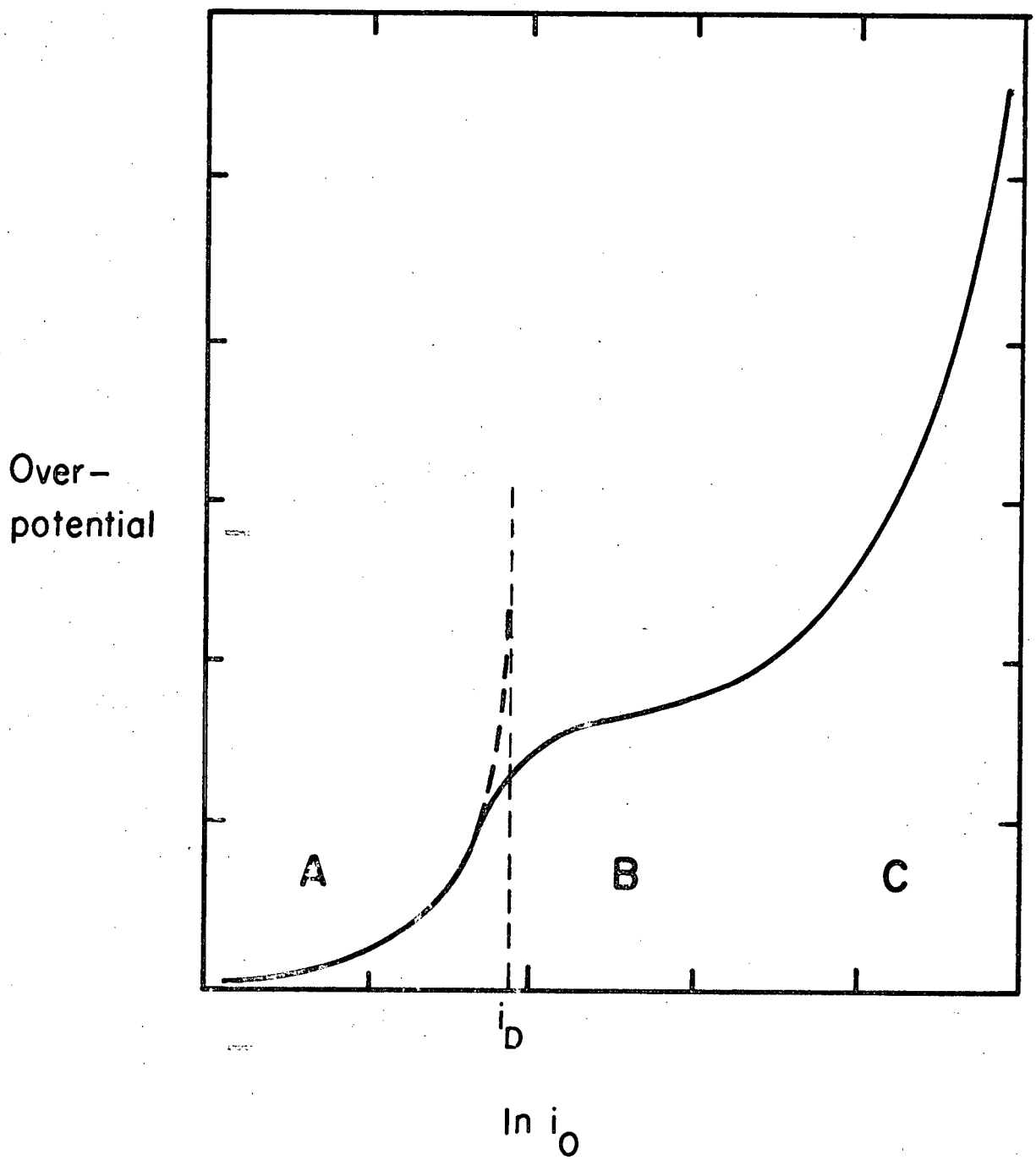

Figure 30. Schematic representation of the anodic polarization curve for pure iron in CaF_2 + Al_2O_3 slags.

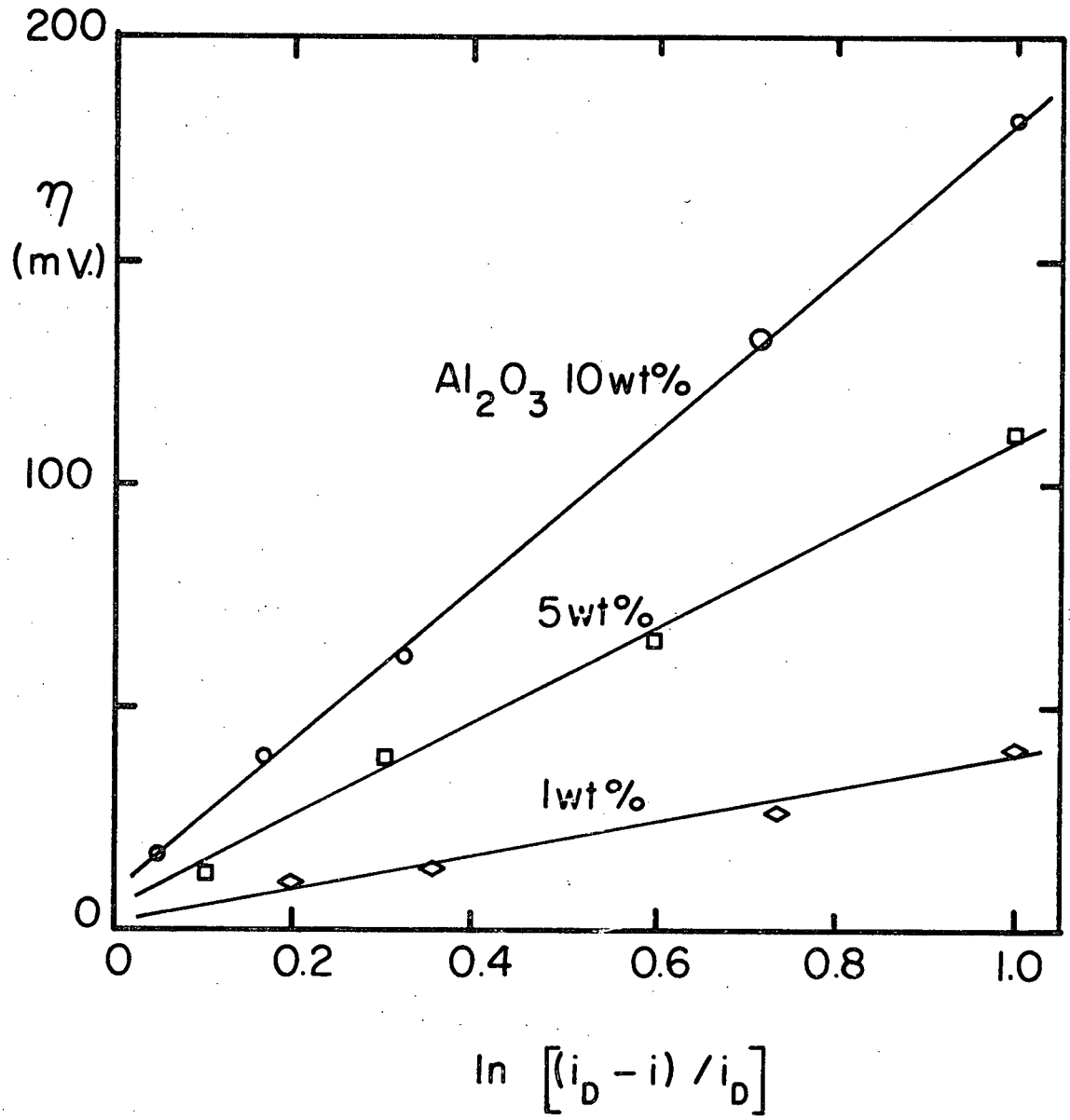

Figure 31. Application of a limiting current density law to anodic polarization of pure iron in CaF_2 + Al_2O_3 slags.

species towards the electrode equals the rate of removal of the ions at the electrode. Such a situation is unlikely in this fused salt system because the solvent is being electrolyzed (there is no solute to be depleted). The simplest anodic process in this case is the reaction

$$Fe_s \rightarrow Fe^{2+} + 2e^- \qquad (4-2)$$

which will not lead to such a limiting law (14). It is, however, possible that the corrosion product, Fe^{2+}, could lead to saturation of the slag at the electrode interface, and that the measured electrode potential would therefore reach some maximum value which would be determined by the equilibrium electrode potential of the Fe/FeO interface. The values of n obtained from Fig. 31 are then simply a fortuitous representation of the exponential diffusion gradient of Fe^{2+} existing in the slag at the electrode interface at current densities too low to saturate the interface. It is therefore reasonable to expect the values of n to vary with slag oxide content which should not occur if a single diffusion limited reaction involving oxide ions was taking place.

When the current density at the electrode is sufficiently high, saturation of the interface in the anodic corrosion product takes place, and the curves enter section B on the schematic plot, Fig. 30. It is necessary to stress that the potential difference measured between the working and reference electrodes is established by the potential existing at the iron electrode surface. Thus a higher current density in section B of a given curve will only produce a thicker saturated layer, and will not affect the measured potential, but this is true only if the saturated layer remains ionic in nature, and does not become an electronic conductor.

If the slag remains ionic, the Faradaic process continues to take place at the electrode surface. If the anodic corrosion of iron is indeed the Faradaic process responsible for these results, the rate at which concentration polarization would arise in the slag due to the establishment of a steady state concentration gradient, will depend on the electrode current density and on the slag composition (oxide type and content).

It is of interest to calculate the approximate thickness of this proposed FeO saturated layer. This calculation refers to a pure iron electrode in a Ca F_2 + 2.5 wt. % Al_2O_3 slag. Anodic saturation began at a current of 600 mA. on an electrode whose total exposed area was 2.75 cm^2. Approximately 3.2 sec. was required to saturate the surface and the coulombic density was therefore 0.70 coul. $cm.^{-2}$ For the reaction

$$Fe \rightarrow Fe^{2+} + 2e^-$$

n = 2, and the number of moles of iron corroded is equal to 3.6×10^{-6} moles. $cm.^{-2}$, which is equivalent to 2.6×10^{-4} gm. of FeO per sec. The saturation solubility of FeO in low oxide CaF_2 slags is low and for this slag will be less than 5 wt. %, and an assumed value of 1 wt. % is used. The density of pure CaF_2 at 1500°C. is 2.54 gm. $cm.^{-3}$ and neglecting the change in density (increase) due to saturation with FeO, the weight of saturated slag per unit area will then be 2.6×10^{-2} gm. which has a volume of $1.03 \times 10^{-2} cm.^{-3}$. This latter value contains the assumption that all the FeO produced remains in the vicinity of the electrode surface. Therefore the thickness of the FeO saturated layer at a current density which is high enough to produce saturation will be approximately 100 microns thick.

It is also of interest to calculate the thickness of a diffusion boundary layer in the small scale system. Levich (27) derived an expression for the diffusion boundary layer thickness, δ, for the case of convective diffusion. The driving force for mass transport is the density gradient produced by movement of electro-active species to the electrode surface. The equation so derived should also apply to the case of diffusion of Faradaic reaction products away from the electrode surface into the bulk of the slag, and is:

$$\delta \tilde{=} \frac{x^{1/4}}{0.7\ Pr^{1/4} \left(\frac{gC}{4\nu^2}\right)^{1/4}} \qquad (4\text{-}3)$$

where

x - distance from the upper edge of the plate

Pr - Prandtl No. of the slag

g - acceleration due to gravity

C - concentration of diffusing species at the plate surface

ν - Kinematic viscosity of the slag.

This equation applies to natural convection at a planar electrode surface, however in the case of cylindrical diffusion the divergence of the flux would tend to decrease the diffusion boundary layer thickness. By assuming that the electrode surface is planar, δ can be calculated using the following data:

x = 1 cm.

Pr = 0.12 which is the Prandtl No. of liquid NaCl (28)

C = 2.54×10^{-2} gm. $cm.^{-3}$ for 1 wt. % FeO saturation in low oxide CaF_2 slags

$$\nu = \frac{\mu}{\rho} = \frac{0.6 \text{ poise}}{2.54 \text{ gm.cm.}^{-3}} = 0.24 \text{ cm.}^2\text{sec.}^{-1} \qquad (4\text{-}4)$$

and $$\delta = \frac{1^{1/4}}{(0.7)(.12)^{1/4}\left(\frac{980 \cdot 0.0254}{4 \cdot 0.058}\right)^{1/4}}$$

$$\delta = 0.757 \text{ cm.}$$

Diffusion boundary layer thicknesses in natural convection are found to be substantially greater than in forced convection, and the values of the diffusional fluxes are found to be correspondingly smaller. The calculated value of δ is much larger than would be found in aqueous systems. It is quite likely that the actual diffusion boundary layer thickness in the small scale system is smaller than this calculated value, its thickness being determined by thermal convection in the slag.

There is no phase diagram information available on the CaF_2-Al_2O_3-FeO system, but in analogy with the CaF_2 - Al_2O_3 - MnO system (29) and the CaF_2 - CaO - FeO system (30), (the partial phase diagrams of which are given in Fig. 32, and show the FeO solubility to be strongly composition and temperature dependent), the system is believed to exhibit a large miscibility gap. Hence the corrosion rate at which surface saturation in FeO is attained would be expected to depend strongly on slag composition and temperature. Once the slag of the anodic electrode surface has become saturated in FeO, the potential of the surface may be represented by

$$Fe(s) + O^{2-} \rightarrow \underset{\text{(slag sat'n.)}}{FeO} + 2e^- \qquad (4\text{-}5)$$

This potential will be approximately independent of slag composition as is seen from the approximately constant plateau values in Fig. 8. The overall potential difference which is measured between the reference and working electrode will then be represented by the virtual reac-

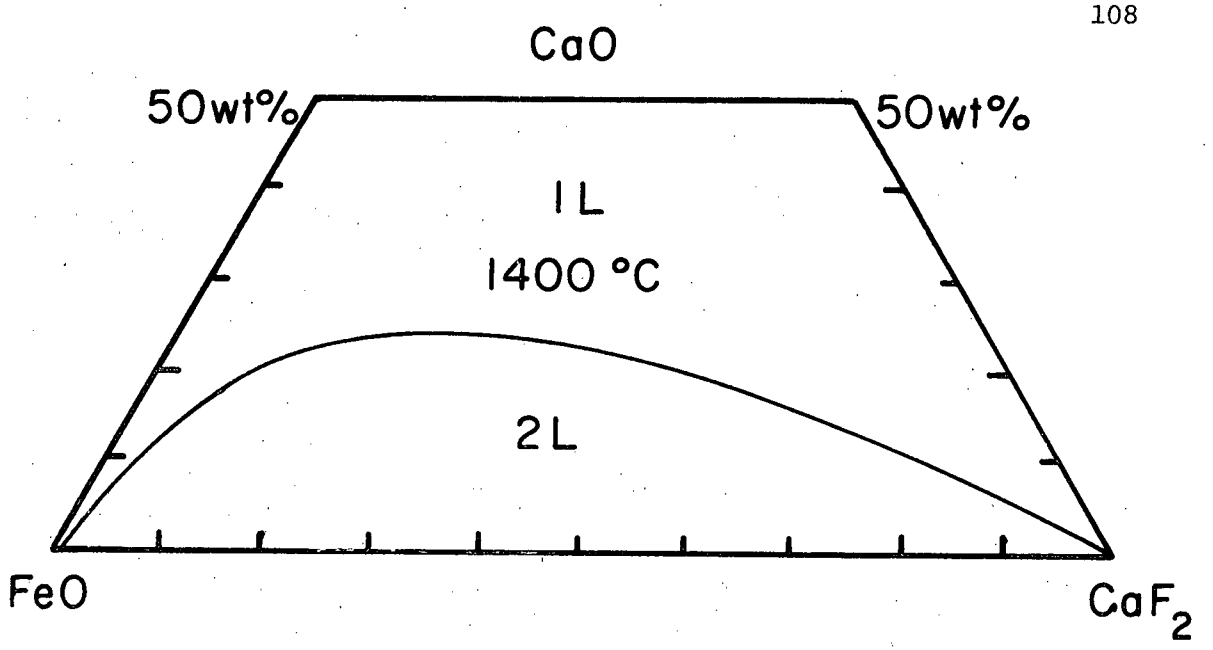

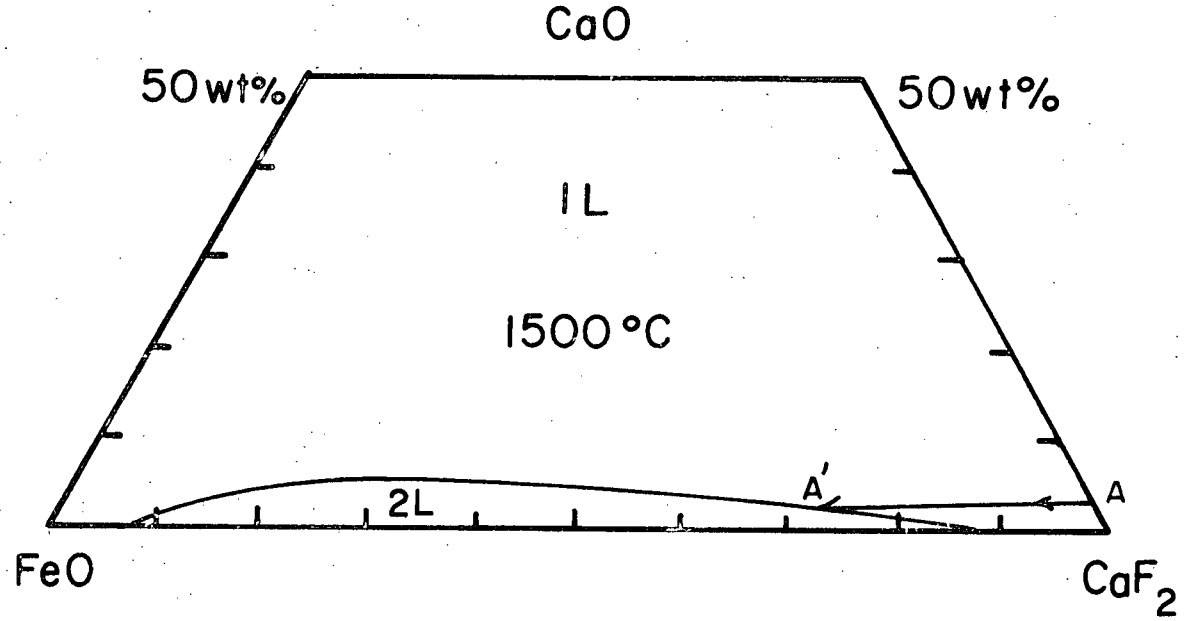

Figure 32. Partial phase diagrams of the system CaF_2-CaO-FeO.

tion:

$$Fe_s + CO_g \rightleftarrows C_{gr} + (FeO)_{(slag\ sat'n)} \qquad (4\text{-}6)$$

which is obtained by adding reactions (2-6) and (4-5). It is difficult to check (4-6) with an exact calculation because the carbon monoxide pressure at the reference electrode is unknown. However, if it is assumed that the effective pressure of CO at the reference electrode is one atmosphere, the potential difference existing between the reference and saturated iron electrode (a_{FeO} at the iron surface is unity) can be calculated using standard thermochemical data (31) at the measured slag temperature of 1480°C (1753°K).

$$C(gr) + \frac{1}{2}O_2(g) \rightarrow CO(g) \quad \Delta F^\circ = 63{,}540 \text{ cal. } (1753^\circ K) \qquad (4\text{-}7)$$

$$Fe(\delta) + \frac{1}{2}O_2(g) \rightarrow \text{"FeO"}(1) \quad \Delta F^\circ = -36{,}496 \text{ cal. } (1753^\circ K) \qquad (4\text{-}8)$$

and $\Delta F^\circ_{rx} = +27{,}044$ cal (1753°K)

$= -nFE^\circ$

so $E^\circ = -586$ mV.

where n = 2 equivalent. $mole^{-1}$.

and F = 23,060 cal. · $volt^{-1}$. $equivalent.^{-1}$

This calculated value of 586 mV. is reasonably close to the observed value of approximately 500 mV. measured as the beginning of sections B in Fig. 8.

At higher current densities in sections B, it is thought that the rate of electron transfer could be accommodated by increasing the ratio of Fe^{3+} to Fe^{2+} by the reaction:

$$Fe^{2+} \rightarrow Fe^{3+} + e^- \qquad (4\text{-}9)$$

in the saturated slag layer, which will have the effect of displacing the measured potential to a higher value. This is seen as the slope of the sections B in Figure 8, and will again be independent of slag composition. As mentioned previously, it was found to be impossible to carry out small scale studies in high oxide slags due to Al_2O_3 precipitation on the electrode and due to the rising liquidus temperature at Al_2O_3 concentrations above the eutectic composition (10 wt. % Al_2O_3). None the less, a trend can be observed if we plot the extrapolated values of the limiting current density (i_D) against the mole % of Al_2O_3 in the slag as shown in Fig. 33. This seems to indicate that as the Al_2O_3 content of the slag is increased, i_D will asymtotically approach a "limiting" value. The practical significance of this is that as long as anodic metal-slag interface current densities are maintained below the i_D curve during D.C. electroslag melting, FeO saturation of the anodic surface will not occur, and oxidation of the metal will be held to a minimum.

It was considered necessary to examine the polarization results to see if there were activation mechanisms present which would have very fast rise and decay time at these temperatures. If such a decay existed, it would be included in the potential difference we have attributed to an ohmic potential gradient seen as the initial rise on the oscilloscope trace. To check this, the "IR" portion of the rise times for a Ferrovac-E anodic electrode in a CaF_2 + 2.5 wt. % Al_2O_3 slag was plotted against the current I, as shown in Fig. 34. The straight line behaviour of the plot excludes the presence of any activation process in these systems (16).

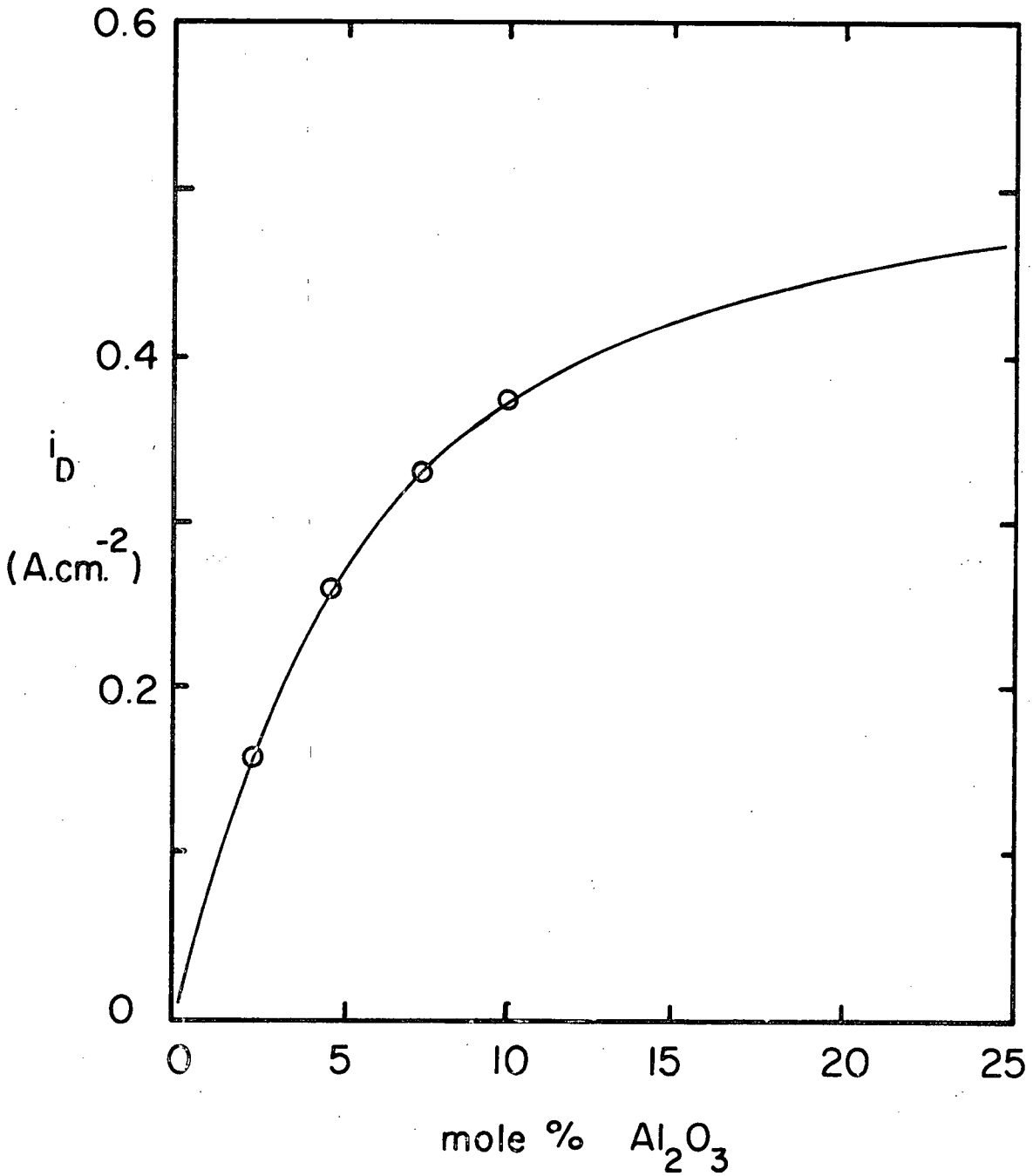

Figure 33. Estimated limiting current density for anodic polarization of pure iron in CaF_2 + Al_2O_3 slags.

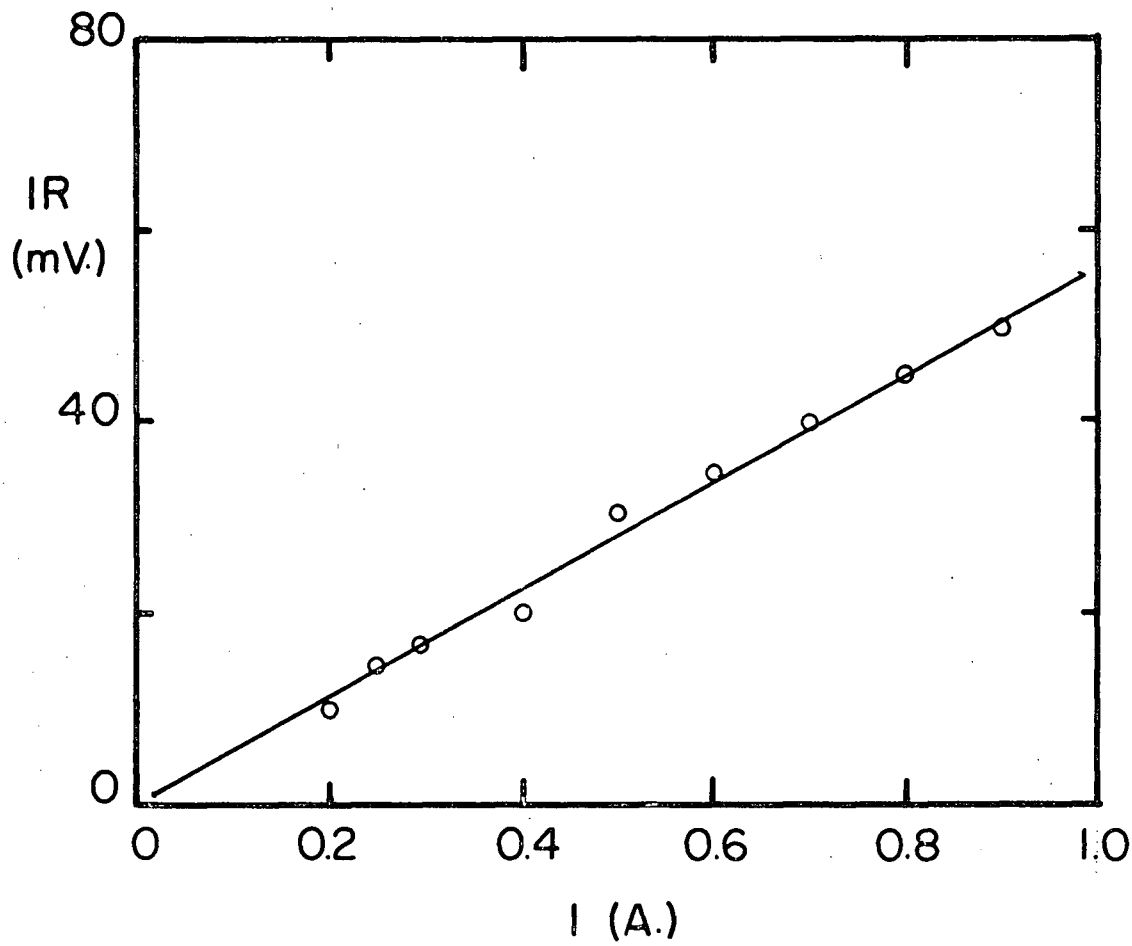

Figure 34. IR drop as a function of applied current, I, for anodic polarization of pure iron in a CaF_2 + 2.5 wt.% Al_2O_3 slag.

It is thought that towards the end of sections B in the anodic polarization curves of Fig. 8, when the rate of electron transfer has become too high to be accommodated by increasing the Fe^{3+}/Fe^{2+} ratio, that gas evolution at the interface is achieved by the reactions:

$$O^{2-} \rightarrow O^{*} + 2e^{-} \qquad (4\text{-}10)$$

$$2O^{*} \rightarrow O_2(g) \qquad (4\text{-}11)$$

It was shown in Fig. 14 that anodic polarization at relatively high current densities produces oxygen in the bulk of the electrode. Fig. 35 is the oscilloscope trace of a high current density anodic pulse on a Ferrovac-E electrode in a low oxide content slag (250 ppm. CaO). The serrated behaviour of the steady-state portion of the curve is characteristic of gas evolution on metal electrodes as observed by Gosh and King (16). It was observed that anodic electrodes showed significant dissolution when polarized at high current density in section B, but not when polarized in section A. This behaviour is expected as a result of formation of liquid FeO on the solid electrode surface, the FeO having a lower melting point ($\sim$ 1380°C) than the iron. The oxidation of the electrode is explained by the following mechanism. During the time when the electrode surface is saturated with FeO, there will be significant diffusion of oxygen into the solid electrode despite the fact that the iron itself is being anodically corroded. When the oxygen content of the surface layer is high enough, FeO forms as a liquid which falls away from the solid electrode producing the observed electrode dissolution.

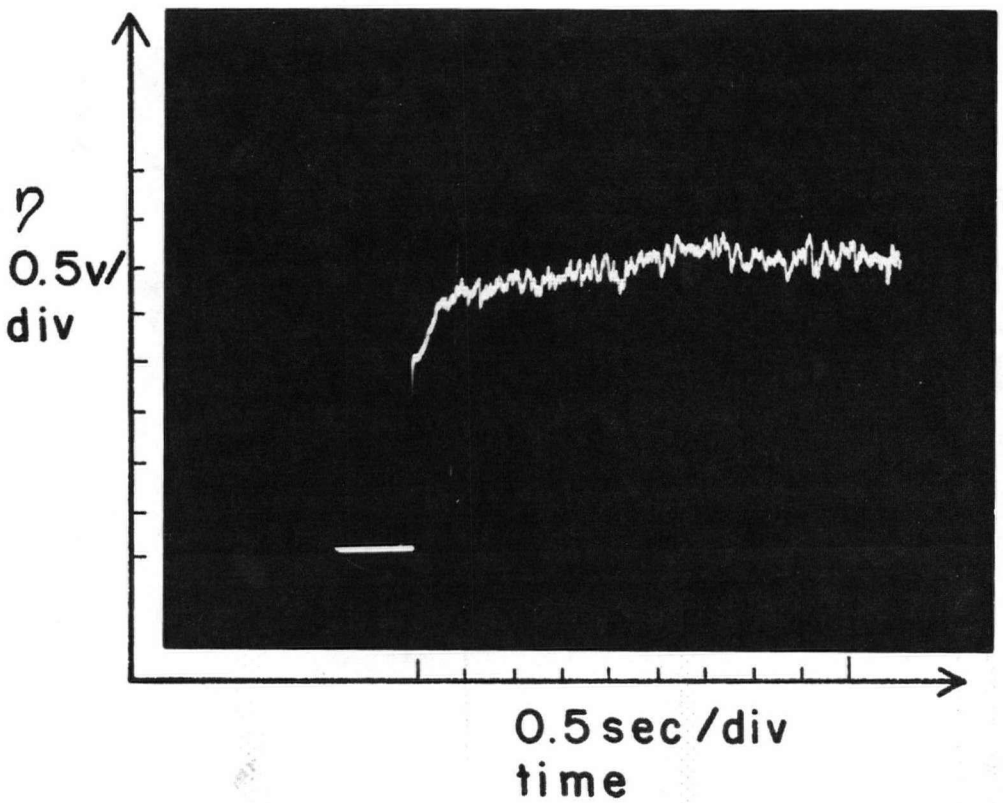

Figure 35. Anodic pulse on pure iron in CaF_2 + 250 ppm CaO. The electrode polarization is seen to transfer from the saturation condition to an arc, as polarization continues i_o = 500 ma.cm^{-2}.

4.3.1 Apparent transition time

The type of anodic polarization curves resulting from a single pulse test as shown in Fig. 12 were found at values of current lying in the middle region of sections B in Fig. 8. At higher and lower current densities, the individual traces exhibited the usual exponential rise and decay behaviour.

The shape of the galvanostatic polarization curve shown in Fig. 12 is qualitatively the same as that expected for a transition between two slow, diffusion controlled processes as described in equation (1-28). Therefore analysis of these curves according to the relationship

$$\eta_d = A + \frac{RT}{nF} \ln \frac{\tau^{1/2} - t^{1/2}}{t^{1/2}}$$

should indicate whether or not the polarization mechanism being studied was indeed a diffusion controlled reaction in which some ionic species in the slag was being depleted at the electrode surface. The transition curves were analysed for applied currents of 0.5 A, 2A., and 3A. and the values of the current density (i_o), the transition time τ, and the product $i_o\tau^{1/2}$ are given below.

I(A.)	i_o(A. cm.$^{-2}$)	τ (sec.)	$i_o\tau^{1/2}$ (A. sec.$^{1/2}$)
0.5	0.18	8.5	2.92
2.0	0.73	1.3	1.14
3.0	1.09	0.8	0.89

It is apparent that the transition time does indeed decrease as the current density increases, but the product $i_o\tau^{1/2}$ is not constant for a given slag, a condition which must be satisfied for such a mechanism.

The diffusion overvoltage is plotted according to equation (1-28) for the three applied currents in Fig. 36 $[f(x) = \ln \frac{\tau^{1/2} - t^{1/2}}{t^{1/2}}]$ and although the points for each current density lie on straight lines, the slopes increase with the current density. Values of n can be calculated by equating the measured slope to $\frac{RT}{nF}$ and are given below.

I(A.)	n (gm. equiv./gm. mole)
0.5	5.2
2.0	3.5
3.0	3.0

The values of n so obtained are not unreasonable in magnitude, but vary over a range which is much wider than would be expected for a correct analysis. Because the values of n and, also, the values of the product $i_o \tau^{1/2}$ are found to be functions of the current density, it must be concluded that the observed transition curves do not arise from diffusional depletion of the slag in some ionic species. This finding agrees with the previously proposed mechanism of anodic corrosion of iron which is a single step diffusion process and would not exhibit a transition time behaviour. The apparent transition times must therefore be explained in another way.

Such an explanation can be found if we examine Figures 32 and 37. Fig. 37 is the oscilloscope trace obtained when repetitive anodic pulses are applied in the "transition" region, at a frequency which maintains part of the saturated FeO layer produced by the previous pulse. Here it is observed that the inflection in the polarization curve is

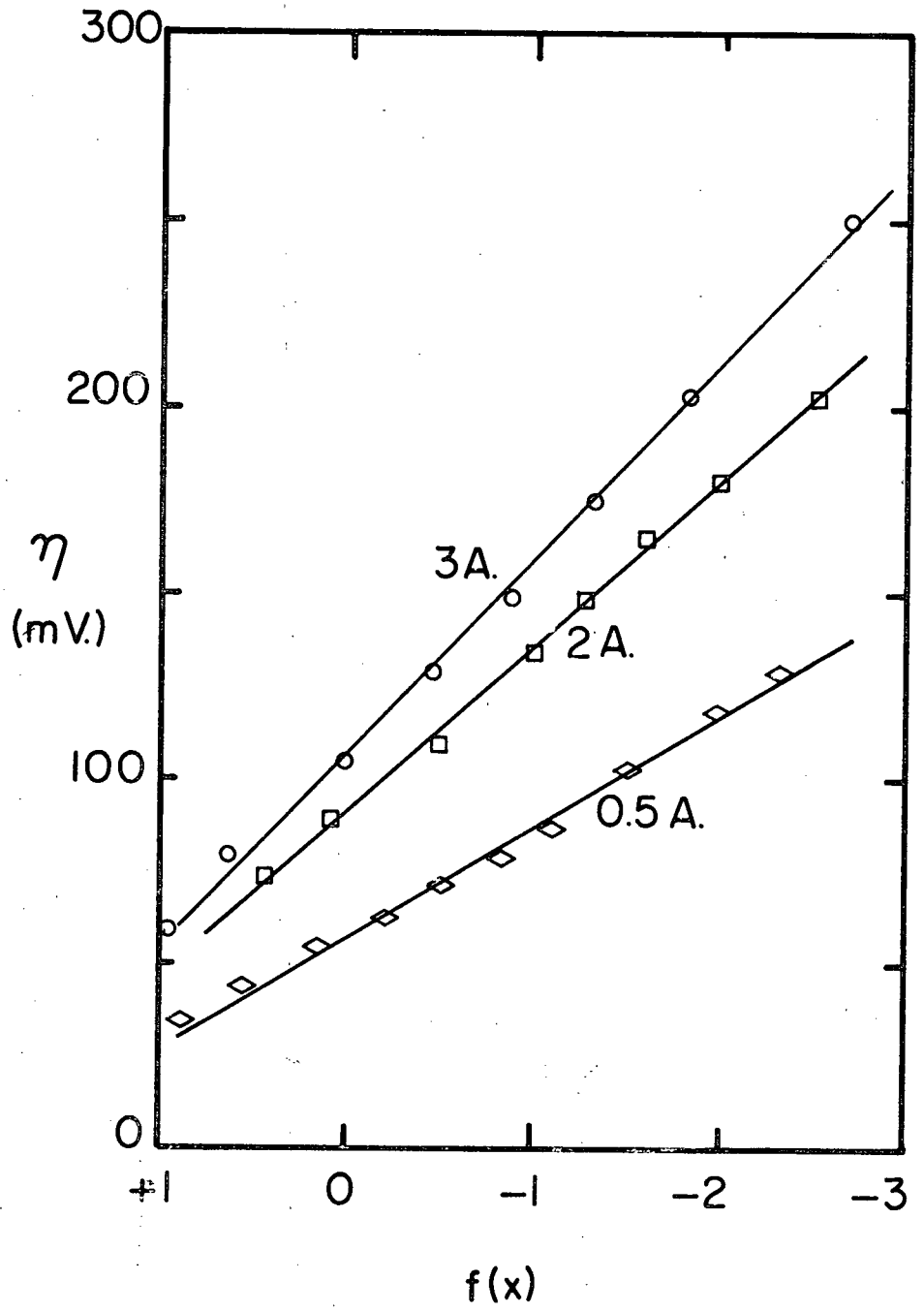

Figure 36. Application of transition time law to anodic polarization of pure iron in CaF_2 + 2.5 wt.% Al_2O_3.

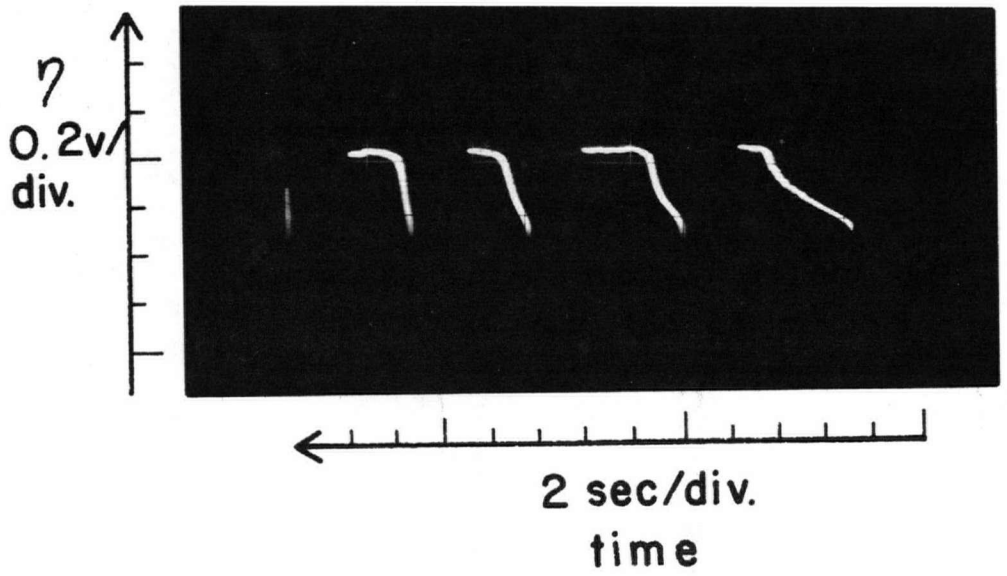

Figure 37. Successive anodic pulses applied to pure iron in CaF_2 + 2.5 wt.% Al_2O_3, showing the disappearance of the apparent transition time when surface saturation is retained between pulses.

gradually removed with successive pulses. This indicates that the transition curves are the result of chemical phenomena rather than electrochemical ones, and can be explained using the single electrode reaction

$$Fe \rightarrow Fe^{2+} + 2e^{-}$$

If we examine the partial phase diagrams of the CaF_2-CaO-FeO system (Fig. 32), we see a two liquid region in a composition range through which the slag at the electrode surface must pass in order to achieve Fe^{2+} saturation. Therefore the first portion of the transition curve, shown as line A-A' in Fig. 32, represents the simple dissolution of Fe^{2+}, while the inflection point indicates the beginning of the two liquid slag system as Fe^{2+} saturation is approached.

4.4 Anodic polarization of pure iron in CaO slags

The anodic polarization behaviour of pure iron electrodes in CaF_2 - CaO slags is shown in Fig. 10. Comparisons of Figures 8 and 10 show that the plateau section B is much more pronounced in Al_2O_3 containing slags than in CaO containing slags where the overpotential at equivalent current density is seen to decrease more rapidly with increasing CaO content. This is probably the combined result of the lower viscosity of CaF_2 - CaO liquids (32) and their higher solubility (30) of Fe^{2+}, as compared with CaF_2 - Al_2O_3 liquids at equivalent oxide content. It was also observed that anodic iron electrodes melted at much lower current densities and CaO contents than they did in an equivalent Al_2O_3 content.

One can speculate, from the results in Fig. 10, that an ESR slag containing 25 wt. % CaO, at a given current density, would not saturate a melting iron electrode in Fe^{2+}, whereas an ESR slag of the same Al_2O_3 content would. This might result in the final metal having a lower oxygen content when melted through the CaO containing slag because of the lower oxidation rate at the anodic surface.

4.5 Cathodic polarization of pure iron in ESR slags

In order to provide a Faradaic mechanism at the slag/metal cathodic interface, we may postulate any combination of the following reactions:

$$Ca^{2+} + 2e^- \rightarrow Ca^* \quad (4\text{-}12)$$

$$Ca^* \rightarrow (Ca°)_{slag} \quad (4\text{-}13)$$

$$Ca^* \rightarrow Ca°_g \quad (4\text{-}14)$$

$$Al^{3+} + 3e^- \rightarrow Al^* \quad (4\text{-}15)$$

$$Al^* \rightarrow [Al]_{FE} \quad (4\text{-}16)$$

$$Al^* \rightarrow (Al°)_{slag} \quad (4\text{-}17)$$

$$Al^* \rightarrow Al°_{\ell} \quad (4\text{-}18)$$

for the appropriate slag cation composition.

In the case of the overall reaction (4-12) and (4-14), the potential seen by the measuring circuit is represented by the equation:

$$(CaO)_{slag} + C_{gr} \rightarrow CO_g + Ca_{(g)} \quad (4\text{-}19)$$

Similarly, the potential seen at an electrode which is cathodically polarizing due to reactions (4-15) and (4-16) is represented by the

reaction:

$$(Al_2O_3)_{slag} + 3\ C_{gr} \rightarrow 3CO_g + 2[Al]_{Fe} \qquad (4\text{-}20)$$

giving potentials:

$$\Delta E^\circ_{4\text{-}19} \tilde{=} 800 \text{ mV}$$

and $$E^\circ_{4\text{-}20} \tilde{=} 400 \text{ mV}$$

at 1812°K, for Raoultian standard states. However, as the observed reaction must involve solution of Al in both the metal and the slag and Ca in the slag, we would not expect to see these potentials as the polarization values.

The form of the cathodic $\eta/\ln i_o$ curves at the lower current densities is again that to be expected from the diffusion of reaction products away from the cathodic interface. One might expect to observe a limiting potential at interface saturation but this will not occur as it did in the anodic cases because there is no electrochemical mechanism by which the interface can remain saturated as the current density is increased above the initial saturation current density. At higher current densities, it is believed that the calcium gas produced forms a soft arc which is very stable and the increase in measured polarization results from the arc resistance. This concept is supported by Fig. 38 which is a plot of the cathodic overpotential against the working current of a pure iron electrode in a CaF_2 + 1 wt. % Al_2O_3 slag. The curve becomes linear after a current of 5 A. (1.8 A. $cm.^{-2}$) which is characteristic of an arc process. In slags with a higher oxide content, it appears that this very stable soft arc does not initiate until higher current densities are attained. This is one way in which the cathodic polariza-

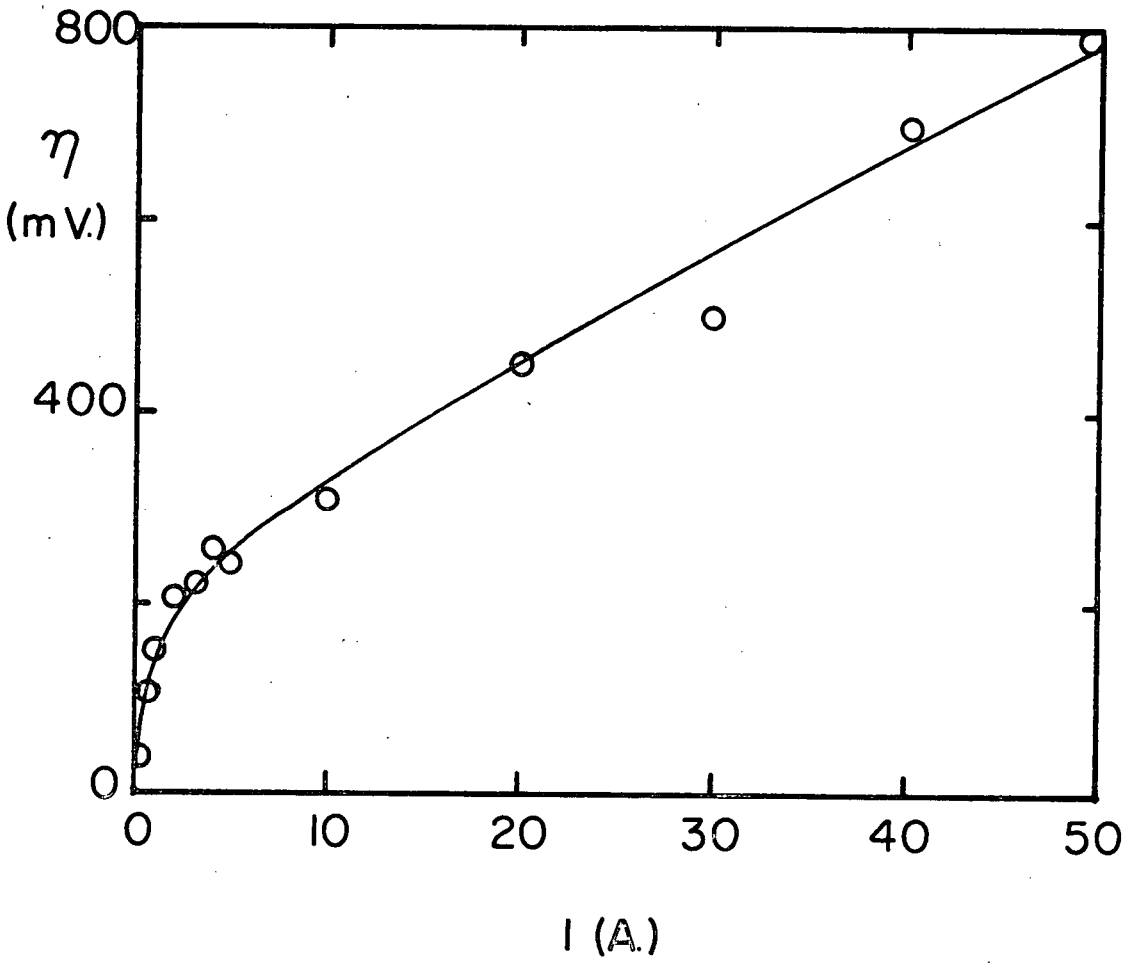

Figure 38. Cathodic polarization of pure iron in a CaF_2 + 1 wt.% Al_2O_3 slag plotted against the applied current.

tion curves can be reasonably explained.

Another possible explanation of the linear behaviour shown in Fig. 38 is that the current density, i_o, and convection boundary layer are related in such a fashion that a linear overpotential-current density plot is obtained. This is based on the assumption that the measured overpotentials do indeed result from a change in activity of a deposited species at the interface, and that this potential can be described in terms of a Nernst equation. This would apply when a steady-state condition is achieved, with the diffusion overvoltage given by

$$\eta_d = \frac{RT}{nF} \ln \frac{c(i)}{\bar{c}}$$

where $c(i)$ is the imposed concentration of the diffusing species at the interface, and $\bar{c}$ is the concentration before current passage (concentration has been substituted for activity). If we assume that the initial curved portion of the plot given in Fig. 39, represents the cathodic deposition of Al in the iron by the reaction:

$$Al^{3+} + 3e^- \rightarrow (Al)_{Fe}$$

and that the linear portion represents the deposition of Ca which subsequently dissolves in the slag, the current density at which the curve becomes linear should be the limiting diffusion current density of Al^{3+} ions in the slag. The diffusion boundary layer can therefore be calculated using equation (1-11).

$$\frac{i}{nF} = D \cdot \frac{(c - \bar{c})}{\delta}$$

when $i = i_D$, $c = 0$.

For the anodic reaction given above, n = 3 and i_D = 1.8 A. cm.$^{-2}$

The slag contains 1 wt. % Al_2O_3 (M.Wt. = 102 gm), and the density of the slag is approximately 2.6 gm.cm.$^{-3}$, therefore $\bar{c}$ = 2.55 x 10^{-4} moles. cm.$^{-3}$

F = 96,500 coul. gm. equiv.$^{-1}$

D = 8.5 x 10^{-5} cm.^{2} sec.$^{-1}$ (33) and δ can be calculated to be 0.347 cm. Therefore the diffusion boundary layer for Al_2O_3 depletion at a cathodic iron surface is approximately 3500 microns thick, a reasonable value for such a system. When the electrode current density exceeds the limiting current density for Al deposition, Ca^{2+} ions must deposit, and the linear portion of the curve must correspond, in the absence of a stable soft arc, to the reaction:

$$Ca^{2+} + 2e^- \rightarrow [Ca]_{slag}$$

where the measured overpotential is determined by the Ca activity at the electrode interface. For Nernst type behaviour, η_d is proportional to ln c, and from equation (1-11), i is proportional to $\frac{c}{\delta}$ ($\bar{c}$ = 0). Therefore i and δ must be related in such a way that the concentration, c, of Ca in the slag at the interface, varies to produce the relationship:

$$i \alpha \ln c$$

and therefore

$$\eta_d \alpha \ln c.$$

Although it is difficult to conceive of such behaviour during electrolysis, it is felt that this explanation is more realistic that the idea of establishing a soft arc at these low current densities.

In high oxide content slags containing Al_2O_3, Al and Ca should be deposited together such that some Al will dissolve in the iron electrode while Al and Ca dissolve in the slag. The fact that Al is produced at a cathodic surface was shown by the electron microprobe studies of an cathodic iron electrode as discussed in Section (2-5).

4.6 Polarization of Fe-Cr alloys and pure chromium

The anodic and cathodic polarization behaviour of AISI 430 stainless steel electrodes was shown in Figures 15 and 16. Very little information can be drawn from these curves except to say that at an equivalent current density and slag composition, the degree of anodic polarization is less on a stainless steel electrode than on a pure iron electrode. No B regions, or plateaus were found on the anodic polarization curves of these electrodes. At low current densities, the anodic reaction is thought to be

$$Cr \rightarrow Cr^{3+} + 3e^{-} \qquad (4\text{-}21)$$

As the current density is increased, and the Cr concetnration at the interface decreases due to preferential anodic corrosion, iron will start to corrode to produce a build up of Cr^{3+} and Fe^{2+} ions at the electrode interface.

The cathodic polarization curves (Fig. 16) show a behaviour similar to the cathodic curves for pure iron shown in Fig. 9. This would indicate that the cathodic reaction is not appreciably influenced by the presence of Cr as an alloying element in the iron matrix.

The concentration gradient of Cr at the surface of an AISI 430 stainless steel shown in Fig. 17 gives ample evidence of the preferential anodic corrosion of Cr from Fe-Cr alloys. As indicated previously the removal of Cr took place at a current efficiency of only 10%. This means that even at this relatively low current density, the anodic reaction was accounted for in the main by corrosion of iron, not chromium. One might expect to observe an anodic polarization plateau established by FeO saturation in the slag because of the fact that Cr removal accounts for only 10% of the current passage. However, no plateau was observed because the potentials measured were established by corrosion of both Cr and Fe such that the effect of the Cr was to mask the Fe plateau.

The anodic polarization curves for the Fe -1 wt. % Cr alloy shown in Fig. 18 can also be explained using the concept of Cr depletion at the electrode surface. Prior to current passage, the electrode surface has a Cr concentration of 1 wt. %. Upon passage of current, the electrode polarizes to produce a plateau at approximately 230 mV., the value of which is determined by the Cr content at the surface. As current passage proceeds, the Cr is quickly depleted at the surface and anodic corrosion of iron takes place causing the measured potential difference between the reference and working electrodes to increase to the plateau value of an anodic iron electrode. Upon current interruption, the measured polarization decay is therefore that of an iron electrode as shown by decay polarization curve in Fig. 18.

The anodic polarization curve of pure chromium (Fig. 19) exhibits a plateau at a potential between 200 and 300 mV. This plateau arises from saturation of the slag at the interface in Cr^{3+} ions and is therefore

comparable to the plateaus found for anodic iron electrodes in CaF_2 - Al_2O_3 slags. The potential difference existing between the graphite reference electrode and the Cr^{3+} saturated surface is represented by the equation:

$$3\,C_{(gr.)} + Cr_2O_{3(\beta)} \rightarrow 2\,Cr_{(s)} + 3\,CO_{(g)} \qquad (4\text{-}22)$$

From the free energies given below (T = 1809°K),

$$3\,Cr_{(s)} + \frac{3}{2}\,O_{2(g)} \rightarrow 3\,CO_{(g)} \quad \Delta F^\circ = -194{,}007 \text{ cal.} \qquad (4\text{-}23)$$

$$2\,Cr_{(s)} + \frac{3}{2}\,O_{2(g)} \rightarrow Cr_2O_{3(\beta)} \quad \Delta F^\circ = -159{,}481 \text{ cal.} \qquad (4\text{-}24)$$

$$\Delta F^\circ_{rx.} = -34{,}526 \text{ cal.}$$

and $\Delta E^\circ = -250$ mV.

This calculated value agrees very well with the observed value of the plateau.

4.7 Polarization of pure nickel

The small scale studies carried out on an anodic nickel electrode in a $CaF_2 + Al_2O_3$ slag were not suitable for presenting as a polarization curve because at the lower current densities, the electrode would not polarize to a steady state value in the time available during an individual pulse experiment. Steady state polarization was not achieved until the current density was increased to 1.1 A. $cm.^{-2}$ The oscilloscope trace of this test is shown in Fig. 20, and the observed polarization potential is approximately 700 mV, which should correspond to the reaction:

$$C_{(gr)} + NiO_{(s)} \rightarrow Ni_{(s)} + CO_{(g)} \qquad (4\text{-}25)$$

The free energy change for this reaction is calculated as follows at 1726°K:

$$C_{(gr)} + \frac{1}{2} O_{2(g)} \rightarrow CO_{(g)} \quad \Delta F^\circ = -62{,}996 \text{ cal.} \qquad (4\text{-}26)$$

$$Ni_{(s)} + \frac{1}{2} O_{2(g)} \rightarrow NiO_{(s)} \quad \Delta F^\circ = -21{,}325 \text{ cal.} \qquad (4\text{-}27)$$

$$\Delta F^\circ_{rx} = -41{,}671 \text{ cal.}$$

and $\Delta E^\circ = -904$ mV.

The discrepancy between the observed and calculated values for the plateau height might be explained by the relatively long time needed to establish the steady-state polarization in this sytem, a time during which the entire system is cooling. If the system temperature was significantly lower than the assumed temperature of the melting point of nickel, then a calculated ΔE° would also be smaller.

The electronmicroprobe results obtained upon the examination of a cathodically polarized nickel electrode were presented in Fig. 21. Although calcium is insoluble in iron (34), it is soluble in nickel, but the question arises as to whether or not Ca will be deposited in the presence of Al_2O_3 containing slags. Bell (21) considered the interaction between CaO + Al_2O_3 in CaF_2 slags and liquid nickel, and under equilibrium conditions, found that the interaction between the oxides and dissolved Al and Ca in liquid nickel was such that as long as alumina is present in a slag, alumina will react with liquid nickel to a much greater extent than CaO. He stated that Ca would not dissolve in the

metal even when the CaO activity in the slag was 0.56, unless the Al_2O_3 activity was less than 0.00018, which was certainly not the case in the CaF_2 + 8 wt. % Al_2O_3 slag used for electrolysis of the nickel electrode. We must therefore conclude that the Ca containing regions shows in Fig. 21, were not electrochemically formed, but that this calcium was in the nickel in the as received condition.

4.8 Anodic polarization of cobalt

The anodic polarization behaviour of cobalt was very similar to that of nickel in that steady-state polarization could not be attained until the current density was high. Fig. 22 shows the oscilloscope trace obtained at a current density of 2.0 A. $cm.^{-2}$ This shows a measured potential difference of almost 800 mV. which corresponds to the reaction:

$$C_{(gr)} + CoO_{(s)} \rightarrow Co_{(\gamma)} + CO_{(g)} \qquad (4\text{-}28)$$

The free energy change for this reaction is calculated at 1766°K, the melting point of cobalt, as follows:

$$C_{(gr)} + \frac{1}{2} O_{2(g)} \rightarrow CO_{(g)} \quad \Delta F° = -63{,}803 \text{ cal.} \qquad (4\text{-}29)$$

$$Co_{(\gamma)} + \frac{1}{2} O_{2(g)} \rightarrow CoO_{(s)} \quad \Delta F° = -26{,}010 \text{ cal.} \qquad (4\text{-}30)$$

$$\Delta F°_{rx} = -37{,}793 \text{ cal.}$$

and $\Delta E° = -819$ mV.

This figure of 819 mV. agrees very well with the measured value. If the rise times in Figures 20 and 22 are compared, it is apparent that the cobalt rise time is much faster and the degree of system cooling is therefore kept to a minimum. The faster rise times so observed must be a result of a difference in saturation solubility of CoO and NiO in CaF_2 slags.

In silicate melts, it is found that the saturation solubility of oxides of transition metals decreases according to the order Cr, Fe, Ni, Co, and it is possible that a similar trend exists in the slags presently studied.

4.9 Anodic polarization of an Fe-C alloy

As stated in section (2.5.7) the anodic polarization of an Fe-C electrode significantly decreased its carbon content. This observed carbon loss must have taken place by evolution of carbon-monoxide gas despite the fact that there is often a bubble nucleation problem associated with carbon-monoxide evolution. It is not surprising, however, that carbon monoxide evolution occurred because, according to Distin et. al. (35), there will be no nucleation barrier at an iron surface containing 0.8 wt. % C when it is in contact with FeO saturated slag.

From this experiment one can conclude that carbon loss during D.C. ESR could be quite substantial.

4.10 High current density polarization

The visual observation of arc effects at very high current densities on both anodic and cathodic surfaces is supported by the behaviour of the polarization curves shown in Fig. 13. It is evident that at sufficiently high current densities the electrode surface displays an essentially linear overpotential/current density behaviour which is unexplainable by a diffusion controlled mechanism. However, it would be the case if the observed polarization resulted from the resistance of

a gas film around the electrode (36). Such an arc could arise in either of two ways. Firstly, the electrode reaction could evolve gas, either $Ca_{(g)}$, $O_{2(g)}$ or $F_{2(g)}$ at a rate sufficient to create a steady-state gas envelope around the electrode. At the high temperature at the tip, sufficient electron transport would be possible in this envelope to transfer the electrode reaction to its outer (slag/gas) surface, thus retaining the electrode reaction, and hence the arc would be self-sustaining. Fig. 35 shows the formation of such a condition in a CaF_2 + 250 ppm. CaO slag. The electrode first polarizes, in this case anodically, then evolves gas at a higher potential. The anodic reaction here would be the initial formation of a saturated layer of FeO at the electrode surface, by reaction (4-2), which would be instantly followed by reaction (4-9). When the rate of these reactions is insufficient to sustain the current density imposed by the current source, reaction (4-11) will be initiated, evolving a gaseous species to form the arc, which produces a significant increase in the polarization potential. This region of arcing is section C in Fig. 30. This situation is probably the phenomenon referred to in the literature as a "soft" arc, since although the effect is visible as a sudden increase in radiation, it has no characteristic arc splutter. The initiation of such an arc is very similar to the initiation of the "anode effect" in aluminum electrolysis (37), and as with the anode effect, the current density required for anodic arc formation is strongly dependent on the oxide content of the slag. As in the case of the transition into the FeO saturation condition at lower anodic current densities, we can only use an approximate extrapolation to extend our findings to higher

TABLE XI

CRITICAL CURRENT DENSITY ESTIMATION

ELECTRODE POLARITY	SLAG CaF_2 + wt. % oxide	ESTIMATED CURRENT DENSITY FOR ARC INITIATION $A.cm.^{-2}$
+	25 Al_2O_3	250
-	25 Al_2O_3	400
+	5 Al_2O_3	150
-	5 Al_2O_3	200
+	0	10
-	0	25
+	5 CaO	300
-	5 CaO	400
+	25 CaO	500
-	25 CaO	500

oxide slags. However, since the current density at the point of arc initiation marks the upper limit for the working of a stable electroslag process electrode, we feel that such an approximation will provide valuable operating information. The anodic and cathodic current limitation figures are shown in Table XI.

The electrode current density in the U.B.C. electroslag furnace is approximately 100 A. $cm.^{-2}$, while in a commercial electroslag furnace, the current density on an 18 in. diameter electrode at a current of 15 kA. is approximately 10 A. $cm.^{-2}$ Both of these current densities are below the estimated values of critical current density for arc initiation in a 25 wt. % Al_2O_3 slag. On the other hand, the current densities in electroslag welding are very high. For a wire diameter of 1/8 in. and a process current of 450 A., the electrode current density is approximately 3×10^4 A. $cm.^{-2}$ This current density is far greater than that required for arc initiation and electroslag welding must therefore operate as a submerged arc process.

A second possible mechanism for such arc initiation is heat generation by Joule heating in the polarized slag layer leading to local boiling in the slag. This has been considered from a theoretical standpoint (38) in analogy with the Leidenfrost phenomenon, and may operate in the present case. It is possible to calculate the required current density to boil the slag at the electrode tip using the following model.

Consider a conical polarized electrode with a surface area of 11.3 $cm.^2$ (an average electrode tip). Joshi (32) calculated the heat transfer coefficient, h, between slag and electrode to be:

$$h \tilde{=} 1 \text{ cal.}^{\circ}\text{C}^{-1} \text{ sec.}^{-1} \text{ cm.}^{-2}$$

If the assumption is made that all of heat generated by current passage through the polarized slag layer is transferred to the electrode at this value of h, it is possible to calculate the current density needed to raise the slag temperature at the interface to its boiling point. The heat transfer equation is

$$q = h \cdot A \cdot \Delta T \quad \text{cal. sec.} \tag{4-31}$$

where A is surface area of transfer, and ΔT is the temperature difference across the interface. By assuming that the slag is at its boiling point and the metal (Fe) is at its melting point.

$$\begin{aligned} \Delta T &= \text{B.P.}_{CaF_2} - \text{M.P.}_{Fe} \\ &= 2509^{\circ}\text{C} - 1538^{\circ}\text{C} \\ &= 971^{\circ}\text{C} \end{aligned}$$

Therefore, for these assumptions,

$$\begin{aligned} q &= 1 \times 11.3 \times 971 \\ &\tilde{=} 11{,}000 \text{ cal. sec.}^{-1} \end{aligned}$$

If the voltage drop in the polarized slag layer is assumed to be 10 V. the power dissipation is given by:

$$P = 10I \text{ watts}$$

where I is the current in amps. Multiplying P in kW by the factor 0.24 converts P to kcal. sec.^{-1} Therefore the current can be calculated as follows:

$$I = \frac{P}{10} A$$

$$11 \text{ kcal. sec.}^{-1} = \frac{11}{.24} \text{ kW.}$$

$$= 45.9 \text{ kW.}$$

$$\text{Therefore } I = \frac{45.9}{10} = 4.59 \text{ kA.}$$

$$= 4590 \text{ A.}$$

The electrode current density would then be

$$i_o(\text{A. cm.}^{-2}) = \frac{4590}{11.3} \tilde{=} 400 \text{ A. cm.}^{-2}$$

This is an unreasonably high current density, even in view of the initial assumptions and one can therefore conclude that arc initiation by this means is very unlikely.

The evolution of gas on the working electrode will only alter the measured polarization through its effect on the Fe^{3+}/Fe^{2+} ratio of the slag at the slag/gas interface. When gas bubbles are evolved, the increase in polarization overvoltage observed is due to the increase in ohmic resistance in the region of the working electrode surface. Although the calcium fluoride used contained only a small quantity of oxide (250 ppm), and extensive precautions were taken to exclude oxygen from the system, there were no indications that fluoride species were involved in the polarization reactions in "pure" calcium fluoride, as evidenced by changes in, for example, the anodic polarization times. It is probable that the low levels of oxygen present in the fluoride were sufficient to provide a saturated layer on the working electrode since oxide solubility in "pure" calcium fluoride is very small.

The observations made on the cathodic process indicate that the arc initiation condition must be associated with the production of $Ca_{(g)}$.

In CaF_2 + CaO slags, this is evidently the only possible mechanism, and should occur at electrode potentials of approximately 1 volt with respect to the graphite reference electrode. In CaF_2 + Al_2O_3 slags, the mechanism should remain the same, but the observed potentials at arc initiation will be markedly different from the CaF_2 + CaO case due to the effect of Al_2O_3 on the CaO activity.

4.11 Electroslag process polarization

The values of anodic and cathodic polarization on melting electrodes in the melting unit given in Figures 23→26 agree well with the extrapolated small scale polarization results. One can therefore conclude that neither the obviously different hydrodynamic regime at the ESR electrode nor the fact that the electrode is continuously melting have a significant effect on the polarization reactions. We may also conclude that the substantial (8%) 360 Hz ripple present in the D.C. rectifier circuit has no detectable effect on the reactions. The few anodic and cathodic overpotential values obtained on melting AISI 1095 and AISI 430 steel electrodes are approximately the same as those measured on pure iron electrodes at equivalent current densities. This indicates that the alloying elements had no appreciable depolarizing effect and that our findings on pure iron electrodes apply to all iron-based materials.

CHAPTER 5

DISCUSSION OF MELT PROGRAM RESULTS

5.1 Introduction

The purpose of the melt program was to investigate the chemical and thermal effects which occur during D.C. electroslag melting, and explain these effects in terms of the Faradaic reaction mechanisms proposed in Chapter 4.

The more important findings of the melt program are shown to be:

1. Chemical effects exist during D.C. electroslag melting. In the case of pure metals, oxidation occurs at the anodic surface to produce ingots with a final oxygen content which is dependent principally on the electrode polarity. Deposition of Al occurs at the cathode surface and the Al-O interaction is partially responsible for oxygen removal from the ingot pool.

2. Thermal effects are present during D.C. electroslag melting. They apparently arise from excess heat generation in the polarized slag layer at the liquid metal/liquid slag interfaces. These effects result not in a higher slag temperature but, in the case of an anodic electrode, in a higher specific melt rate and, in the case of an anodic ingot, in a larger liquid metal volume in the ingot pool.

3. In the case of D.C. electroslag melting of alloys, the chemical effects result in significant losses of easily oxidizable alloying elements. Alloy depolarization is small.

4. All of these effects can be explained in terms of both Faradaic reaction mechanisms and mass transfer phenomena at the two metal/slag interfaces.

5.2 Effect of electrode polarity on oxygen content

The oxygen analysis results of the ingots made in the melt program show that ingots made on the D.C. electrode negative mode have a much higher final oxygen content than ingots made on the electrode positive mode, independent of atmospheric interactions. This fact is best illustrated by examining the melt record results of Ferrovac-E ingots (Table III) in which the average oxygen content of electrode negative ingots melted through CaF_2 + 25 wt. % Al_2O_3 slag is 480 ppm. O, while ingots made on the electrode positive mode in the same slag have an average oxygen content of 185 ppm. O. As shown in the melt records, there are actually three types of electrode positive melting possible. The first type is the standard electrode positive mode in which the maximum rate of power input is controlled by the voltage at which arcing to the "insulated" mold occurs (~19 V.). To operate at a higher voltage, it was necessary to paint the inner surface of the copper mold with boron-nitride paint as described in Chapter 3. In this type of electrode positive melting [+(im)] it was possible to melt at higher applied voltages without arcing to the mold (see ingots 37, 38, and 41). These in-

gots had an average oxygen content of 140 ppm. O which is only slightly lower than that of the normal electrode positive (+) ingots. Two ingots were made in the third type of electrode positive mode which is electrode positive with a live mold, [+(lm)]. In this mode the mold was purposely made to carry current being connected to the power return circuit with its own leads and current shunt. It was found that in this mode approximately 90% of the process current passed through the live mold circuit, and ingots 35 and 83 made this way in a CaF_2 + 25 wt. % Al_2O_3 slag had the higher oxygen content (760 ppm. O). Three ingots made using A.C. power (34, 36 and 40) had an average oxygen content of 215 ppm. O. As shown in Table III, ingot 36 was made using a live mold connection, while ingot 40 was made in an insulated mold, but these conditions appeared not to affect the final oxygen content to any extent.

This observed dependence of the oxygen content on the electrode polarity can be explained using the findings of the small scale studies. Consider first the case of the ingot being made in the electrode negative mode. The electrode is cathodic and the ingot anodic such that Al and Ca will be deposited at the melting electrode tip. The Ca will dissolve in the slag and Al will dissolve at a steady-state rate into the liquid iron film on the electrode tip. Therefore, the metal droplets which detach from the tip will contain dissolved aluminum which will be carried to the liquid metal pool ofthe solidifying ingot. In the U.B.C. electroslag rig, the current density at an anodic ingot tip is high enough to saturate the slag at the interface in FeO, and iron oxide will be dissolving continuously into the liquid metal pool. Depending on the relative concentrations of

Al and O in the liquid, oxide inclusions will nucleate and grow as solidification proceeds. The inclusions that are trapped by the solidifying interface represent the final oxygen content of the ingot metal. This is a very simplistic view of inclusion formation and entrapment in which no consideration has been given to the problems of inclusion nucleation or Al loss from the drops as they pass through the iron-oxide saturated anodic interface.

Ingots made in the electrode positive [+] or electrode positive with an insulated mold [+(im)] mode will pick up Al and O by the same means with the exception that the electrode is anodic and the ingot cathodic. Why, then, do electrode negative ingots have a higher final oxygen content? This can be explained by considering the location of the anodic reaction sites in the two cases. The ingot current density is approximately one-half that of the electrode tip current density, but the operating current in the U.B.C. electroslag rig is sufficiently high to saturate an anodic ingot surface in FeO. In electrochemical terms an anodic ingot surface is equivalent to an anodic electrode tip, and the observed dependence of final ingot oxygen content on electrode polarity must therefore arise from differences in the rate of metal oxidation at the two possible anodic surfaces. Anodic liquid iron surfaces are exposed to FeO saturated slag which represents an unlimited supply of oxidant, and the rate of oxygen dissolution must be controlled by the liquid metal flow characteristics at these interfaces. A melting electrode has a liquid film on the surface which is approximately 200μ thick (4). As will be shown in Section (5.6), the amount of oxygen which dissolves in the melting electrode metal is equal to 1600 ppm.

O for pure iron electrodes. It was not possible to calculate an equivalent value for the amount of oxygen dissolution at an anodic liquid ingot surface, because too little is known about the fluid flow conditions in the ingot pool. However, due to the larger surface area at the pool, one can speculate that more oxygen will be dissolved at an anodic ingot. One must now consider how this oxygen is removed from the liquid metal, because the observed final ingot oxygen contents are much lower than the calculated oxygen content. In the case of the anodic electrode, the metal droplets could conceivably lose some of their dissolved oxygen during the time the drops fall through the slag, especially when one considers the fact that oxygen is surface active in iron and the drop surface therefore presents a large amount of the dissolved oxygen to the refining action of the slag. Also when the drops reach the cathodic ingot surface, they must pass through a layer of strongly deoxidizing slag containing metal produced by the cathode reaction. It is therefore reasonable to expect that the bulk of the oxygen dissolved in a melting anodic electrode will be removed from the metal before the metal becomes part of the ingot pool proper. In the case of an anodic ingot pool which is in contact with an FeO saturated slag, the only supply of deoxidant is that which is transported to the pool by the metal drops. Then drops will contain electrochemically produced aluminum which will react with the dissolved oxygen in the ingot metal to form inclusions, some of which will dissolve in the slag. The dependence of the final ingot oxygen content on electrode polarity can therefore be explained in terms of differences in oxygen dissolution rates at the ingot and electrode and the chemical interaction between the electrochemically produced products.

The fact that live mold electrode positive ingots have the highest oxygen content of any mode can be explained if we again consider the electrochemical reaction sites. The anodic surface is the electrode tip which behaves in the same manner as the anodic surface in any other mode by dissolving oxygen in the melting metal. In this mode, the bulk of the current flows to the mold and the path of lowest resistance should be a radial one, orthogonal to the electrode tip. It seems unreasonable to propose that the process current passes through the solidified slag skin to the Cu mold. It would be more plausible to have the current transferred through a "soft arc," (section 4.10) established between the liquid slag and the copper mold. As discussed in Section (1.3.3) such an arc might conduct both electronically and ionically, with the principal Faradaic site as the arc/slag interface. Hence the ingot/slag interface has little cathodic deoxidizing capability and thus will not substantially alter the electrode metal composition. We would expect then that the ingot pool contain large amounts of dissolved oxygen.

5.3 Inclusion types

As previously indicated in Chapter 1, electroslag processing ensures that no large inclusions are present in the ingot metal. Electron microprobe examination of ingot specimens produced in the present melt program show this to be the case. Fig. 39 shows the appropriate electron microprobe pictures obtained upon examination of ingot no. 27 (FVE. el.-ve) while the pictures in Fig. 40 were obtained from the AISI 430 stainless steel ingot (No. 61). Both ingots contained small round inclusions of high

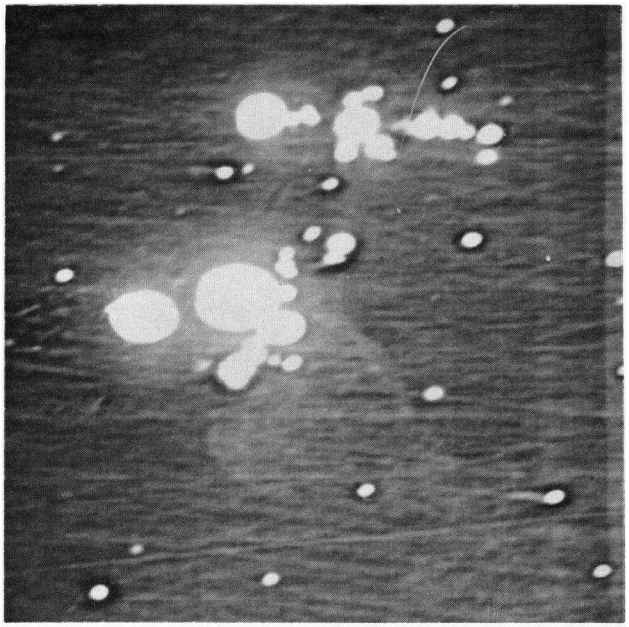

A.E.I. X 1200

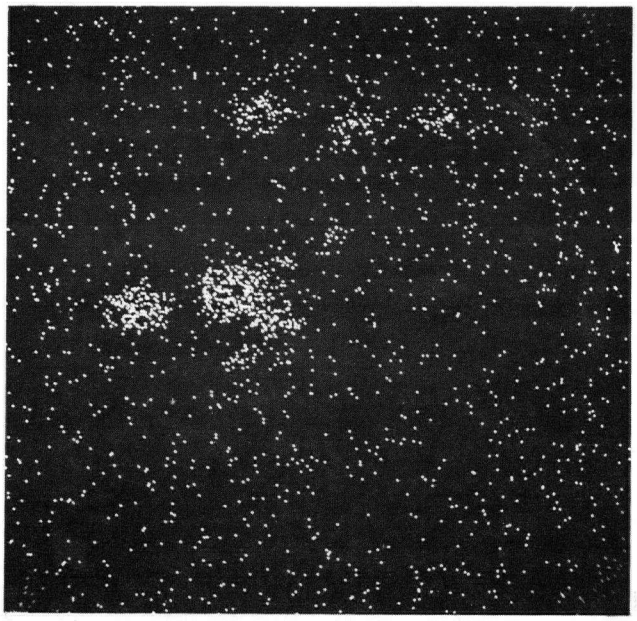

Al X-ray X 1200

Figure 39. Section from interior of Ferrovac-E electrode negative ingot showing Al containing inclusions.

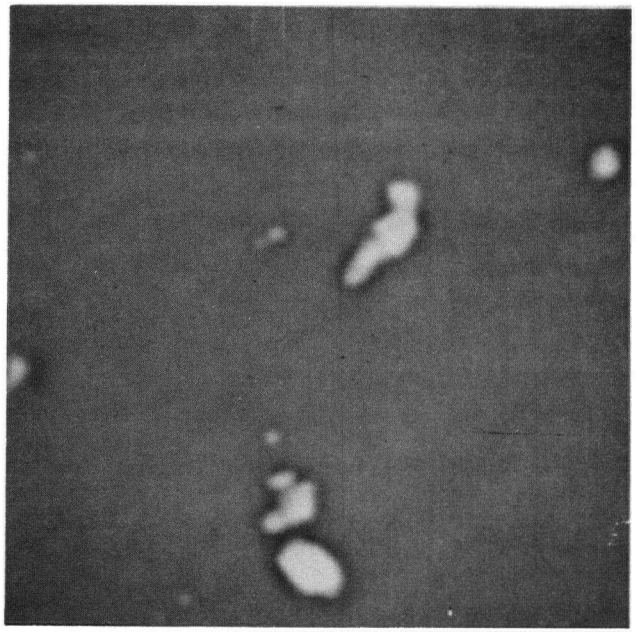

A.E.I. X 2100

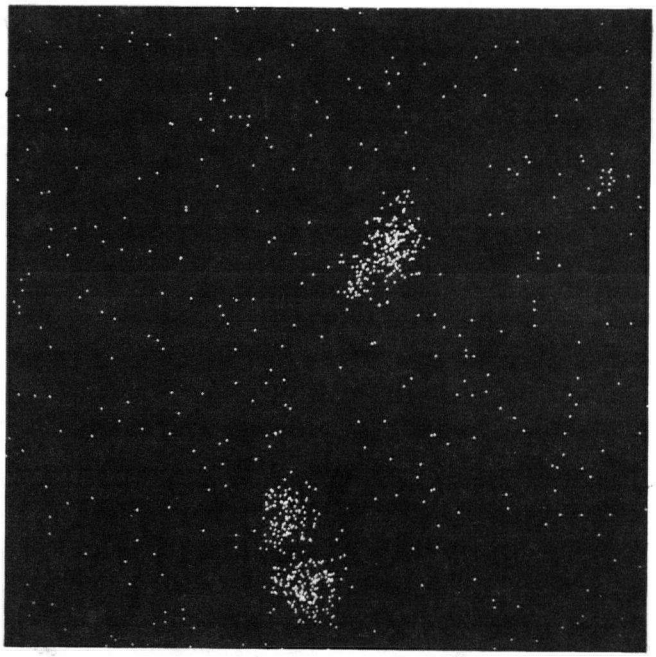

Al X-ray X2100

Figure 40. Section from interior of AISI 430 stainless steel ingot showing Al containing inclusions.

aluminum content. The same type of inclusions were found in most of the ingots examined whether they were made from AISI 1095 steel or essentially pure nickel. Inclusion formation and composition during electroslag processing will not be discussed here, having been adequately covered by Bell (21). Evidence of inclusion removal by flotation was found upon examination of the top surface of ingot 30 as shown in Fig. 41. This shows a large number of alumina inclusions which were about to enter the slag. These inclusions were larger than those found in the bulk of the ingot and they appear to have formed by agglomeration of smaller inclusions. This produced inclusions with a larger effective radius which were able to float out of the ingot pool. This observation indicates that the measured oxygen content of the ingots is lower than the electrochemically produced oxygen content.

It must be noted that the final ingot oxygen and aluminum contents in pure iron were far higher than would be produced by equilibration of iron with alumina. This is shown to be true in Fig. 42 which is a plot of experimentally determined Al and O contents of pure iron in equilibrium with alumina of unit activity at 1600°C (21). The residual Al and O contents of ingots 25, 41, and 83 are shown to lie well above the equilibrium contents. This supports the argument that the electrochemical reaction products are responsible for the observed ingot inclusions.

With respect to removal of inclusions present in the starting electrode metal, it has been noted (39) that the electrode tip is the site at which these inclusions are most efficiently removed. As discussed previously, this is not the case with respect to removal of electrochemically formed inclusions.

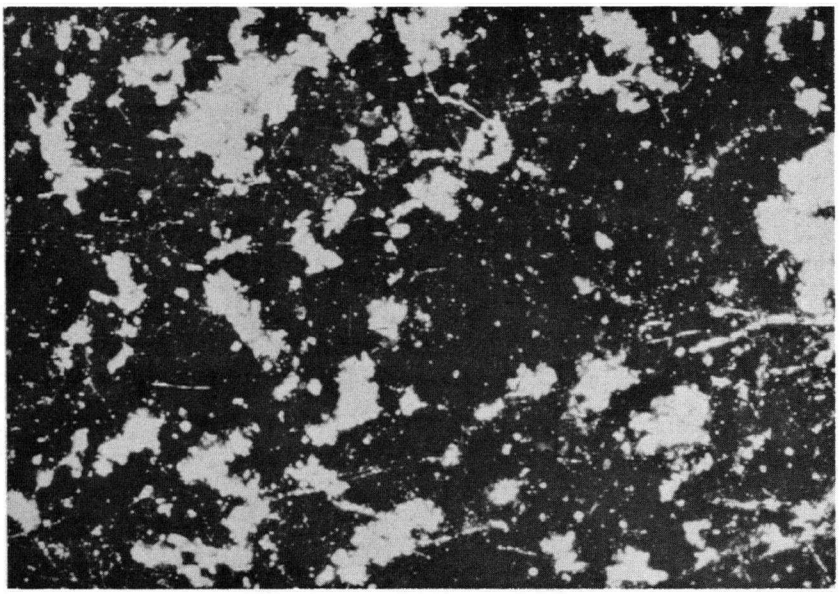

Figure 41. Alumina inclusions on the top of a Ferrovac-E electrode negative ingot.

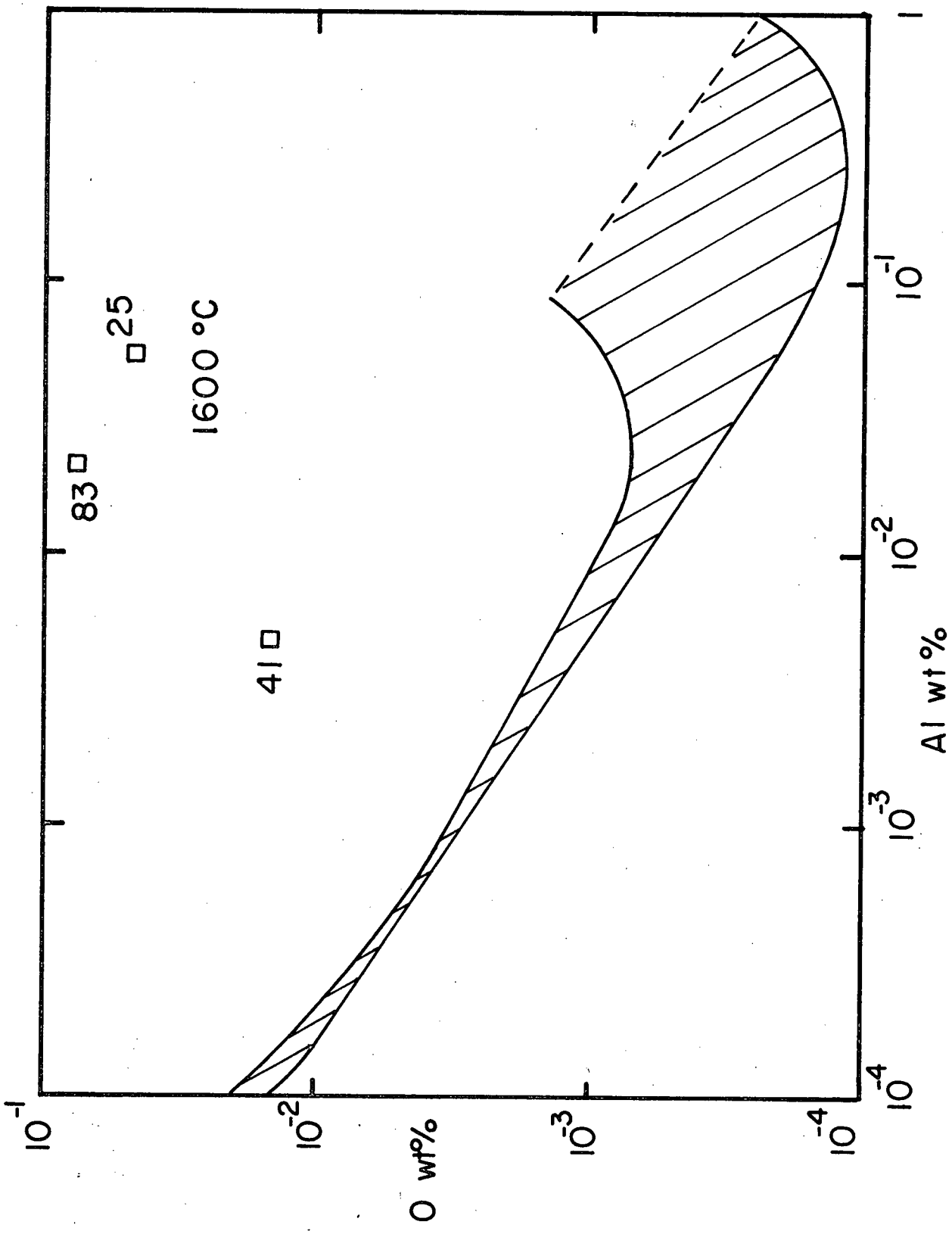

Figure 42. Al and O in liquid iron in equilibrium with unit activity Al_2O_3 at 1600°C. Experimental data falls within the hatched area.

5.4 Effect of specific coulombic density (Z) on the final oxygen content

As presented in Chapter 3, it was postulated that the final ingot oxygen content could be correlated to a parameter, Z, which took into account the operating current density and the melt rate. There may indeed exist such a relationship, but the range of stable operating current densities available on the U.B.C. electroslag rig is limited. Hence, we were unable to vary Z over a sufficiently wide range for the postulate to be examined with respect to the final ingot oxygen content. Despite the limited amount of data, a trend does appear to exist. If one examines the values of Z and oxygen content for ingots 31→33 in Table III (el. +ve.), it can be seen that the lowest oxygen content corresponds to the lowest value of Z, but this may simply be a reflection of the higher melt rate of ingot 31. Examination of the data for the electrode negative ingots in Table III shows the same trend in that ingot 77 has the lowest oxygen content as well as the lowest value of Z and the highest melt rate. However, although the approach appears entirely reasonable, the range of accessible experimental data is insufficient to adequately test our initial postulate.

5.5 Effect of atmosphere control

Two types of atmospheric control were used during the melt program. The argon fume hood produced a relatively oxidizing atmosphere (up to 1% O_2) whereas the argon gas cap atmosphere purity depended solely on the purity of the argon in use. Etienne (4) states that the atmospheric oxidation rate during melting is dependent upon exchange reactions between slag and atmosphere which in turn are controlled by diffusion of multiple valence ions (Fe^{2+}/Fe^{3+}) in the slag. He also concluded that electrode

oxidation above the slag was unimportant as a means of atmosphere oxygen transport to the melting metal. His final conclusion is that the partial pressure of oxygen in the atmosphere bears little relation to the amount of atmospheric oxidation except when the actual rate of supply of atmospheric oxygen is less than the limiting rate of oxygen transfer at the slag/atmosphere interface. If one compares the oxygen contents of Ferrovac-E ingots made in the argon fume hood (23, 72, 24, and 74)with those of the Ferrovac-E ingots made in the argon gas cap (25→30, and 31→33) it is obvious that the different atmospheres have had very little effect on the oxygen content in either the electrode negative mode or the electrode positive mode. One must therefore conclude that the ingot oxygen contents are a result of metal oxidation by the FeO-saturated slag layer produced by electrochemical reactions at the anode. The oxidizing power of this anodic slag layer is much greater than any atmospheric oxidation processes which might have existed during melting in the U.B.C. electroslag rig.

5.6 Diffusion of oxygen into an anodic electrode

As previously discussed (5.2) a melting anodic iron electrode is exposed to slag saturated in FeO. Oxygen dissolves in the liquid electrode film to establish a steady-state rate of oxygen transfer to the melting metal. Etienne (4) developed a mathematical model by consid-

ing an idealized situation in which the liquid metal film flows down a conical electrode tip under the influence of gravity, neglecting the effects of surface tension and momentum transfer from the slag to the liquid metal film. The total weight of oxygen Q_o transferred per unit time across the slag/metal interface is the same as the flow rate of oxygen at the system exit (electrode tip) which may be calculated by integration of the diffusion flow equation over the entire area of the electrode cone, A. The flux of oxygen can then be wirtten as:

$$Q_o = 2\,A[O]_i \sqrt{\frac{D_{o,m}}{\pi t_e}} \quad \text{gm. sec.}^{-1} \tag{5-1}$$

using $A = \frac{\pi R^2}{\cos\theta}$

$[O]_i$ - concentration of O in Fe at slag metal interface,

= 0.2 wt. % (saturation of Fe at 1550°C).

= 0.014 gm. cm.$^{-3}$

$D_{o,m}$ - diffusion coefficient of O in Fe

$\cong 3 \cdot 10^{-4}$ cm.^{2} sec.$^{-1}$ (40)

It has been assumed that the diffusion boundary layer is small compared to the film thickness and the situation therefore reduces to diffusion in a semi-infinite medium. The exposure time, t_e, of a surface element travelling between the base of a cone and the tip is given by:

$$t_e = \left(\frac{2\pi\cos\theta}{3\dot{W}_m'}\right)^{2/3}\left(\frac{\mu_m}{\rho\, g \sin\theta}\right)^{1/3}\left(\frac{R}{\cos\theta}\right)^{5/3}\frac{\Gamma(5/6)\,\Gamma(1/3)}{\Gamma(7/6)} \tag{5-2}$$

where

$\dot{W}_m$ - melt rate in gm. $sec.^{-1}$

= 1.94 gm. $sec.^{-1}$ for electrode positive

$\dot{W}_m'$ - total volumetric melt rate in $cm.^3$ sec^{-1}

$= \frac{\dot{W}_m}{\rho} = 0.277$ $cm.^3 sec.^{-1}$

$\rho = \rho_m - \rho_s$ - effective density of liquid iron due to slag buoyancy

$= 7.0 - 2.6 = 4.4$ gm. $cm.^{-3}$

μ_m - viscosity of molten iron

= 0.05 poise.

R - electrode radius

= 1.59 cm.

θ - base angle of cone

= 45° (average of electrode tips)

g - acceleration due to gravity

$\frac{\Gamma(5/6)\,\Gamma(1/3)}{\Gamma(7/6)}$ - Eulerian functions which evolve from integration of t_e

= 3.259

and $t_e = 0.976$ sec. for the conditions stated above.

$A = 11.234$ $cm.^2$

and Q_o can now be calculated to be:

$Q_o = 3.10 \times 10^{-3}$ gm. $sec.^{-1}$

The weight % of oxygen transported into the melting electrode metal is then found by dividing Q_o by $\dot{W}_m$, and is equal to 0.16 wt. % O or 1600 ppm O. This figure of 1600 ppm O represents the theoretical amount

of oxygen dissolved in the metal during the melting of pure iron in the electrode positive mode. Comparing this with the observed final oxygen contents of pure iron electrode positive ingots (185 ppm O), it appears that the bulk of the dissolved oxygen is lost between the drop detaching from the electrode tip and metal solidification in the ingot. In sections (5.2) and (5.3) it was shown that oxygen might be lost by dissolution of oxide in the slag during the time the drops fall through the slag and by inclusion floatation from the ingot pool. Ingot 83 (Table III) was made in the electrode positive live mold mode [+(lm)] and examination of the slag cap showed that droplets of iron were retained in the slag cap. The larger droplets were analyzed for their total oxygen content and were found to contain 1750 ppm O. This figure is close to the theoretically calculated oxygen content of 1600 ppm O. These drops had been exposed to the slag for a finite length of time but still retained a high oxygen content. It therefore appears that oxide loss during drop fall through the slag is negligible and that inclusion flotation and removal from the ingot pool must account for the removal of the electrochemically produced oxygen.

In order for aluminum containing inclusions to nucleate homogeneously in the ingot pool, there must be high supersaturation of both aluminum and oxygen in the metal. This is in contrast with Bell's findings (21). He found that ingots made with A.C. power had low supersaturations of aluminum and oxygen and inclusions were nucleated only at the freezing ingot interface. Inclusion flotation in D.C. ingots is "short range" and occurs in the ingot pool near the slag/metal interface because

this interface is the electrochemical reaction surface at which the high supersaturations are produced. For this reason inclusion flotation is probably independent of convective motion in the pool.

5.7 Drop size and surface tension

The drop size and surface tension data presented in Table VI, shows a marked dependence of drop size on the electrode polarity during melting. These differences must arise from the effect of oxygen on the interfacial tension at the slag/metal interface. Drops produced at electrode positive electrodes are the smallest because they have a high oxygen content arising by the mechanism of anodic saturation of the electrode tip in FeO. Drops from cathodic electrode are larger because they have no appreciable oxygen content and in fact should be deoxidized by the dissolved aluminum produced by the cathodic processes taking place. A.C. electrode drops are the largest, even larger than electrode negative drops, despite the fact that A.C. slags have a higher bulk concentration of FeO (Table X) which should decrease the interfacial tension at the drop/slag interface. This disparity may simply arise from the cathodic electrode containing aluminum produced by Faradaic processes. In general these findings support our interpretation of the electrochemical phenomena occurring at anodic and cathodic electrode tips, and they agree with the findings of Whittaker (5). Our estimated values of interfacial tension are not unreasonably different from the value of approximately 800 dynes. $cm.^{-2}$ found by Yokabashvili et. al (41) for the interfacial tension between CaF_2 + 25 % Al_2O_3 slag and mild steel.

5.8 Significance of iron in the slag caps

The results presented in Table X show that slags used during electroslag processing pick up iron in the form of iron-oxide. There is no detectable iron in these slags before they are used, therefore the observed iron contents arise by chemical and electrochemical means during remelting. In the electrode negative mode (ingot 39), the bulk of the slag cap is very clean in appearance, with only a very thin layer of FeO containing slag at the ingot pool/slag interface. Both electrode positive slag caps (ingots 31 and 37) have a substantially thicker layer of FeO containing slag at the ingot pool/slag interface. These visual observations of the slag caps agree with the analysis shown in Table X.

In order to consider the possibility of simple chemical formation of FeO in the slag, one must study the thermodynamics of the Fe-Al_2O_3 system. Three possible reactions which may produce FeO in the slag are:

$$3\,Fe_{(l)} + Al_2O_{3(s)} \rightarrow 3\,FeO_{(l)} + 2[Al]_{Fe} \qquad (5\text{-}3)$$

$$2\,Fe_{(l)} + Al_2O_{3(s)} \rightarrow 2\,FeO_{(l)} + Al_2O_{(g)} \qquad (5\text{-}4)$$

$$Fe_{(l)} + Al_2O_{3(s)} \rightarrow FeO_{(l)} + 2\,AlO_{(g)} \qquad (5\text{-}5)$$

These reactions, however, are all highly endothermic and hence would produce no FeO during electroslag melting. Therefore any FeO occurring in the slag must have an electrochemical origin. The FeO produced at the anode represents only one-half of the overall electrochemical reaction, and there must also be an equivalent amount of electrochemically produced calcium and aluminum dissolved in the slag during melting.

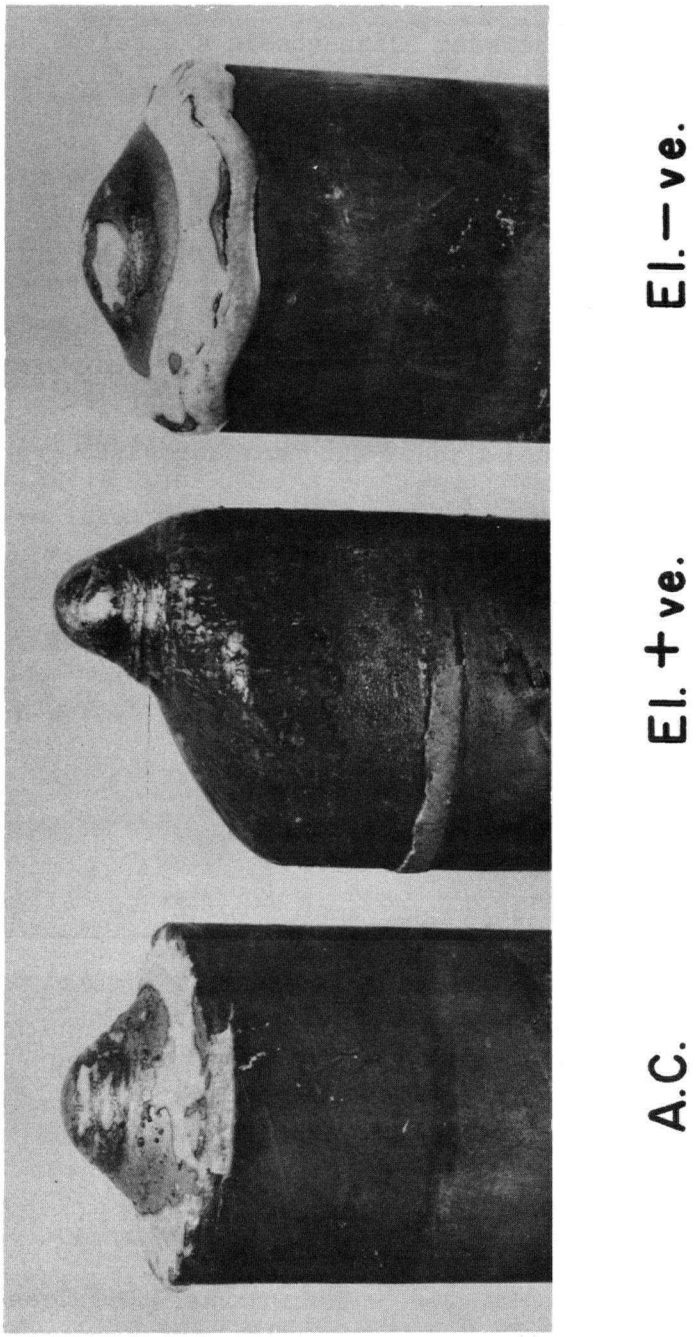

Figure 43. Various electrode tips showing oxide present on an anodic iron electrode tip.

One can envisage a steady-state rate of production of both anodes and cathodic components, the bulk of which dissolve in the slag and continuously back-react in the slag as shown below:

$$(Ca \text{ and } Al)_{slag} + (FeO)_{slag} \rightarrow (CaO \text{ and } Al_2O_3) + Fe_l \quad (5\text{-}6)$$

Thus steady-state amounts of the electrochemical products are present in the total slag cap. When the current is interrupted and electrochemical reactions cease, the back-reaction will continue presumably until the slag caps solidifies and a residual FeO content is retained in the slag. An equivalent amount of residual Ca and Al must also be retained and, in the case of Ca, will be present as Ca^{+} or Ca_2^{2+} ions in the solidified slag. Presently available analytical methods are inadequate to detect this amount without ambiguities.

One must also consider why the FeO containing slag in an electrode position slag cap is found near the ingot/slag interface. This is not immediately clear, but it must arise from density effects in the slag cap since the FeO was produced in the electrode region. Fig. 43 shows pictures of clean electrode tips produced by melting in the electrode negative or A.C. mode and a heavily oxidized electrode tip produced by melting in the electrode positive mode. This lends support to the proposed model requiring FeO saturation at an anodic surface.

5.9 Melt rate and heat generation

An important effect associated with electrode polarization is heat generation at the electrode tip. The average specific power consumption when melting Ferrovac-E electrodes in CaF_2 + 25 wt. % Al_2O_3 slags is

12.6 kWs. · gm.$^{-1}$ in the electrode negative mode and 10.6 kWs. · gm.$^{-1}$ in the electrode positive mode. We know from our small scale studies that at the operating electrode and ingot current densities, an anodic surface is polarized to a greater degree than a cathodic surface. The heat generation due to current passage through these anodic and cathodic polarization resistances is therefore greater at an anodic electrode, and it is evident that the heat transfer pattern in the electrode slag/interface region is such that the heat generated in the polarized slag layers is transferred efficiently into the electrode melting process. The effect is thus seen in specific melting efficiency and not directly in a slag temperature distribution. Similarly, the heat generation at an anodic ingot surface manifests itself by producing a greater liquid metal volume than is observed in a cathodic ingot.

It was also noted that A.C. power produced the most efficient melting with a specific power consumption of 7.7 kWs. · gm.$^{-1}$ If polarization effects did not exist, then there is no reason why there should be any differences in the melting efficiency between A.C. and D.C. melting. This disparity can be explained by using an electrochemical argument. The cathodic products during D.C. melting are calcium and aluminum, both of which are soluble in CaF_2 slags, and substantially increase the slag conductivity. Joshi (32) found a 35% increase in slag conductivity when melting with D.C. power as compared to A.C. power. With a higher conductivity slag, heat generation is decreased and the melting efficiency decreases. This is in agreement with the melting efficiencies observed in this study.

5.10 Calcium oxide slags and ingot porosity

The insolubility of calcium in iron was quite apparent when Armco iron ingots were made in CaF_2 + CaO slags. The cathodic electrochemical product is calcium which dissolves in the slag while, in the electrode negative mode, the ingot is efficiently oxidized. The solidifying ingot metal therefore had a high oxygen content but no dissolved aluminum and the result was carbon-monoxide blow hole formation by the carbon-oxygen reaction:

$$[C]_{Fe} + [O]_{Fe} \rightarrow CO_g \qquad (5\text{-}7)$$

The carbon content of Armco iron is .012 wt. % and was sufficient to produce ingots of high porosity. In the case of ingot 52 melted in the electrode negative mode in a 25 wt. % CaO slag, bubble formation was so drastic that iron bubbles would form on the top of the liquid pool and rise up to contact the melting electrode. This is admittedly an extreme case, but such conditions cannot be tolerated during commercial electroslag processing.

5.11 Effect of increasing ingot/electrode diameter ratio

In an attempt to produce a wider variation in Z, ingots were prepared using the electrode/ingot diameter ratio as a variable. Ingots 75 and 76 were made using 3.2 cm. diameter Ferrovac-E electrodes but they were melted into a 7.6 cm. dia. copper mold instead of the usual 5.5 cm. dia. copper mold. Ingot 76 was made in the electrode negative

mode and had a final average oxygen content of 548 ppm. O which is somewhat greater than the 480 ppm. O measured as the average oxygen content of 5.5 cm. ingots. Ingot 76 was made in the electrode positive mode [+(lm)] and had an average oxygen content of 153 ppm. O which lies inside the range of oxygen contents measured for 5.5 cm. electrode positive ingots. The higher final oxygen content of ingot 75 must have arisen in part, because of the lower current density at the anodic ingot surface, a lower current density which still saturated the interface in FeO and produced more efficient net electrochemical oxidation of the iron. The higher current density at the cathodic electrode interface may have resulted in less efficient aluminum transfer to the melting electrode and therefore less efficient deoxidation of the ingot pool. These results would indicate that the ingot pool/slag interface is the most important electrochemical reaction site during D.C. electroslag melting.

5.12 Effect of aluminum addition at the electrode during melting

Experiments were carried out in which aluminum wire was attached to Ferrovac-E electrodes to make ingots 80 and 81. In these ingots, if all the aluminum from the wire was dissolved in the iron during melting, the aluminum content would be 2000 ppm. The aluminum analysis results given in Table VII show that there was efficient transfer of aluminum into the ingot metal. These aluminum analysis figures are total aluminum figures because both matrix aluminum and aluminum in inclusions are counted by the neutron activation technique. The lower than normal total oxygen content of ingot 80 (259 ppm. O as compared to an average of 480 ppm. O) indicates that the added aluminum was respon-

sible for a higher than normal rate of inclusion formation and removal. The presence of the excess aluminum at the melting cathodic electrode increased the drop size to 3.46 gm. as shown in Table VI, a drop size comparable to the A.C. drop size. The effect of aluminum wire on the oxygen content of ingot 81 made in the electrode positive mode is unexpected in view of our other observations. The final ingot oxygen content (576 ppm. O) was much greater than the normal electrode positive ingot oxygen content of 185 ppm. O. One would have expected the aluminum to prevent excessive oxygen dissolution in the melting electrode metal, but this apparently does not occur even though the aluminum was transferred efficiently to the ingot which had a final Al content of 2621 ppm. This agrees with the results given in Table VI which show the drop size of ingot 81 was not appreciably greater than the drop size of a normal electrode positive ingot. These results could be explained on the basis that both oxygen and aluminum are transferred efficiently into the ingot pool. The oxide inclusions subsequently precipitating would be higher in aluminum content than normal electrode positive ingots, and might be less efficiently removed into the slag. Hence the net effect of adding aluminum is to retain oxygen as ingot oxide particles.

5.13 Alloy losses during remelting

5.13.1 AISI 1095 steel

The ingot analysis results given in Table VIII show that there were significant losses in carbon and silicon during remelting, but no manganese loss. Ingot 67 melted in the electrode positive mode lost 6%

of its initial carbon but no silicon, while ingot 68 melted in the electrode negative mode lost 7% of its carbon and 27% of its initial silicon content. These alloy losses must be associated with the anodically produced layer of FeO containing slag at the anodic interface whether this interface be at the electrode or the ingot pool. In the case of ingot 67 the carbon loss should occur at the electrode. The lack of silicon loss in this mode of melting can be explained if one considers that a continuous supply of high carbon liquid metal is exposed to the oxidizing interface at such a rate that the carbon level will never be depleted sufficiently to permit silicon oxidation. Why then is silicon loss experienced in the electrode negative mode? The anodic ingot is being oxidized during melting to such an extent that the carbon at the interface is sufficiently depleted to allow silicon to oxidize. By assuming an ingot pool/slag interface temperature of 1600°C, and neglecting the interaction effects between carbon and silicon, it can be shown that the equilibrium oxygen content of iron with 0.975 wt. % carbon is approximately 20 ppm. O, an oxygen level too low to oxidize silicon. Silicon will not oxidize at this temperature until the oxygen level is above approximately 80 ppm. O which could not be reached under equilibrium conditions unless the carbon level is depleted to approximately 0.2 wt. % at an interface. Therefore silicon oxidation only occurred in the electrode negative mode (anodic ingot) because the degree of mixing at the ingot pool/slag interface was low. Hence the rate of carbon transport to this interface was insufficient to accommodate the rate of oxidation. In the electrode positive case, the rate of carbon supply to the anodic

interface was sufficiently high and no silicon losses were observed. The fact that no silicon containing inclusions were found in these ingots tends to substantiate the idea that silicon losses took place at the ingot pool/slag interface. The oxygen contents reported in Table V are higher than both of the C-O or Si-O equilibrium values. This supports the proposal that inclusion precipitation is taking place in the ingot pool surface region and not in the bulk of the pool.

5.13.2. AISI 430 stainless steel

The ingot analyses information given in Table IX shows that chromium, silicon, and sulphur were lost during the melting of AISI 430 stainless steel, and that the total alloy losses were greatest in the electrode negative mode. These observations again show that the anodic ingot surface is capable of more efficient oxidation of alloying elements than is the anodic electrode tip. The lower rate of metal transport through the ingot surface produces a longer exposure time to the oxidizing anodic slag interface than is encountered at an anodic electrode. A calculation following the lines indicated in Section (5.5) was done for the known melt rate and electrode diameter of this material, and Q_o, the flux of oxygen into an anodic electrode tip was found to be 2.0×10^{-3} gm. $sec.^{-1}$ If it is assumed that an equivalent amount of chromium is oxidized to the Cr^{3+} state and dissolves in the slag, this corresponds to a chromium loss of 0.22 wt. % from the alloy, which is close to the observed chromium loss of 0.19 wt. % in the electrode positive mode. The solubility of oxygen in pure Fe-Cr alloys is relatively high, (~400 ppm at 1600°C in Fe-20 wt. % Cr) but the presence of 0.26 wt. % Si in the alloy decreases

the oxygen solubility to 100 ppm. O. In the absence of dissolved Al one would expect to find Si containing inclusions in this material. However this was not observed, and the inclusions found could only have been formed in a silicon-depleted region.

5.14 Remelting of nickel electrodes

The melt record results of the two nickel ingots are given in Table V. Ingot 69 melted in the electrode negative mode has a low oxygen level of 7 ppm., while ingot 71 melted in the electrode positive insulated mold mode has a relatively high oxygen content of 326 ppm. O. This is contrary to the findings for pure iron ingots in which electrode negative ingots had the higher oxygen content. The inclusions in ingot 71 were found to be aluminum containing, whereas ingot 69 contained a very large number of carbon-monoxide blow holes. The dependence of final oxygen content of these nickel ingots appears to have arisen from a combination of chemical and electrochemical means. It is possible that the rate of aluminum deposition in the cathodic electrode of ingot 69 was low, and the carbon-oxygen reaction in the ingot pool removed most of the anodically produced oxygen. However, in the electrode positive case, aluminum and possibly calcium were deposited in the ingot pool more efficiently to produce a sufficient concentration of deoxidizing elements which consumed the anodic oxygen to form inclusions. Most of these were trapped during ingot solidification. The corollary of this is that if ingots were made from nickel with a negligible carbon content, then the electrode negative ingot would have the higher oxygen content.

5.15 A.C. melting of pure iron

The electrochemical phenomena occurring at the two slag/metal interfaces during A.C. melting are extremely difficult to study. The asymmetry of the anodic and cathodic polarization curves on pure iron suggests a mechanism by which a degree of electrochemical rectification could occur. If this was so, then there would be a net chemical effect. Bell (21) measured oxygen contents in pure iron A.C. ingots which were in excess of the theoretically predicted oxygen level that would be produced by equilibration with Al_2O_3 containing slags. He also measured a substantial D.C. current (5→10 A.) in the melting unit which did not arise from the A.C. power source. It can therefore be concluded that electrochemical rectification does occur during A.C. electroslag processing of pure iron, and that this D.C. current deposits oxygen in the metal which gives rise to non-metallic inclusions.

5.16 Electrochemical phenomena in commercial ESR

It is necessary to consider the findings of this study in relation to commercial D.C. ESR practices.

It is apparent that the current density at the anodic surface, whether it be the electrode or the ingot, should be maintained below the current density at which interface saturation in FeO occurs. In this way, metal oxidation during melting will be kept to a minimum and alloy losses will be less extreme. In view of the fact that the current densities in commercial ESR furnaces are lower than those used in U.B.C. furnace, this condition should be satisfied when using slags with a high

oxide content.

The mechanism of drop formation on a commercial electrode is one of multiple drop formation and is therefore quite different from that in a smaller furnace in which drops form one at a time. It is not known what effect this will have on the rate at which the Faradaic reaction products enter the melting metal. It is also difficult to define the effective electroactive surface area and any model developed for such an electrode tip will be very complicated.

Convective movement in the liquid ingot pool will be important with respect to inclusion nucleation in the liquid metal and inclusion removal by flotation. Little is known about the flow patterns in the liquid pool and it is therefore unreasonable to speculate about such phenomena.

CHAPTER 6

CONCLUSIONS

The observations made in the melt program can be interpreted on the basis of the anodic and cathodic Faradaic reaction mechanisms proposed to explain the results of the small scale studies. The predominant anodic reaction at pure iron surfaces in $CaF_2 + Al_2O_3$ slags and $CaF_2 + CaO$ slags is the anodic corrosion of iron according to:

$$Fe \rightarrow Fe^{2+} + 2e^-$$

At sufficiently high current densities the slag adjacent to the anodic interface becomes saturated in Fe^{2+} ions, which is formally equivalent to iron oxide saturation. This saturation condition leads to oxidation of the electrode metal. The cathodic reaction at iron surfaces is proposed to be the deposition of aluminum at low current densities and the codeposition of both aluminum and calcium at higher current densities. Aluminum dissolves in iron and chemical reaction in the ingot pool between the electrochemically produced oxygen and aluminum produces alumina or aluminum containing inclusions in the final ingot metal. These inclusions are typically small (<20 microns) in diameter. The proposed anodic and cathodic reactions have a high net reversibility even at high current densities, therefore the slag composition remains essentially unchanged during remelting.

At equivalent electrode anodic and cathodic current densities in the U.B.C. electroslag furnace a higher degree of anodic polarization

is observed. The heat generation due to this polarization resistance manifests itself as a lower specific power consumption in the electrode positive mode. At excessively high current densities, an arc is established at the electrode tip and the melting conditions become extremely unstable due to arc heat generation at the electrode tip.

As has been observed by other workers, alloy losses of easily oxidized elements are very substantial during D.C. melting. Results from the present studies on the galvanostatic pulsing of iron alloy anodes demonstrate that such losses are associated with negligible alloy depolarization. Thus the polarized anode behaves essentially as if it were a pure iron surface.

It appears, from this work, that the ingot pool/slag interface is the most important reaction site with respect to electrochemical oxidation and deoxidation reactions. Such reactions occur in a manner essentially independent of the atmosphere.

REFERENCES

1. M. Etienne and A. Mitchell: Proc. Sec. Symp. on ESR technology, Part II, Mellon Institute, Sept. 1969.

2. G.K. Bhat, J.B. Tobias, and R.L. Kennard: Proc. Sec. Symp. on ESR technology, Part I, Mellon Institute, Sept. 1969.

3. B.I. Medovar et al: Electroslag Remelting, State Scientific and Techn. Publ. House of Literature on Ferrous and Nonferrous Metallurgy, Moscow, 1963.

4. M. Etienne: Ph.D. Thesis, U.B.C., Oct. 1970.

5. D.A. Whittaker: Ph.D. Thesis, McMaster University, 1968.

6. W. Holzgruber and E. Plöckinger: Berg-u Huttenw. Monatshefte, 1968, Vol.113, pp. 83-93.

7. W. Holzgruber, K. Petersen, and P.E. Schnider: Trans. Int. Vac. Met. Conf., p.518, Am. Vac. Soc., 1968.

8. R. Roberts: Proc. Sec. Symp. on ESR technology, Part II, Mellon Inst., 1970.

9. P.P. Evseev: Avtom. Svarka, 1967, Vol. 176, p.42.

10. R.W. Ure: J. Chem. Phys., 1957, Vol.26, pp. 1363-73.

11. J.S. Anderson: "Nonstoichiometric Compounds," Am. Chem. Soc., Wash. D.C., 1963, pp.1-22.

12. M. Blander: "Molten Salt Chemistry", Interscience, pp. 367-421, 1964.

13. B.R. Sundheim: "Fused Salts", McGraw-Hill Co., 1964, p.272.

14. K.J. Vetter: "Electrochemical Kinetics", Academic Press, New York, 1967.

15. B.J. Welch and N.E. Richards: "Extractive Metallurgy of Aluminum" Vol. 2, pp. 15-30, Interscience, New York, 1963.

15a. A.F. Alabyshev, M.F. Lantratov and A.G. Morachevskii: "Reference Electrodes for Fused Salts," Sigma Press, 1965.

16. A. Gosh and T.B. King: Trans. TMS-AIME, 1969, Vol. 245, pp.145-52.

17. P. Delahay: "New Instrumental Methods in Electrochemistry", p.350 ff., Interscience, New York, 1965.

18. A. Mitchell and B. Burel: J.I.S.I. 1970, Vol.208, p.407.

19. J. Cameron, M. Etienne, and A. Mitchell: Met. Trans., July 1970, Vol. 1, pp. 1839-1844.

20. J. Campbell: J. Metals, July 1970, Vol. 22, No.7, pp.23-35.

21. M. Bell: Master's Thesis, U.B.C., July, 1971.

22. G.P. Smith: "Molten Salt Chemistry", p.427, Interscience, New York, 1964.

23. V.D. Shantarin, O.A. Esin and V.N. Boronenkov: Elektrochimiya, 1967, Vol. 3(6), pp.775-79.

24. G.A. Toporushev and O.A. Esin: Izv. Vysshikh Uchebnykh Zavedince, Vol.6, 1964, pp.21-27.

25. S. Pizzini, R. Morlotti and E. Romer: Euratom Report, EUR 804 e, 1965.

26. H.A. Laitenen, C.H. Liu and W.S. Ferguson: Anal. Chem., 1960, Vol. 30, p.698.

27. V.G. Levich: "Physiochemical Hydrodynamics", Prentice-Hall, 1962.

28. M. Stewart: Ph.D. Thesis, U.B.C., Dec. 1970.

29. P.N. Smith and M.W. Davies: Trans. Section C, Inst. Min. Met., Vol.80, 1971, pp.C87-92.

30. D.A.R. Kay, A.Mitchell and M. Ram: J.I.S.I., Vol. 208, 1970, pp. 141-46.

31. J.F. Elliot, M. Gleisser and V. Ramakrishna:"Thermochemistry for Steel Making", Vol.2, Addison-Wesley.

32. S. Joshi: Ph.D. Thesis, U.B.C., Aug. 1971.

33. B. Burel: Master's Thesis, U.B.C. June 1969.

34. D.L. Sponsellor and R.A. Flinn: Trans. AIME, Vol. 230, June 1964, p. 776.

35. P.A. Distin, G.D. Hallett and F.D. Richardson: J.I.S.I., Vol.206, p.821.

36. E. Manthey and E. Conzelmann: Z. fur das Elektrochemie, Vol. 32(7), 1962, pp. 330-36.

37. H.H. Kellog: J. Electrochem. Soc., Vol. 97(4), 1950, pp. 131-41.

38. P. Drossbach: Z. fur das Elektrochemie, Vol. 56(1), 1951, pp.38-41.

39. M.M. Klyuev and Yu. M. Mironov: Electrometallurgy, Vol. 6, 1967, pp. 480-83.

40. L.S. Darken and R.W. Gurry; "Physical Chemistry of Metals", McGraw Hill, 1953.

41. S.B. Yakabashvili and I.I. Frumin: Avt. Svarka., No.10, 1962, pp. 41-45.